COUPLING OF NITRATE, CARBON AND HEAT IN WARM WATERS OF THE WESTERN EQUATORIAL PACIFIC: CONSEQUENCES FOR ESTIMATING NEW PRODUCTION AND AIR-SEA EXCHANGE OF CARBON DIOXIDE

By

Daniela Turk

SUBMITTED IN PARTIAL FULFILLMENT OF THE
REQUIREMENTS FOR THE DEGREE OF
DOCTOR OF PHILOSOPHY
AT
DALHOUSIE UNIVERSITY
HALIFAX, NOVA SCOTIA
1999

Contents

List of Tables

List of Figures

Abstract

Recent studies indicate that the western equatorial Pacific Warm Pool may play an important role in interannual and decadal climate variation, global new production, and global atmosphere CO_2 concentration. In this study, I compared the rates of new production and air-sea exchange of CO_2 in the western equatorial Pacific Warm Pool during normal conditions (December 1995/January 1996 and January 1997), during a moderate El Niño event (November/December 1994), and during the strongest El Niño event (December 1997/January 1998) in recent history. As an aid for interpreting and understanding of these processes I used both direct measurements and a box model.

Direct measurements of the rate of nitrate uptake (new production) along the equator (from 145°E to 165°W) show that interannual variations in new production in the western and central equatorial Pacific correlate well with the change of the nutricline depth during the eastward expansion of the Warm Pool depending strongly upon the severity of the El Niño event. The analysis of nitrate, carbon, and heat balances in the western equatorial Pacific indicates that—in non- El Niño conditions—vertical turbulent diffusion is primarily responsible for both the loss of heat and the supply of nitrate and inorganic carbon to the euphotic zone.

Based on this conclusion on the importance of vertical processes, I developed a box model that allows estimation of the rates of new production and air-sea CO_2 exchange in the Warm Pool from the net surface heat flux, elemental ratios, and the C:N ratio of the organic matter sinking from the euphotic zone. The model predictions agree qualitatively with the direct measurements. The model may provide a means for estimating the rates of new production and air-sea CO_2 exchange over the large areas of equatorial Pacific using the remotely-sensed data. The results of this study may also be useful in further understanding of the role of the western equatorial Pacific in biogeochemical cycles and climate variations, and for assessment of this part of the ocean for future fisheries demands.

Symbols and Abbreviations

∇	Gradient operator	[m^{-1}]
APE	Atom percent excess	
$AP^{13}C_{inc}$	Atom % of ^{13}C in incubated sample	
$AP^{13}C_{n}$	Atom % of ^{13}C in natural sample	
$AP^{13}C_{tic}$	Atom % of ^{13}C in total inorganic carbon	
c_p	Specific heat of seawater	[J kg^{-1} K^{-1}]
c_{pa}	Specific heat of air	[J kg^{-1} K^{-1}]
^{13}C	Carbon isotope concentration	[mmol m^{-3}]
C_e	Turbulent exchange coefficients for latent heat	
C_h	Turbulent exchange coefficients for sensible heat	
CEP	Central equatorial Pacific	
	(165°E to 165°W along the equator)	
CO_2	Carbon dioxide	
DCM	Deep chlorophyll maximum	
D_{ez}	Depth of the 1 per cent of the surface PAR	[m]
D_{be}	Depth of the entrained water	[m]
DIC	Dissolved inorganic carbon	[mmol m^{-3}]
DOC	Dissolved organic carbon	[mmol m^{-3}]
DON	Dissolved organic nitrogen	[mmol m^{-3}]
e_a	Water vapor pressure	[Pa]
E	Enhancement factor	
e_s	Saturation water vapor pressure	[Pa]
E	Irradiance vector	[J m^{-2} s^{-1}]
$E_d(O-,\lambda)$	Spectral downwelling irradiance	[W m^{-2} nm^{-1}]
	below the surface	
EUC	Equatorial Undercurrent	
f	Discrimination factor	
Fe	Iron	[nM]

F_{CO2}	Air-sea flux of carbon dioxide	[mmolN m^{-2} d^{-1}]
g	Gravitational acceleration	[m s^{-2}]
$HNLC$	High–nutrient–low–chlorophyll regime	
k_s	Michaelin-Menton half saturation constant	[mmol m^{-3}]
$\mathbf{K}$	Eddy diffusivity vector	[m^2 s^{-1}]
K_h	Horizontal eddy diffusivity coefficient	[m^2 s^{-1}]
K_v	Vertical eddy diffusivity coefficient	[m^2 s^{-1}]
$K(z,\lambda)$	Spectral attenuation coefficient	[m^{-1}]
L	Latent heat of vaporization	[$2.5 \cdot 10^6$ J Kg^{-1}]
N^2	Square of buoyancy frequency	[s^{-2}]
N_a	Ambient nitrate concentration	[mmol m^{-3}]
^{15}N	Nitrate isotope concentration	[mmol m^{-3}]
n_c	Fraction of sky covered by cloud	[tenths]
NO_3	Nitrate concentration	[mmol m^{-3}]
p	Atmospheric pressure	[Pa]
pCO_2	Partial pressure of carbon dioxide	[μatm]
PAR	Photosyntheticaly available radiation	[quanta cm^{-2} s^{-1}]
PON	Particulate organic nitrogen	[mmol m^{-3}]
POC	Particulate organic carbon	[mmol m^{-3}]
P_c	New production, carbon units	[mmolC m^{-2} d^{-1}]
P_n	New production, nitrogen units	[mmolN m^{-2} d^{-1}]
p_C	Biological uptake of inorganic carbon	[mmolC m^{-3} d^{-1}]
p_N	Biological uptake of nitrate	[mmolN m^{-3} d^{-1}]
R	Carbon to nitrogen ratio of the organic matter	[mol:mol]
R_h	Relative humidity	[%]
Ri	Richardson number	
q_s	Saturation humidity	
Q_n	Net surface heat flux	[W m^{-2}]
Q_p	Penetrative irradiance	[W m^{-2}]

Q_l	Latent heat flux	[W m^{-2}]
Q_s	Sensible heat flux	[W m^{-2}]
Q_i	Shortwave solar radiation	[W m^{-2}]
Q_t	Longwave solar radiation	[W m^{-2}]
S	Salinity	[psu]
S_x	Sink/source of x	
SST	Sea surface temperature	[°C]
SSH	Sea surface height	[m]
t	Time	[h]
T	Temperature	[°C]
T_a	Temperature of air	[°C]
T_s	Sea surface skin temperature	[°C]
u	Zonal component of velocity	[m s^{-1}]
u_w	Wind speed	[m s^{-1}]
U_a	Normalized uptake at ambient nitrate concentration	
U_{a+t}	Normalized uptake at nitrate concentration after isotope addition	
w	Vertical component of velocity	[m s^{-1}]
WEP	Western equatorial Pacific (145°E to 165°E along the equator)	
v	Meridional component of velocity	[m s^{-1}]
z_d	Depth of euphotic zone	[m]
α	Albedo	
ϵ	Mixing ratio	
ρ	Density of sea water	[kg m^{-3}]
ρ_a	Density of air	[kg m^{-3}]
σ	Stefan-Boltzmann constant	[5.67 · 10^{-8} W $m^{-2}K^{-4}$]

Acknowledgments

I would like to thank my supervisor Marlon Lewis for encouraging me to pursue my Ph.D., and for his support and advice. I thank my co-supervisor Dan Kelley for his constructive ideas and criticism. My sincere gratitude goes to the members of my supervisory committee, Glen Harrison, Neil Oakey and John Cullen, for their helpful suggestions and advice.

I wish to extend my gratitude to Chuck McClain and the Tropical Ocean Team for being my second scientific family. I thank Ichio Asanuma, Michio Aoyama, Takeshi Kawano, and crew members of R/V Kaiyo and Mirai for giving me the opportunity to participate in wonderful field expeditions. I also gratefully appreciate the cooperation of Scott McLean, Cyril Dempsey and Gary Maillet in field experiments. My sincere thanks goes to all the people in the 2nd floor D-lab, past and present, for their friendship and support.

I wish to thank my family for their love, patience and encouragement. Special thanks goes to my husband for his invaluable support and for inspiring me to pursue my graduate work. Finally I would like to thank my friends Tera, Bostjan, Gordana, Barbara and Lio for their encouragement. Thanks to Michael and his family for making my life in Halifax enjoyable. This thesis is dedicated to Franc Hren.

Chapter 1

Introduction

The western equatorial Pacific Warm Pool represents a large area of the world's ocean system (Fig. 1.1) and may play a dominant role in interannual and decadal climate variation (Rasmusson and Carpenter, 1982; Godfrey and Lindstrom, 1989). It has been observed that the western equatorial Pacific undergoes strong fluctuations (e.g. SST, SSH, thermocline depth, winds, precipitation) on time scales of 3 to 5 years associated with El Niño (McPhaden et al., 1986; McPhaden and Picaut, 1990; Webster and Lukas, 1992). The initiation of El Niño is mediated by small changes (approximately 0.4 degrees over a period of 3 months) in the sea-surface temperature (SST) in this area of the ocean (Rasmusson and Carpenter, 1982); the temperature changes are due to small variations in the different components of the heat budget of the surface mixed layer (the components of net surface heat flux, gains and losses from the upper layer by fluid transport of heat, and penetrating irradiance).

Seasonal and interannual fluctuations associated with El Niño also affect the total primary production in the equatorial Pacific (Barber and Chavez, 1983; Chavez and Barber, 1985; Mackey et al., 1995) as well as the new production (Barber and Kogelschatz, 1989), which can be, at steady-state, defined as the net input rate of newly available nitrogen to the euphotic zone (Dugdale and Goering, 1967; Lewis et al., 1986). In the open ocean, the main external source of nitrogen appears in the form of nitrate (Dugdale and Goering, 1967; Eppley and Peterson, 1979), although some studies have suggested that atmospheric

sources of nitrate and dinitrogen fixation may also be important (Capone and Carpenter, 1982; Carpenter and Romans, 1991; Walsh, 1996; Karl et al., 1997). The nitrate is supplied to the upper ocean layer primarily by upwelling and/or vertical turbulent transport from the deep ocean (Lewis et al., 1986). Given a steady-state assumption, new production represents the amount of organic nitrogen exported out of the surface ocean (Eppley and Peterson, 1979). Assuming that nitrate and carbon are taken up in the euphotic zone and exported downward in approximately Redfield ratio (106 C atoms per 16 N atoms), new production is also a measure of the flux of organic carbon from the surface waters to the deep ocean. In a one-dimensional system, the loss of organic carbon from the surface layer is compensated by a supply of inorganic carbon from deep waters, and by a flux of carbon across the air-sea interface. Hence, new production may play an important role in the ocean's carbon cycle, and the air-sea exchange of carbon across the sea surface. However, the degree to which the new production determines the rate of CO_2 removal from the atmosphere still has yet to be elucidated (Lewis, 1992; Platt et al., 1992).

Since the western Pacific Warm Pool accounts for a large portion of the world's ocean, it may markedly affect the global new production (Barber and Chavez, 1991; Peña et al., 1994). It is therefore of great practical interest to determine the rates of new production in this area of the ocean and how the new production is modified during El Niño conditions.

So far, rates of new production have been estimated indirectly from calculations of nitrate transport in the central/eastern (east from 165°E) equatorial Pacific (Chavez and Barber, 1987; Carr, 1995) as well as by direct measurement of nitrate assimilation by the resident phytoplankton population (Peña et al., 1992; Wilkerson and Dugdale, 1992; Dugdale et al., 1992; McCarthy et al., 1996; Rodier and Le Borgne, 1997). Peña et al. (1994) estimated new production in the Warm Pool ($T > 26$°C) from the net surface heat flux and nitrate-temperature correlation. In the eastern part of the equatorial Pacific, the upwelling, and usually to a lesser degree, turbulent vertical transport, brings the cold and nitrate-rich water into the upper well-lit surface layer (Wyrtki, 1981; Philander et al., 1987). In the western equatorial Pacific (west from 165°E) however, the nutricline is deeper than in the

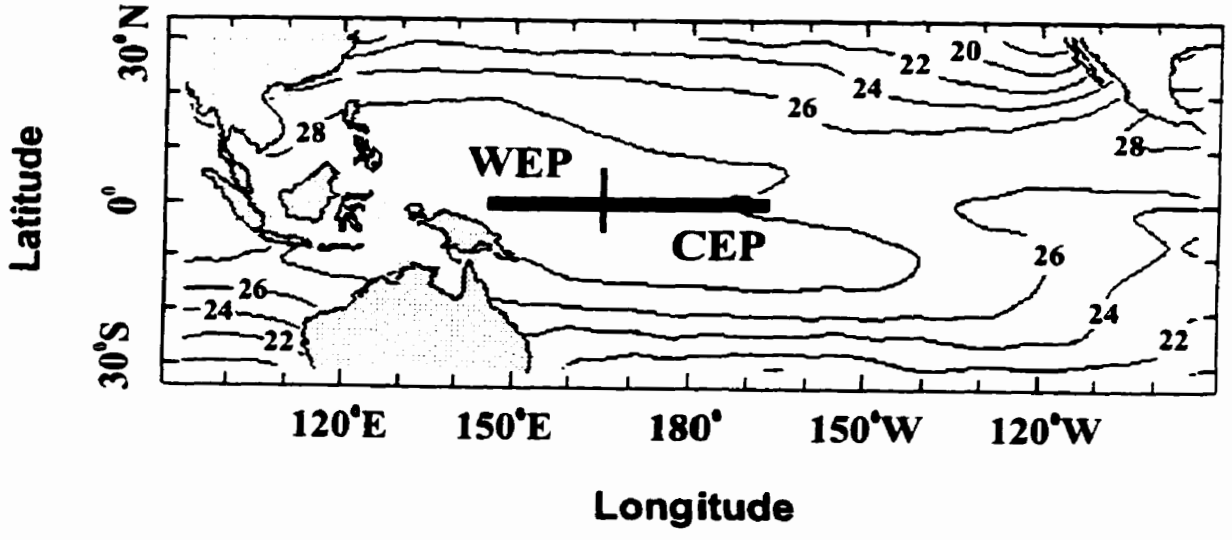

Figure 1.1: Annual SST in the tropical Pacific (Levitus, 1994). Black line represents a cruise track along the equator in the western equatorial Pacific-WEP (from 145°E to 165°E) and central equatorial Pacific-CEP (from 165°E to 165°W), where data were collected.

eastern equatorial Pacific (Barber and Kogelschatz, 1989), and the vertical advective transport brings warm and nitrate-poor water to the surface from above the nutricline. It has been also indicated (Peña et al., 1994) that, within this region, the turbulent vertical transport from below the nutricline into the upper surface layer is relatively more important than the upwelling and thus may primarily determine the rate of new production.

The equatorial Pacific may also have a profound effect on global atmospheric CO_2 concentrations since it is potentially the strongest oceanic source of CO_2 (Keeling and Revelle, 1985; Tans et al., 1990). As with sea surface temperature (SST) and new production, the interchange of carbon between the atmosphere and ocean undergoes interannual fluctuations associated with El Niño conditions (Inoue and Sugimura, 1992; Ishii and Inoue, 1995; Feely et al., 1995; Hisayuki et al., 1996). The air-sea CO_2 flux is determined by the partial pressure difference of CO_2 across the air-sea interface and the coefficient of gas exchange. However, the assessment of these terms is not easy to perform. Firstly, the rates of gas exchange have a strong nonlinear dependence on the wind velocity (Liss and Merlivat, 1986; Wannikhof, 1992) which remains to be completely understood. Secondly, the surface distribution of CO_2 partial pressure is inadequately known in the western equatorial Pacific and exhibits pronounced seasonal and spatial variability (Inoue and Sugimura, 1992; Inoue and Ishii, 1996; Inoue et al., 1996).

The prerequisite for understanding how the SST, the new production, and the air-sea carbon flux are modified under El Niño conditions in the western equatorial Pacific is an evaluation of the heat, nitrate, and carbon balances in the upper surface layer. Recent studies showed that the temperature and the concentration of nitrate are correlated in deeper water and, therefore, their vertical fluxes from the deeper ocean to the upper layer may also be related (Lewis, 1992; Peña et al., 1994). I will show here that the same statement can be made for dissolved inorganic carbon. Under steady-state conditions, and in the absence of significant horizontal advection and diffusion, the net heat flux at the ocean's surface has to be balanced by the vertical flux of heat by fluid transport and penetration of light to deeper water; the vertical fluxes of nitrate and dissolved norganic carbon may thus be intimately tied to the surface heat fluxes. The simultaneous study of fluxes of heat, nitrate, and carbon

would provide further insight into the relation between SST, the new production, and the air-sea CO_2 exchange during normal and El Niño conditions.

The task of relating El Niño and variation of SST is fraught with difficulties due to inadequacy of models which would satisfactorily predict the SST; as a consequence, predictions of SST with climatological surface heat fluxes are invariably too high (e.g. Philander et al., 1987; Chen et al., 1994). The fluctuations of new production in the western equatorial Pacific during El Niño are also poorly understood, since direct measurements are scarce. The difficulties in directly measuring the air-sea exchange of CO_2 were outlined above. It is thus of great importance to determine the new production and air-sea exchange of CO_2 from other parameters for which more frequent measurements with better spatial resolution are available.

No simultaneous direct measurements of heat, nitrate, and carbon fluxes in the western equatorial Pacific are available at the present time. The goal of my thesis is to analyze the relation between El Niño and changes in the upper ocean heat content, the new production, and the air-sea exchange of CO_2, in a manner that incorporates field measurements and modeling. The specific goal is to determine interannual variations in the vertical transports of heat, nitrate, and dissolved inorganic carbon from below the nutricline (thermocline) into the surface upper layer (euphotic zone), their inter–relationships, and their influence on biological production and air-sea exchange of CO_2 in the western equatorial Pacific Warm Pool.

The scope of this research is defined by the following objectives:

- To measure biological ^{15}N–nitrate uptake (the new production) in the western (145°E to 165°E) and central (165°E to 165°W) equatorial Pacific during normal and El Niño conditions (Chapter 2).

- To determine what processes primarily govern the distribution of heat, nitrate and carbon in the western Pacific Warm Pool (SST> 29°C) (Chapter 3).

- To indirectly estimate the new production and air-sea carbon exchange over the large area of western equatorial Pacific Warm Pool (SST> 29°C) from measurements of

the net surface heat fluxes (Chapter 4).

The null hypothesis is that there are no quantitatively identifiable differences in the rate of heat storage, new production and air-sea carbon exchange between normal and El Niño conditions.

Chapter 2 presents the methodology, results, and discussion of direct measurements of the new production. Chapter 3 describes the estimation of terms in the advection-diffusion equation and discussion of assumptions used in development of a box model. Chapter 4 presents the box model that couples the new production and air-sea exchange of carbon and measurements of the model parameters in the Warm Pool of the equatorial Pacific. Chapter 5 contains general conclusions.

Chapter 2

Geographical distribution of new production in the western/central equatorial Pacific during El Niño and normal conditions

2.1 Introduction

During El Niño, the east-west asymmetry of observed physical variables (such as SST, sea surface height (SSH), thermocline depth) in the western and central equatorial Pacific is altered due to the eastward expansion of the Warm Pool. Chemical and biological patterns in the western and central equatorial Pacific are also altered as a result (e.g. Barber and Kogelschatz, 1989; Delcroix et al., 1992; Peña, 1992; Radenac and Rodier, 1996; Mackey et al., 1995), but the nature and causative factors are insufficiently understood.

In this chapter, I describe observations of physical, chemical, and biological variables in both the western-WEP (145°E to 165°E) and central-CEP (165°E to 165°W) equatorial Pacific during normal conditions (December 1995/January 1996, and January 1997), during a moderate El Niño event (November/December 1994), and during the strongest El

Niño events recorded in recent history (December 1997/January 1998). I have attempted to understand better the physical and chemical environment, and associated biological response, in terms of the new production. The specific objective was to measure directly and compare the rates of new production in the western and central equatorial Pacific during both El Niño and normal conditions, two tasks which have not been previously done.

It has been observed that, during El Niño conditions, the thermocline and nutricline rise in the western part (WEP) and deepen in the central part (CEP) of the equatorial band; this phenomenon is a consequence of the eastward expansion of the Warm Pool (Barber and Kogelschatz, 1989). In the west, the pool of nutrient–rich water is raised closer to the surface, and more nitrate is potentially available in the euphotic zone compared to normal conditions; accordingly, the rate of new production should increase in the WEP during El Niño (Fig. 2.1). On the other hand, in the central equatorial region, the nutricline deepens during El Niño, and consequently upwelling—which is confined to relatively shallow waters—brings warm and nutrient poor water from above the nutricline to the surface. Nitrate supply into the euphotic zone is thus decreased and the rate of new production should also decrease in the CEP during El Niño (Fig. 2.1).

The assumption was made that variations in phytoplankton production in the WEP and CEP during El Niño and normal conditions are mainly regulated by the availability and flux of nitrate. Previous studies have shown that the biological production and phytoplankton biomass in the eastern equatorial Pacific can be limited by other nutrients, such as silica and iron (e.g. Dugdale and Wilkerson, 1998; Landry et al., 1997; Cullen 1995). However, these studies were performed eastward from our cruise track, where nitrate is always present at the surface due to the upwelling of nitrate-rich subsurface waters. In the area where our measurements were conducted I observed residual phosphate and silica, in absence of nitrate, in the surface waters, which implies these nutrients did not limit production. Measurements of iron were not performed on our cruises. Previous studies have suggested that iron concentrations are sufficient to support the phytoplankton uptake and growth in the WEP, as a result of eolian iron supply from Asia (Barber and Chavez, 1991), and input of iron to surface waters from the Equatorial undercurrent (EUC) (Coale et al., 1996; Wells et

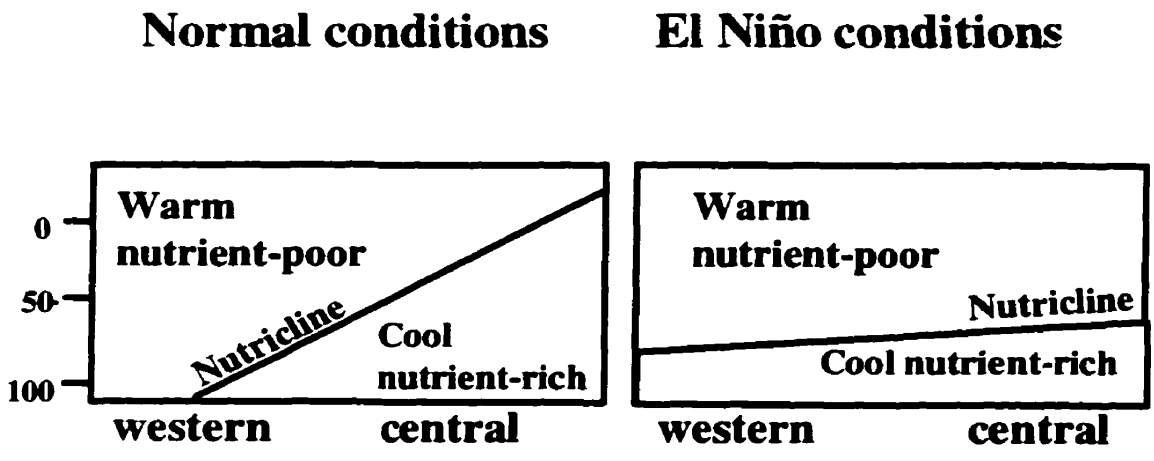

Figure 2.1: Schematic diagram of nutricline depth in the western and central equatorial Pacific during normal and El Niño conditions.

al., 1999). These concentrations decrease eastward (Duce and Tindale, 1991) and may limit productivity in the CEP during normal conditions when nitrate is present at the surface.

Here I tested the hypothesis that the rates of new production increase in the western equatorial Pacific and decrease in the central equatorial Pacific during El Niño conditions relative to normal conditions mainly due to variations in the nutrient supply to the euphotic zone that are associated with eastward expansion of the Warm Pool.

2.2 Methods and data

Data were collected on board R/V Kaiyo and R/V Mirai during four cruises; in November/December 1994, December 1995/January 1996, January 1997, and December 1997/January 1998 in the western/central Pacific on a transect along the equator from 145°E to 165°W (Fig. 1.1). In January 1997, the transect extended only along the equator from 165°E to 165°W. The physical and chemical variability during these conditions was determined using CTD observations and measurements of nutrients (nitrate, phosphate, and silicate) at discrete depths. The distributions of phytoplankton biomass were defined using the pigment (chlorophyll *a*) data and the new production was obtained from measurements of biological uptake of nitrate labeled with ^{15}N.

2.2.1 CTD measurements, nutrients and pigments

CTD measurements were performed using a tethered free-fall SeaWiFS Profiling Multichannel Radiometer System (Satlantic). Vertical profiles of temperature and conductivity were measured with approximately 0.2–0.3 m resolution to a depth of 200 to 350 m.

Concentrations of nutrients (nitrate, phosphate, and silica) were measured on samples collected by Niskin bottles at each station at 18 sampling depths from 0 to 300 m. Nutrients were analyzed using a Bran-Luebbe continuous flow autoanalyser (Model TRAACS 800). Nitrate concentrations were determined using the method described by Strickland and Parsons (1972). During the cruise in December 1995/January 1996, the nitrate concentrations in surface waters (where nitrate was below detection limits of the autoanalyzer,

i.e., < 0.1 mmol m^{-3}), were also determined by an analytical chemoluminescent method (Garside, 1982). The method of Murphy and Riley (1962) was used for the determination of phosphate concentrations, while silicate concentrations were obtained by the standard AAII molybdate-ascorbic acid method.

Measurements of chlorophyll *a* were also taken at each station at 15 sampling depths from 0 to 150 m. Chlorophyll *a* concentrations were measured fluorometrically as follows. First, seawater samples were filtered through 0.4 μm pore size Nuclepore filters. Next, phytoplankton pigments were extracted with 6 ml N,N-Dimethylformamide (DMF) and were finally analyzed by a spectrofluorophotometer, Shimadzu RF-5000. The spectrofluorophotometer was calibrated using Sigma Chlorophyll *a* standard (*Anacystsis nidulans*). The concentrations of chlorophyll *a* were determined by the Moran (1981) method (with the detection limit of 0.01 mg m^{-3}).

2.2.2 Biological uptake of nitrate and inorganic carbon

Uptake rates of labeled ^{15}N-nitrate and ^{13}C-inorganic carbon were measured by simulating *in situ* incubation (Harrison, 1983; Harrison, 1992) to determine the rates of new and total primary production in the western and central equatorial Pacific. Water samples were collected using Niskin bottles at the surface, and four or five depths in the euphotic zone, corresponding to nominal specific optical depths (viz., 100, 50, 30, 15, and 1 per cent of surface PAR, respectively). PAR was determined from vertical profiles of the spectral distribution of downwelling irradiance and upwelling radiance that was measured with a high precision profiling spectroradiometer (Satlantic) at each station. Niskin bottles were retrofitted with silicon tubing to eliminate toxicity from black rubber (Price et al., 1986). Samples were dispensed into one-liter polycarbonate bottles and inoculated with $Na^{15}NO_3$ and , $Na^{13}HCO_3$ in such a way that concentrations of added isotopes were about 10 per cent of ambient concentrations of nitrate and inorganic carbon. In those cases for which nitrate was below detection limits of conventional analytical methods (Autoanalyzer), 50 nM isotope was added to the water sample. The bottles were placed into clear plastic tubes wrapped with neutral density screens corresponding to light levels at the depth from which

samples were taken. Samples were incubated for three hours (from approximately noon to 3 p.m.); at the end of the incubation period, samples were filtered onto precombusted GF/F glass fiber filters and dried in a dessicator.

The ^{15}N and ^{13}C enrichments of particulate organic nitrogen (PON) and particulate organic carbon (POC) concentrations (mg m^{-3}) were determined using mass spectrometric analysis (Owens, 1988). The uptake rate of nitrate into cells (mmol m^{-3} ^{-1}h) was calculated as (Dugdale and Goering, 1967),

$$p_N = \frac{[APE]\,[PON/14]\,(N_a + {}^{15}N)}{100\,{}^{15}N\,\Delta t}. \tag{2.1}$$

where APE is atom percent excess (calculated as the difference between atom percent enrichment measured by mass spectrometric analysis, and natural abundance of ^{15}N in sea water (0.3664)), ^{15}N (mmol m^{-3}) is the concentration of the labeled nitrate added to the medium, N_a is the measured ambient nitrate concentration (mmol m^{-3}) using an autoanalyzer (see Section 2.2.1), and Δt is the time of incubation expressed in hours. The ambient nitrate concentrations in the surface waters were assumed to be zero when they were below detection limits of the autoanalyzer. Daily rates of nitrate uptake were approximated by multiplying hourly rates by 14 (i.e., an empirically derived relationship between hourly and daily uptake rates based on time-course measurements in the equatorial region (McCarthy et al., 1996)). Uptake rates of nitrate were integrated over the depth of euphotic zone at each station. The assumption was made that nitrate uptake is the predominant source of new production.

The uptake of inorganic carbon p_C (mg m^{-3} h^{-1}) into cells was computed as

$$p_C = \frac{POC\,(AP^{13}C_{inc} - AP^{13}C_n)}{\Delta t\,(AP^{13}C_{tic} - AP^{13}C_n)\,f} \tag{2.2}$$

where POC is particulate organic carbon (mg m^{-3}), $AP^{13}C_{inc}$ is the atom % of ^{13}C in incubated sample, $AP^{13}C_n$ is the atom % of ^{13}C in natural sample (natural abundance), $AP^{13}C_{tic}$ is the atom % in total inorganic carbon, Δt is the duration (hours) of incubation, and f is the discrimination factor of ^{13}C (f=1.025). $AP^{13}C_n$ was assumed to be equal 1.12. Daily rates of carbon uptake were approximated by multiplying hourly rates by 12.

2.3 Results

2.3.1 Zonal distributions of temperature, salinity, and density

The general features of the physical environment in the equatorial western Pacific during both normal and El Niño conditions have been described extensively elsewhere (Delcroix et al., 1992; Ando and McPhaden, 1997; Delcroix and Picaut, 1998). In this subsection, I shall concentrate on the variability of those physical factors that may be important for determining the changes in new production in this area during El Niño conditions. Contour plots of temperature, salinity, and density were computed using kriging with a linear semivariogram model (Curran, 1988).

Temperature distribution. The zonal sections for temperature distributions in the upper 300 m along the equator from 147°E to 165°W are shown in Fig. 2.2 for December 1995/January 1996 and January 1997 (normal conditions), and for November/December 1994 and December 1997/January 1998 (El Niño conditions). Temperature contours during normal conditions show a typical pattern (Halpern, 1980; Barber and Chavez, 1991) with isotherms sloping upward eastward from approximately 170°E. In December 1995/January 1996, the Warm Pool ($T > 29$°C) covered the WEP (147°E–165°E region) with a thick isothermal layer (about 100 m). The center of the thermocline, i.e., the depth of the 20°C isotherm (Ando and McPhaden, 1997), was at approximately 170 m. Values of SST were larger in the western ($T \geq 29$°C for 147°E–170°E region) than in the central ($T \leq 28$°C for 177°E–165°W region); presumably, this difference was due to equatorial upwelling of the subsurface water in the central region. The temperature distribution during January 1997 showed a similar pattern as during December 1995/January 1996 with the Warm Pool expanding slightly further toward the east.

During El Niño (November/December 1994, December 1997/January 1998), the Warm Pool water ($T > 29$°C) expanded eastward over the entire length of our cruise track. Compared to normal conditions, the 20°C–thermocline was closer to the surface (150 m in

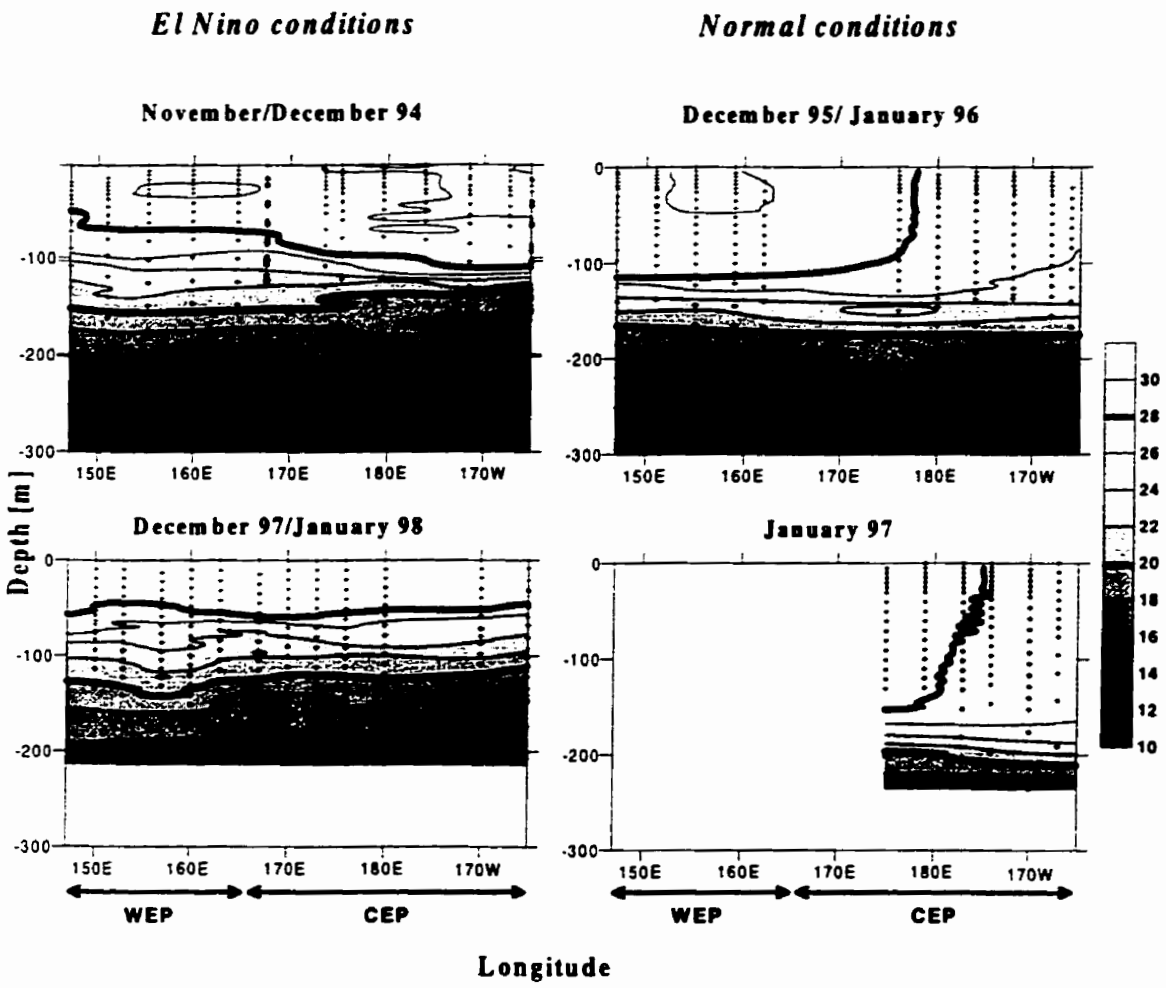

Figure 2.2: Zonal sections of temperature [°C] along the equator from 147°E to 165°W during normal conditions (right) and El Niño (left). For January 1997, data were available from 175°E to 165°W only. Bold lines represent $T = 28$°C (upper), and $T = 20$°C (lower). Crosses represent sampling depths.

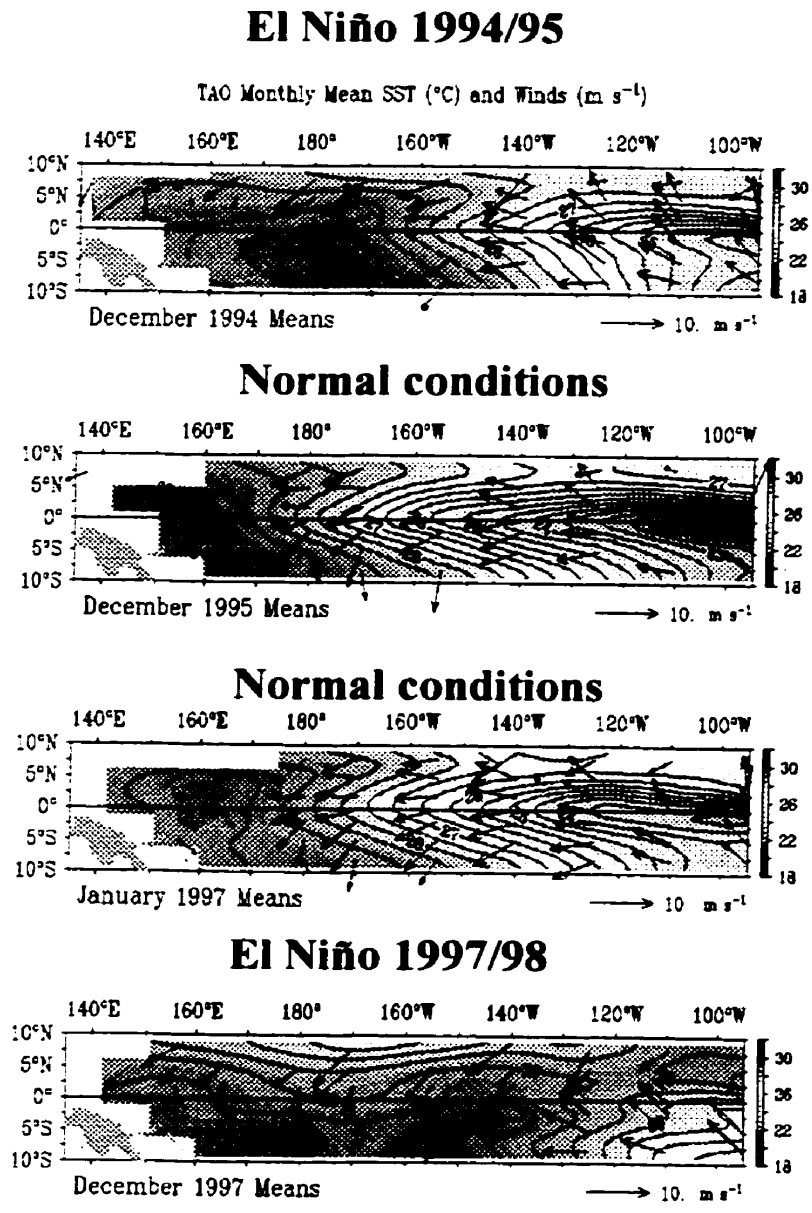

Figure 2.3: Monthly mean SST [°C] and winds [m s^{-1}] from TOGA-TAO buoy array in the tropical Pacific for December 1994, December 1995, January 1997, and December 1997.

November/December 1994, and 120 m in December 1997/January 1998). My observations agree with monthly mean SST data from the TOGA-TAO buoy array in the equatorial Pacific, as shown in Fig. 2.3.

Salinity distribution. Fig. 2.4 shows salinity distributions in November/December 1994 (El Niño) and in December 1995/January 1996 (normal conditions). In normal conditions, low salinity surface waters ($S < 34.6$ psu) were confined to the western region (147°E–170°E). Surface salinity increased from 34.2 psu (at 147°E) up to 35.4 psu east of the date line (179°W–165°W region), while at intermediate depths (150–210 m), high salinity water was observed.

During El Niño conditions, low salinity surface waters ($S < 34.0$ psu) extended eastward over the entire region. Similarly to the normal conditions, a layer of high salinity water ($S > 35.4$ psu) was observed at intermediate depths (100–200 m).

Density distribution. Density distributions in November/December 1994 (El Niño) and in December 1995/January 1996 (normal conditions) are depicted in Fig. 2.4. For normal conditions, the density contours in the central region follow the temperature distribution by sloping upward from 170°E–165°W. The relation between temperature and density sections is more complex in the western region where the depths of the largest density gradients corresponded to those of the largest temperature gradients (at 120–140 m). However, the upper layer (0–100 m) was isothermal but featured a gradual increase of the density; in this layer, density was primarily determined by the salinity (see Fig. 2.4). During El Niño, the general features typical for the Warm Pool in normal conditions were also observed throughout the region of interest, with the pycnocline found at 100–120 m.

Barrier layer thickness The upper and lower boundaries of the barrier layer (i.e., nearly isothermal, but salinity stratified layer between the base of the mixed layer and the top of the thermocline) were defined as the depths where $\partial S/\partial z \geq 0.01$ psu m^{-1} and $\partial T/\partial z \geq 0.05$°C/m, respectively (Lukas and Lindstrom, 1991). Using these definitions, the thickness of the barrier layer in the WEP during December 1995/January 1996 (normal conditions)

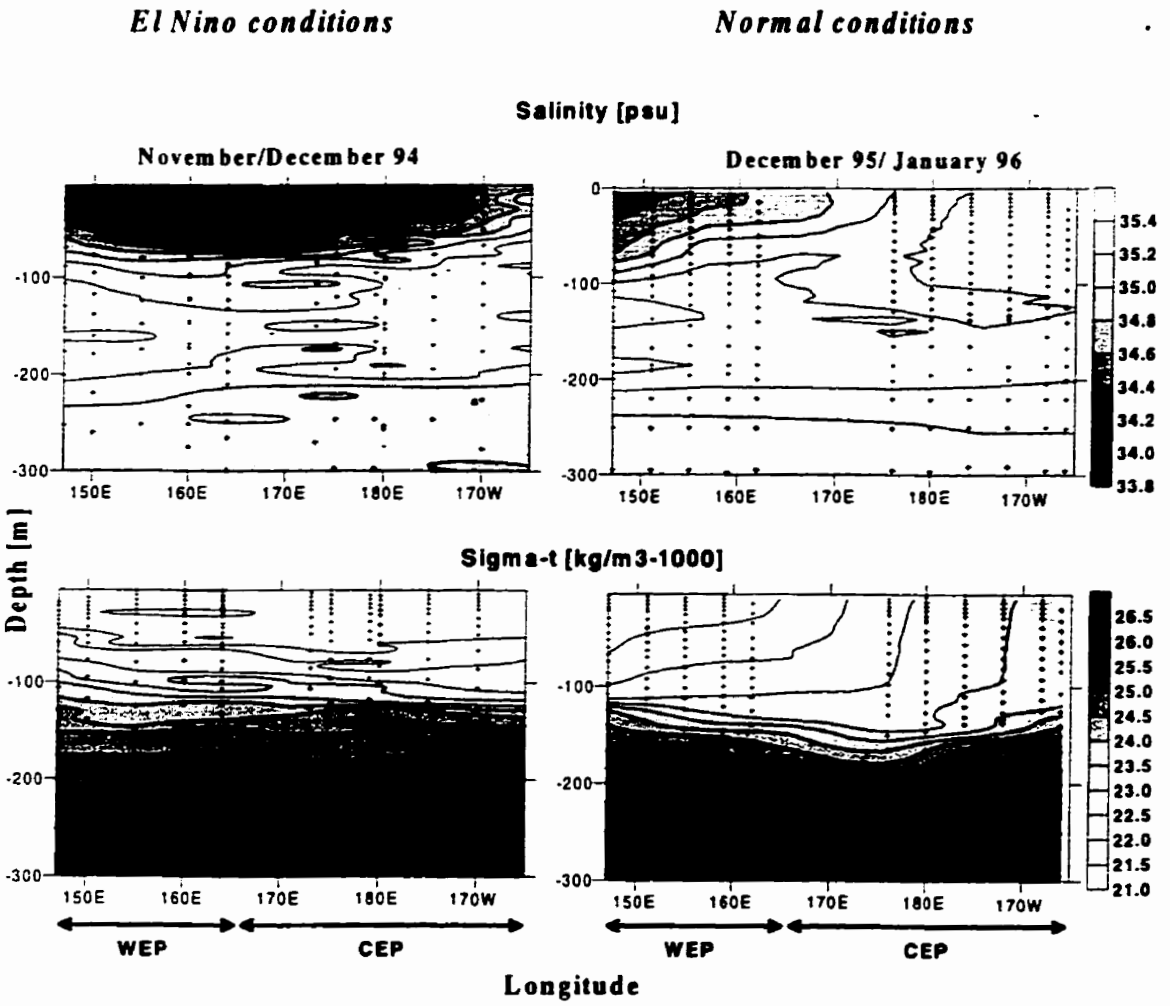

Figure 2.4: Zonal sections of salinity, and density along the equator from 147°E to 165°W during normal conditions–December 1995/January 1996 (right) and moderate El Niño–November/December 1994 (left). Crosses represent sampling depths.

was between 40–50 m, with the upper boundary 40 m below the surface. During November/December 1994 (El Niño), the upper boundary moved closer toward the surface (30 m) and the barrier layer became correspondingly thinner (20–30 m). It has been suggested (Lukas and Lindstrom, 1991) that the barrier layer obstructs the vertical mixing of heat and nutrients from the thermocline/nutricline into the upper surface layer. If the biological production in the surface layer is limited by the availability of nutrients, the thickness of the barrier layer may potentially have an effect on the rates of new production in this part of the ocean.

2.3.2 Zonal distributions of nitrate, phosphate and silicate

The zonal sections for nitrate distributions in the upper 300 m along the equator from 147°E to 165°W, as measured by an Autoanalyzer, are shown in Fig. 2.5 for December 1995/January 1996, and January 1997 (normal conditions), and for November/December 1994, December 1997/January 1998 (El Niño conditions). Data for January 1997 were collected only in the central region (175°E to 165°W). The zonal sections for phosphate, and silicate distributions for November/December 1994, and December 1995/January 1996 are presented in Fig. 2.6 as a representative case for El Niño and normal conditions, respectively. Contour plots of nutrients were computed using kriging with a linear semivariogram model (Curran, 1988).

Nitrate distribution. Distributions of nitrate concentrations followed the pattern of temperature during both normal and El Niño conditions. In normal conditions, nitrate concentrations were on average undetectable by Autoanalyzer (< 0.1 mmol m^{-3}) in surface waters (0-90 m) in the WEP (147°E–165°E); these concentrations increased eastward from 170°W (> 4 mmol m^{-3}) indicating upwelling of nutrient rich subsurface waters. The depth of the 16 mmol m^{-3} isopleth (approximation for the center of the nutricline (Barber and Chavez, 1991)) in the warm waters was approximately 250 m.

During El Niño, nitrate was depleted in surface waters (0–80 m in November/December 1994 and 0–50 m in January 1998) through the entire area of study. The depth of the

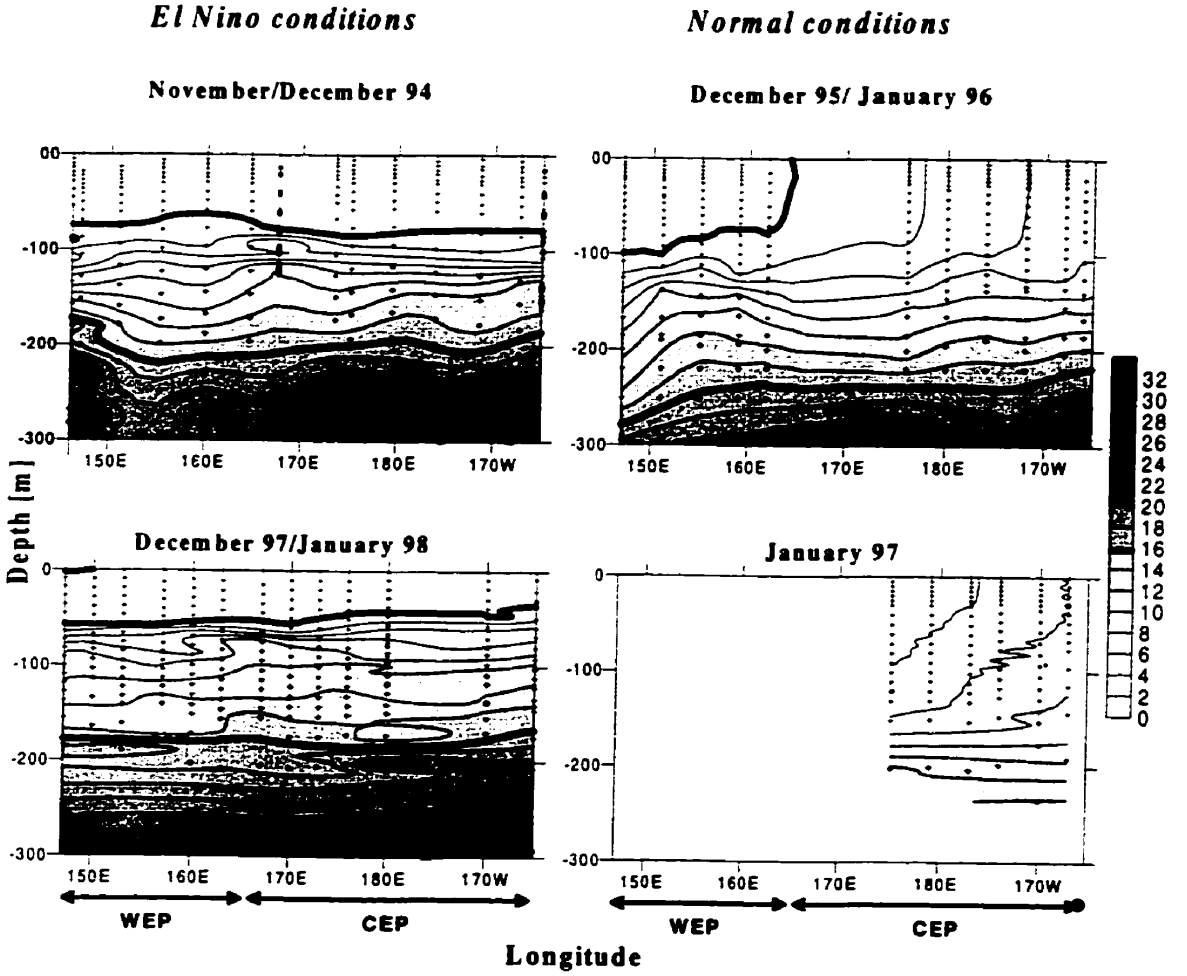

Figure 2.5: Zonal sections of nitrate measured by autoanalyzer (mmol m^{-3}) along the equator from 147°E to 165°W during normal conditions (right) and El Niño (left). For January 1997 data were available from 175°E to 165°W only. Bold lines show $NO_3 = 0.2$ mmol m^{-3} (upper), and $NO_3 = 16$ mmol m^{-3} (lower). Crosses represent sampling depths.

nutricline in the western Pacific decreased during El Niño conditions (approximately 210 m in November/December 1994 and 180 m in December 1997/January 1998) compared to normal conditions.

Table 2.1 shows the average ($\pm SD$) low-level nitrate concentrations [nM] in surface waters (where nitrate was below detection limits of the autoanalyzer) for six stations in the western equatorial Pacific (from 147°E to 165°W) for December 1995/January 1996 (normal conditions) determined by the analytical chemoluminescent method. The average value of nitrate concentration in the upper 80 m was 30 ± 25 nM.

Table 2.1: Average nitrate concentrations ($\pm SD$) [nM] in the surface waters for six stations in the western equatorial Pacific during December 1995/January 1996 determined by the analytical chemoluminescent method.

Depth	NO_3
0	20 ± 11
10	47 ± 38
25	20 ± 30
40	34 ± 21
50	12 ± 20
80	54 ± 37

Phosphate and silicate distribution. The vertical distributions of phosphate and silicate also followed the temperature pattern. During normal conditions, surface silicate concentration ranged from 2 mmol m^{-3} in the Warm Pool to 3 mmol m^{-3} in the central part. During El Niño conditions, the silicate distribution was vertically uniform in surface waters over the whole region with concentration of ca. 2 mmol m^{-3}. Phosphate concentrations were low (i.e., < 0.2 mmol m^{-3}) but not depleted at the surface during El Niño, while in normal years they increased eastward from 0.2 mmol m^{-3} to 0.5 mmol m^{-3}.

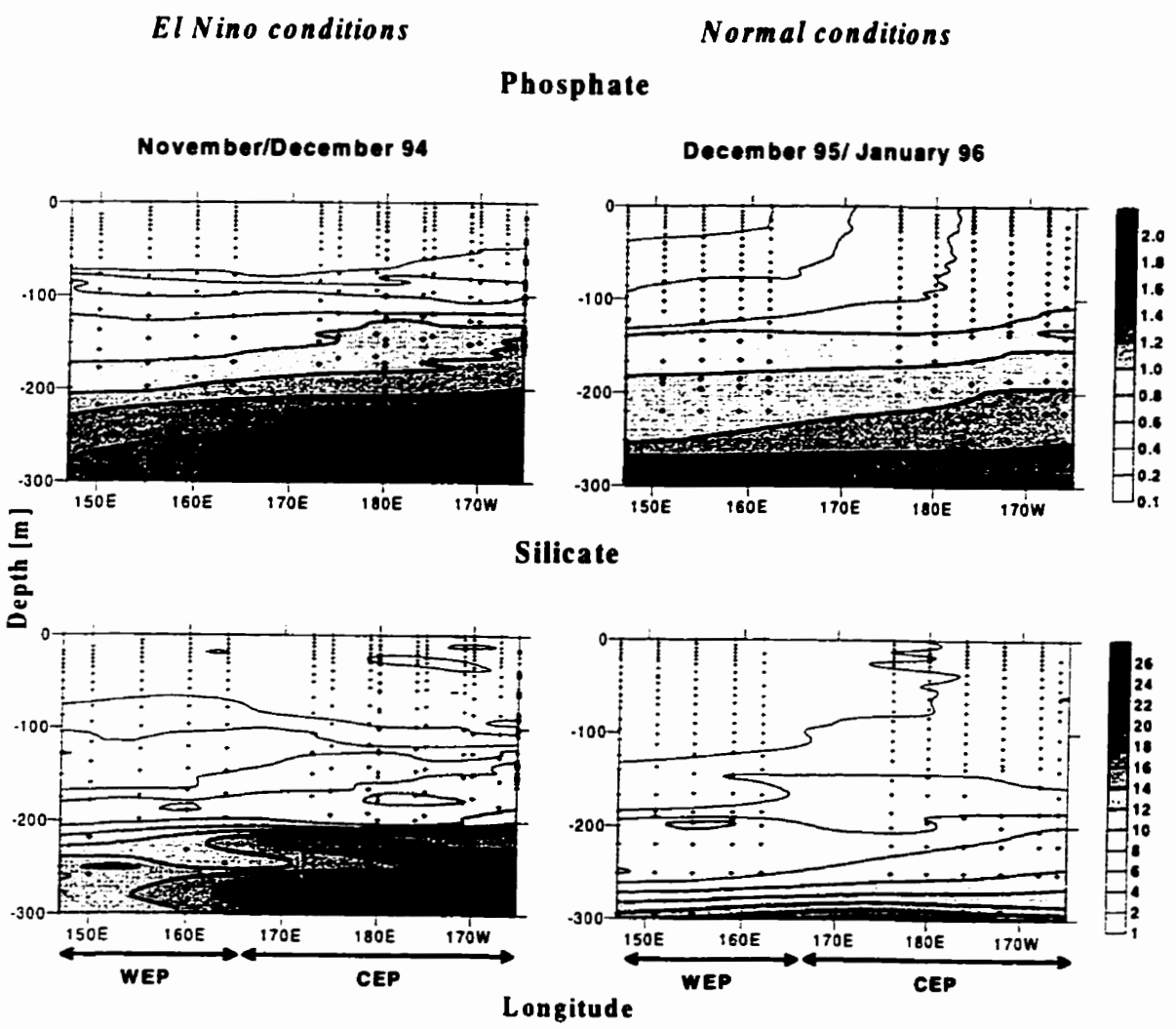

Figure 2.6: Zonal sections of phosphate [mmol m^{-3}] and silicate [mmol m^{-3}] along the equator from 147°E to 165°W during normal conditions–December 1995/January 1996 (right) and moderate El Niño–November/December 1994 (left). Crosses represent sampling depths.

2.3.3 Zonal distribution of chlorophyll *a*

The zonal sections for chlorophyll *a* distributions in the upper 150 m along the equator from 147°E to 165°W are shown in Fig. 2.7 for December 1995/January 1996 and January 1997 (normal conditions), and for November/December 1994 and December 1997/January 1998 (El Niño conditions).

During normal conditions, the distribution of chlorophyll *a* concentration showed typical tropical structure (Herbland and Voituriez, 1979; Cullen, 1982) with maximum concentrations > 0.4 mg m^{-3} at 90 m in the region near 160°E, and high concentrations (> 0.25 mg m^{-3}) between 50 and 100 m throughout the region of interest. The influence of equatorial upwelling was reflected (similar to the nitrate and temperature distributions) in the chlorophyll *a* distributions which had a surface enrichment (concentrations > 0.2 mg m^{-3}) east of approximately 171°E.

During El Niño conditions, surface chlorophyll *a* concentrations were low (< 0.15 mg m^{-3} within 40–50 m of the surface) throughout the entire region of investigation. In November/December 1994, the maximum concentrations (> 0.4 mg m^{-3}) were found at 75 m in the 151°E–161°E region with high concentrations (> 0.25 mg m^{-3}) extending from 75 to 100 m through the entire region. In December 1997/January 1998, the chlorophyll *a* maximum, with concentrations > 0.4 mg m^{-3}, was at 50–70 m.

Depth integrated (to 150 m) chlorophyll *a* values (mg m^{-2}) are shown in Fig. 2.8 for both normal and El Niño conditions. Table 2.2 shows the integrated values of chlorophyll *a* averaged over the western and central equatorial Pacific. The integrated values during normal conditions showed no zonal trend in the western region (147°E–165°E region), but gradually increased toward the east. During El Niño conditions, there was no clear zonal trend throughout the region of investigation; in addition, the average integrated values in the central part were markedly lower (23.2 ± 2.2 mg m^{-2} in November/December 1994 and 24.9 ± 4.1 mg m^{-2} in December 1997/January 1998) than during normal conditions (34.6 ± 3.3 mg m^{-2} in December 1995/January 1996 and 33.3 ± 3.3 mg m^{-2} in December

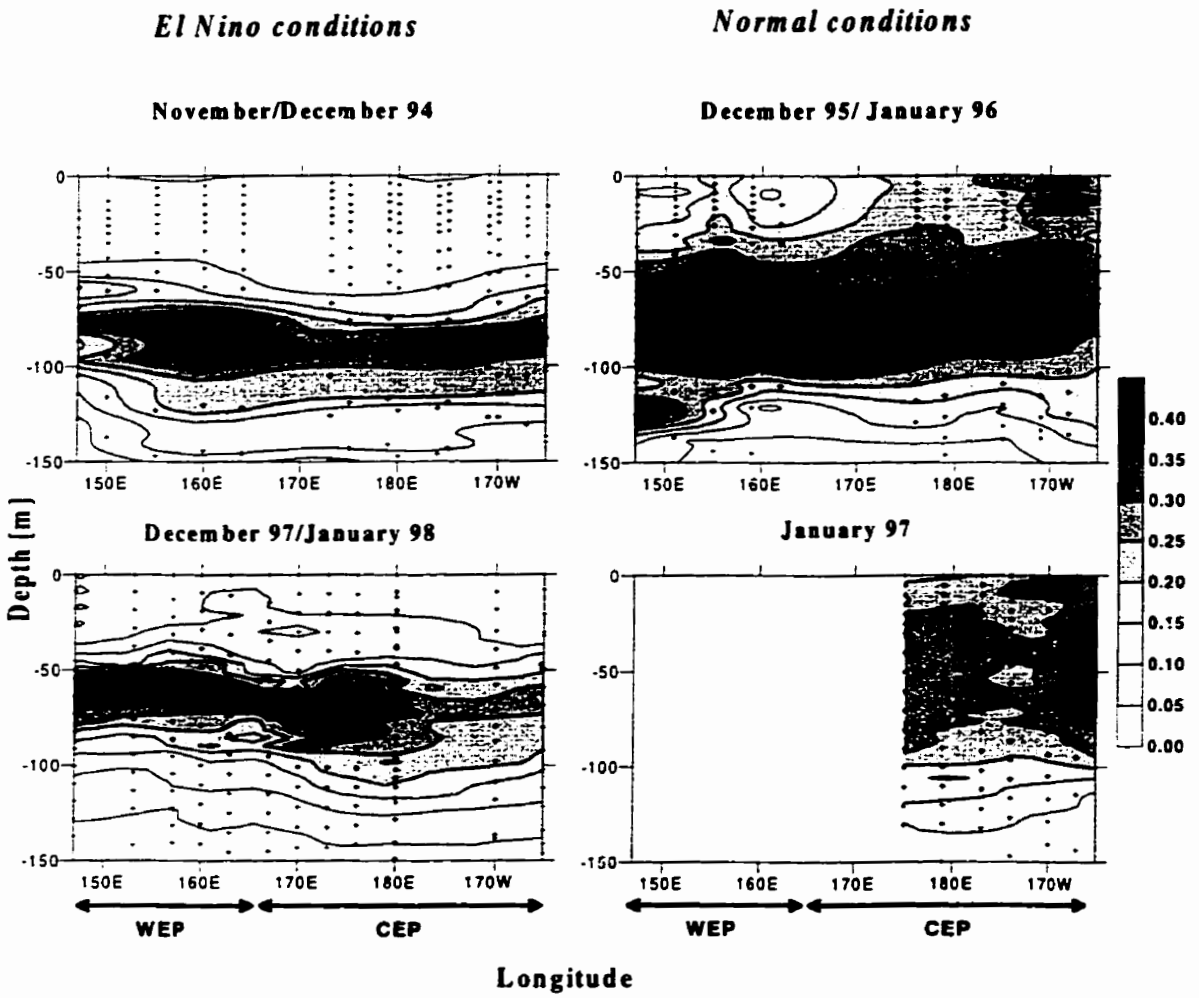

Figure 2.7: Zonal sections of chlorophyll *a* [mg m^{-3}] along the equator from 147°E to 165°W during normal conditions (right) and El Niño (left). For January 1997 data were available from 175°E to 165°W only. Crosses represent sampling depths.

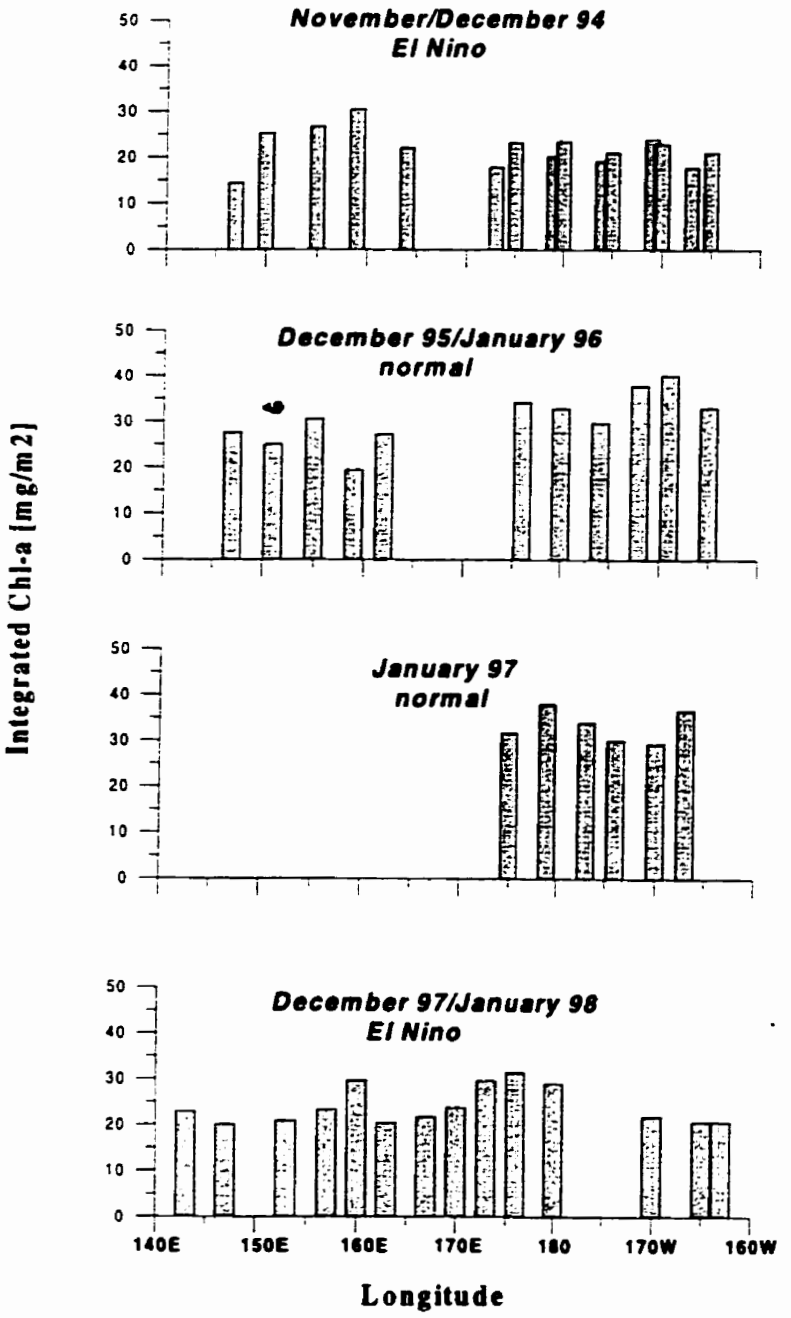

Figure 2.8: Depth integrated values of chlorophyll *a* [mg m^{-2}] along the equator from 147°E to 165°W for December 1995/January 1996, and January 1997 (normal conditions), and for November/December 1994, December 1997/January 1998 (El Niño conditions). For January 1997 data were available from 175°E to 165°W only.

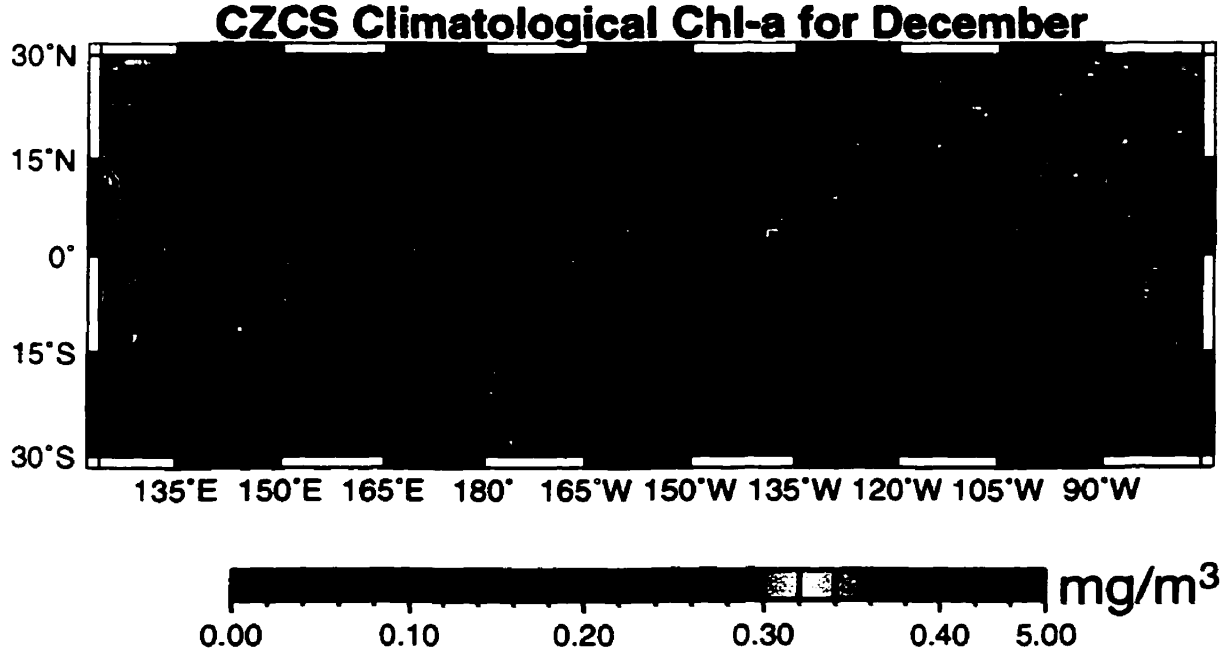

Figure 2.9: CZCS climatological chlorophyll *a* distribution in tropical Pacific for December. The white line represents 0.1 mg m^{-3} of chlorophyll *a*.

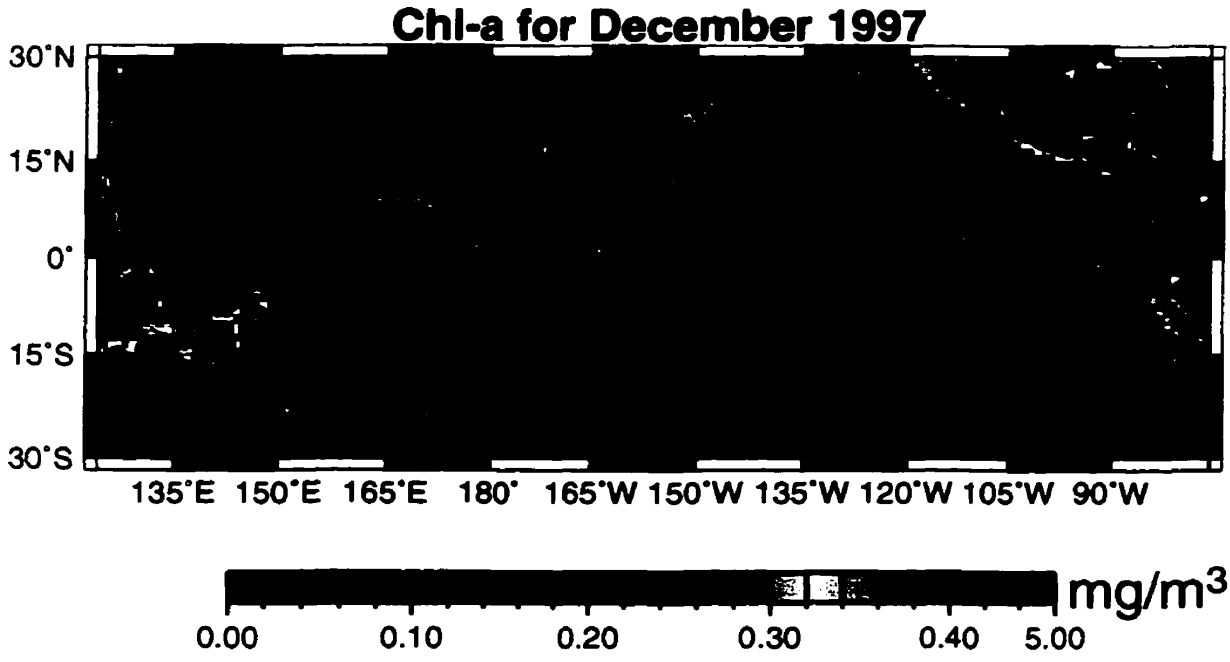

Figure 2.10: SeaWiFS chlorophyll *a* distribution in tropical Pacific for December 1997. The white line represents 0.1 mg m^{-3} of chlorophyll *a*.

1997/January 1998). This observation is in agreement with CZCS climatological chlorophyll *a* distribution in tropical Pacific for December, as representative for normal conditions (Fig. 2.9), and SeaWifs chlorophyll *a* distribution in tropical Pacific for December 1997 (Fig. 2.10).

Table 2.2: Depth-integrated (0 to 150 m) values of chlorophyll *a* (mg m^{-2}) in the western and central equatorial Pacific for December 1995/January 1996, and January 1997 (normal conditions), and for November/December 1994, December 1997/January 1998 (El Niño conditions.) For January 1997 data were available from 175°E to 165°W only.

	Western	No.St	Central	No.St
El Niño (Nov/Dec 94)	23.8 ± 5.3	5	23.2 ± 2.2	10
Normal (Dec 95/Jan 96)	25.9 ± 3.7	5	34.6 ± 3.3	6
Normal (Jan 97)			33.3 ± 3.2	7
El Niño (Dec 97/Jan 98)	25.5 ± 3.3	5	24.9 ± 4.1 7	

2.3.4 Zonal distribution of new production

The zonal sections for distributions of ^{15}N uptake (new production) in the upper 120 m along the equator from 147°E to 165°W are shown in Fig. 2.11 for normal and El Niño conditions. The uptake rates were calculated using Eq. 2.1 and assuming the ambient nitrate concentrations in the surface waters were equal zero when they were below detection limits of the autoanalyzer (< 0.1 mmol m^{-3}).

During normal conditions, the uptake rates were not strongly depth-dependent in the region west of 162°E. The surface nitrate uptake was small (< 0.002 mmol m^{-3} d^{-1}) west of approximately 162°E and then abruptly increased to > 0.005 mmol m^{-3} d^{-1} near 165°E and remained high in the central region (up to 0.05 mmol m^{-3} d^{-1}). Here, higher uptake rates than in the deep water were found in the upper layer (0–40 m) with the maximum rates located between 20 and 30 m.

During El Niño, the rates of new production in the upper layer (0–40 m) of the central region were markedly lower than during normal conditions. In November/December 1994,

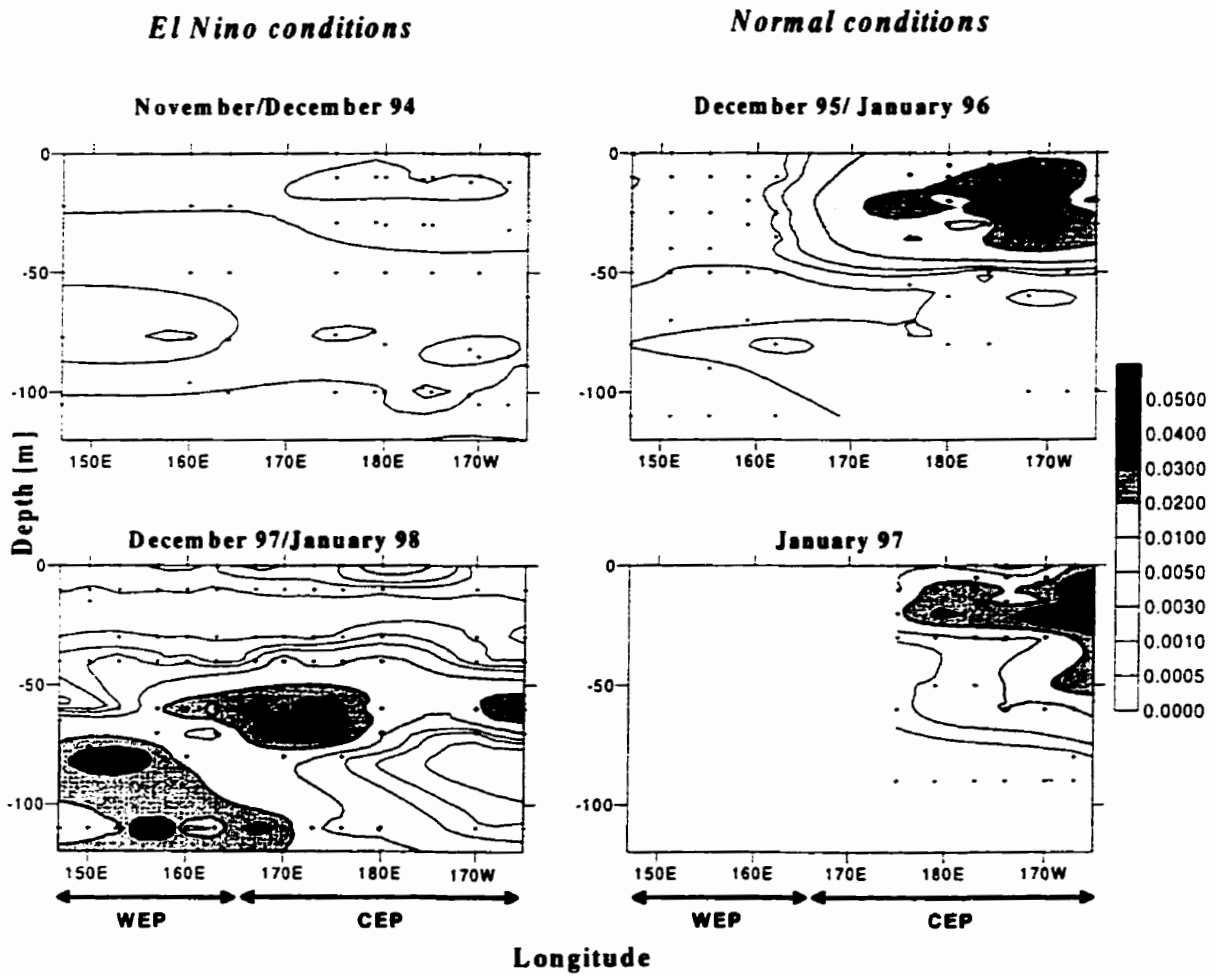

Figure 2.11: Zonal sections of the rate of new production [mmol m^{-3} d^{-1}] along the equator from 147°E to 165°W during normal conditions (right) and El Niño (left). For January 1997 data were available from 175°E to 165°W only. Crosses represent sampling depths.

the surface values were small (< 0.002 mmol m^{-3} d^{-1}) throughout the area. West of approximately 163°E, I observed a small increase in the rate of new production between depths of 40 to 60 m; however, due to generally small values of the rates of new production in this region, it is difficult to consider this a significant increase.

In December 1997/January 1998, the new production rates markedly increased below 40 m with values > 0.02 mmol m^{-3} d^{-1}. These values are an order of magnitude higher than those observed in November/December 1994; they are comparable to new production rates in surface waters of the central part during normal conditions.

Table 2.3: Depth-integrated (0 to 120 m) ^{15}N–nitrate uptake (mmol m^{-2} d^{-1}) in the western and central equatorial Pacific.

	Western	No. St.	Central	No. St.
El Niño (Nov/Dec 94)	0.19 ± 0.10	4	0.19 ± 0.07	9
Normal (Dec 95/Jan 96)	0.15 ± 0.05	5	1.37 ± 0.52	6
Normal (Jan 97)			1.49 ± 0.82	6
El Niño (Dec 97/Jan 98)	1.16 ± 0.47	6	1.25 ± 0.75	7

The integrated values of new production averaged over the western and central equatorial Pacific are presented in Table 2.3. Fig. 2.12 shows the zonal dependency of the new production integrated over the depth of euphotic zone for normal and El Niño conditions. As can be expected from the zonal section distribution (Fig. 2.11), larger mean integrated values were observed during the normal conditions in the central (for 162°E–165°W region, 1.37 ± 0.52 mmol m^{-2} d^{-1} in December 1995/January 1996, and 1.49 ± 0.82 mmol m^{-2} d^{-1} in January 1997) than in the western part (0.15 ± 0.05 mmol m^{-2} d^{-1} for 147°E–162°E region). Again, consistent with the features of the zonal sections, the integrated new production during the November/December 1994 El Niño did not vary significantly with respect to longitude; the mean integrated value (0.19 ± 0.09 mmol m^{-2} d^{-1}) taken over the entire region was close to that obtained in the western part during normal conditions. These features reflect the eastward expansion of the warm pool during El Niño. During El Niño 1997/98, the integrated new production rates in the western part increased by an order

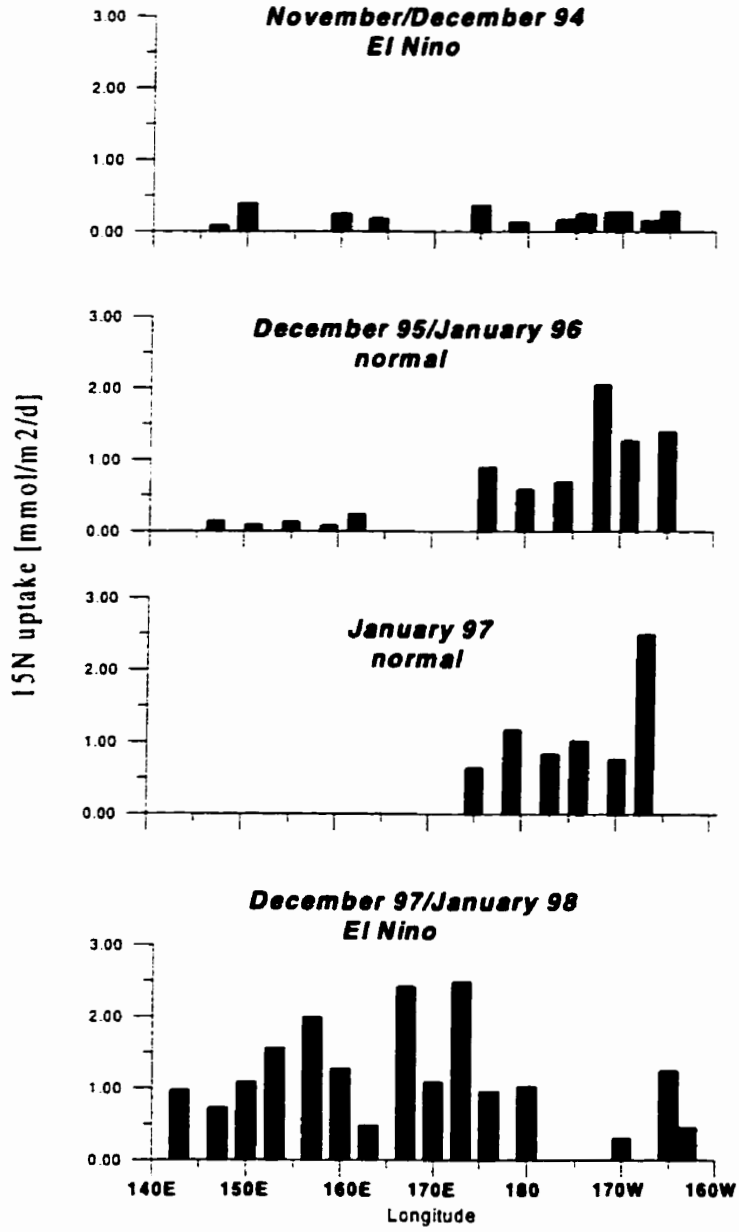

Figure 2.12: Depth-integrated (0-120 m) values of new production [mmol m^{-2} d^{-1}] along the equator from 147°E to 165°W for December 1995/January 1996, and January 1997 (normal conditions), and for November/December 1994, December 1997/January 1998 (El Niño conditions.) For January 1997 data were available from 175°E to 165°W only.

of magnitude compared to normal conditions. In the central part they were comparable to those observed during normal conditions, but displaced downward.

2.3.5 f-ratio

Since measurements of ammonium uptake were not available on our cruises, f-ratios (defined as nitrate uptake/total N-uptake (Eppley and Peterson, 1979)) were estimated as the ratio of integrated nitrate uptake (mmolN m^{-2} d^{-1}) to integrated primary production measured as ^{13}C uptake (mmolC m^{-2} d^{-1}). Nitrate uptake was converted to carbon units using a value of 6.6 (mol:mol) for the C:N ratio (Redfield, 1934). It has been suggested that the C:N ratio can markedly vary in response to changes in nutrient and light limitation (Longhurst and Harrison, 1989; Goldman, 1986), with ratios that exceed the nominal Redfield ratio (up to > 17) in nitrate limited environments (Goldman, 1986; Dauchez et al, 1995). Since nitrate is depleted in surface waters of the western equatorial Pacific the estimated f-ratios may therefore be underestimated using value of 6.6 (mol:mol) for C:N ratio (see Chapter 4).

The estimated values of integrated primary production suggest an f-ratio of 0.02 in the western region during normal conditions (Table 2.4) and 0.11 in the central region (Table 2.5).

Table 2.4: Depth-integrated (0 to 120 m) ^{15}N (mmolN m^{-2} d^{-1}) and ^{13}C uptake (mmolC m^{-2} d^{-1}) and f-ratio (f = (6.6 ^{15}N uptake)/ ^{13}C uptake) in the western equatorial Pacific.

	^{15}N	^{13}C	f-ratio
Normal (Dec 95/Jan 96)	0.15 ± 0.05	45.36 ± 14.63	0.02
El Niño (Nov/Dec 94)	0.19 ± 0.10	7.73 ± 4.06	0.16
El Niño (Dec 97/Jan98)	1.16 ± 0.47	62.21 ± 18.02	0.12

During El Niño 1994/95, the rates of total primary production decreased compared to normal conditions. The estimated f-ratio was 0.16 in the western region (Table 2.4). In the central region, the estimated f-ratio was 0.14, which was slightly higher compared to

Table 2.5: Depth-integrated (0 to 120 m) $^{15}N \pm SD$ (mmolN m^{-2} d^{-1}) and ^{13}C uptake $\pm SD$ (mmolC m^{-2} d^{-1}) and f-ratio (f = (6.6 ^{15}N uptake)/ ^{13}C uptake) in the central equatorial Pacific.

	^{15}N	^{13}C	f-ratio
Normal (Dec 95/Jan 96)	1.37 ± 0.52	81.37 ± 13.13	0.11
El Niño (Nov/Dec 94)	0.19 ± 0.07	8.73 ± 4.5	0.14
El Niño (Dec 97/Jan98)	1.25 ± 0.75	51.88 ± 27.05	0.16

normal conditions (Table 2.5). However, due to uncertainties in estimated new and total production, it is difficult to consider this a significant increase.

During El Niño 1997/98, the integrated primary production in the western region was higher than those observed during normal conditions. The estimated values of integrated primary production suggest an f-ratio of 0.12 in the western equatorial Pacific (Table 2.4), and 0.16 in the central region (Table 2.5).

2.4 Discussion

In this section, I discuss variations in the rates of new production during normal and El Niño conditions as related to changes in the physical, chemical, and biological environment. Firstly, I present the normal structure of the western and central equatorial Pacific, and the responsible mechanisms for the zonal and vertical distributions of observed physical, chemical and biological variables. In the western region of the equatorial band, data from one cruise (December 1995/January 1996) were available to represent normal conditions, while in the central region, two cruises were carried out during normal conditions (December 1995/January 1996, January 1997). Comparison of data indicated that all observed variables showed similar zonal and vertical patterns in the two normal conditions in the central region.

Secondly, I consider two examples of anomalous conditions in more detail: the moderate El Niño conditions 1994/95, and the El Niño in 1997/98, which is considered the

strongest El Niño fluctuation in recent history. In contrast to normal conditions, where I did not observe significant differences in the zonal and vertical distributions of observed variables between two years, I have observed strong variations in the nature of El Niño. I discuss the similarities and the differences between the two anomalous conditions, and the possible causes for the observed variability.

2.4.1 The normal equatorial Pacific structure

Temperature, salinity, density, and nutrients

During normal conditions, the Warm Pool water ($T > 29$°C) was confined to the western part of the equatorial band (147°E–165°E), while in the central region (165°E–165°W), the colder subsurface waters were upwelled to the surface. The salinity at the surface layer was low ($S < 34$ psu) in the western region and increased eastward. At intermediate depths (150–210 m), high salinity water was observed, which may be due to intrusion of subtropical water from the south into the equatorial thermocline (Tsuchiya, 1968). Possible reasons for the eastward increase in surface salinity may include upwelling of intermediate high salinity water and/or lower precipitation over the central Pacific (Ando and McPhaden, 1997).

In the western region, a deep (0–100 m) isothermal layer was observed in the surface layer, while the isohaline layer only extended from the surface to about 50 m. The consequence of the interplay between the dependency of the density on temperature and salinity was the formation of a traditional mixed layer at the upper surface layer (0–50 m) and the nearly isothermal, but salinity stratified, barrier layer (Lukas and Lindstrom, 1991) between the base of the mixed layer and the top of the thermocline (50–100 m). The barrier layer was named by Lukas and Lindstrom (1991) since it acts as a barrier for mixing of colder thermocline waters with the surface layer, and inhibits surface cooling due to entrainment. The processes involved in the formation of the subsurface barrier layer in the western Pacific Warm Pool region include local freshwater forcing and the subduction of saline waters from the central equatorial Pacific (Shinoda and Lukas, 1995). The Warm

Pool region is dominated by nearly one-dimensional processes with the surface heat fluxes balancing the entrainment fluxes at the bottom of the mixed layer (Niiler and Stevenson 1982; Gent 1991). It is also likely that the supply of nitrate into the euphotic zone in the western region is primarily determined by the vertical turbulent flux (Peña et al. (1994); see Chapter 3). Thus the barrier layer potentially has an effect on the nitrate distribution, and rates of new production by isolating the surface water from the deep nutrient rich pool. However, the complete understanding of the role of barrier layer in nutrient distribution and biological production is still not sufficiently understood since the measurements of vertical turbulent fluxes are scarce.

The zonal and vertical distributions of nutrient concentrations (silicate, phosphate and nitrate) followed the pattern of temperature. Higher values of these parameters in the central part were due to the upwelling of relatively cold and nutrient-rich subsurface water. Phosphate and silicate were always present in the surface waters, while nitrate was undetectable in the surface layer of the western region. A possible implication is that in the western part of the equatorial Pacific, the low concentrations of nitrate may limit the rate of new production and phytoplankton biomass, which is consistent with previous studies (Barber and Chavez, 1991).

My observation of the zonal and vertical structure of temperature, salinity, density and nutrients in both the western and central equatorial Pacific during normal conditions are consistent with previous studies in this area (Halpern, 1980; Barber and Chavez, 1991, Mackey et al., 1995, Radenac and Rodier, 1996).

New production, chlorophyll *a*, f-ratio

New production My study indicates that the rates of new production in the western region were low during normal conditions, and were likely limited by low concentrations of nitrate. They were comparable to that measured in the oligotrophic north Atlantic Ocean (Lewis et al., 1986; G. Harrison, personal communication 1998), where, as in the western equatorial Pacific (see Chapter 3), vertical turbulent flux primarily determines the supply of nitrate into the euphotic zone (Lewis et al., 1986; Clark, 1997). My measured integrated

nitrate uptake values were in agreement with indirectly estimated values of new production in the Warm Pool area (i.e., 0.25–0.31 mmol m^{-2} d^{-1}) (Peña et al., 1994). The vertical structure of nitrate uptake showed low values at the surface, likely due to the low supply of nitrate to the surface associated with the presence of the barrier layer, which isolated the surface waters from the deep nutrient rich pool. A slight increase in rates of nitrate uptake was observed at depths 70–80 m, where nitrate became detectable.

In the central equatorial Pacific, the integrated new production rates were an order of magnitude higher than those observed in the western region. My results agree with those of previous studies in the central/eastern equatorial Pacific that estimated new production indirectly from calculations of nitrate transport (Chavez and Barber, 1987; Carr, 1995) and by measurements of nitrate assimilation based on the resident phytoplankton population (Peña et al., 1992; Wilkenson and Dugdale, 1992; Dugdale et al., 1992, McCarthy et al., 1996; Rodier and Le Borge, 1997). However, the rates of new production and biomass in the central equatorial Pacific were lower than would be expected from the high concentrations of nitrate when compared to coastal upwelling regions. This suggests that nitrate was not a limiting factor and that some other mechanism may control the new production and biomass, such as availability of iron (Martin et al., 1991) and silica (Dugdale and Wilkerson, 1998) or grazing of zooplankton (Peña et al., 1990; Cullen et al., 1992; Landry et al., 1997). The vertical structure of nitrate uptake differed from that observed in the western region, where higher uptake rates than in the deeper layer were found in the upper surface layer (0–40 m). This zonally-dependent distribution was supported by the upwelling of nitrate-rich water to the surface in the central part (see Fig. 2.11).

The east-west asymmetry of biological production and biomass in the equatorial Pacific has been discussed by previous authors (Barber and Kogelschatz, 1989). In the central part of the equatorial Pacific, the upwelling, and usually to a lesser degree, turbulent vertical transport, brings cold and nitrate-rich water into the upper well-lit surface layer (Wyrtki, 1981; Philander et al., 1987). In the western equatorial Pacific, however, the nutricline is deeper than in the eastern equatorial Pacific (Barber and Kogelschatz, 1989), and the vertical advective transport brings warm and nitrate-poor water to the surface from above

the nutricline. It has been indicated (Peña et al., 1994) that, within this region, the turbulent vertical transport from below the nutricline into the upper surface layer is relatively more important compared to the corresponding upwelling and thus may primarily determine the new production. The vertical turbulent flux of nitrate in the euphotic zone is small, and as a consequence, the new production is lower than in the central region. However, in the next section we show that the east-west asymmetry of observed variables is altered during El Niño conditions.

Chlorophyll *a* The vertical distribution of chlorophyll *a* in the western region showed typical tropical structure (Herbland and Voituriez, 1979; Cullen, 1982) with low values at the surface that likely resulted from low nitrate concentrations, and maximum concentrations exceeding 0.4 mg m^{-3} at 90 m, i.e., at the depth where nitrate concentrations became detectable. The observed integrated values of chlorophyll *a* in the western region during normal conditions (25.9 ± 3.7 mg m^{-2}) were in agreement with those obtained in earlier studies (23.4 mg m^{-2} at 172°W by Mackey et al., 1995; 20-30 mg m^{-2} at 155°E by Mackey et al., 1997; 15.8 ± 0.6 mg m^{-2} by Barber and Chavez, 1991).

In the central region, the influence of equatorial upwelling was (as for nitrate and temperature distributions) seen in the vertical chlorophyll *a* distributions which had an enrichment at the surface (concentrations > 0.2 mg m^{-3}). The integrated biomass was higher compared to the western region, but by a smaller factor than new production. A possible implication is that grazing regulated biomass in this area of the ocean.

f-ratio The value of the f-ratio (0.02) in the western part during normal conditions was lower than typically observed in oligotrophic areas. The low f-ratio resulted from high values of measured primary production rather than low new production. In the central region, the estimated f-ratio in December 1995/January 1996 was 0.11, which agrees with the values (0.06–0.20) previously reported in the central equatorial Pacific (Peña et al., 1992; Dugdale et al., 1992; Rodier and Le Borgne, 1997). The relatively higher f-ratio in the nitrate–abundant central region compared to the western region, where nitrate is depleted in the upper surface layer agree with previous studies that have observed increase

of f-ratios with higher ambient nitrate concentrations (Harrison et al., 1987). Low f-ratios indicate that regenerated nitrogen primarily supported the phytoplankton production in this area of the ocean.

2.4.2 Zonal and vertical fluctuation during moderate El Niño 1994/95

Temperature, salinity, density and nutrients

I observed that during El Niño 1994/95, the Warm Pool water ($T > 29$°C) expanded eastward (147°E–165°W) compared to normal conditions (147°E–165°E). Low salinity surface waters ($S < 34.0$ psu) extended eastward over the entire region, which agrees with earlier observations (Henin et al, 1997; Delcroix and Picaut, 1998). It has been demonstrated that surface salinity anomalies during El Niño conditions are mainly due to local variations in precipitation (Ando and McPhaden, 1997). During El Niño, precipitation is enhanced in the central equatorial Pacific and reduced in the western equatorial Pacific compared to normal conditions (Delcrox and Henin, 1991; Ando and McPhaden, 1997). As during normal conditions, a layer of high salinity water ($S > 35.4$ psu) was observed at intermediate depths (100–200 m). The thermocline moved closer to the surface in the western region and deepened in the central region, while the low salinity surface water extended eastward. As a consequence, the barrier layer developed across the entire region. In the western region, the upper boundary of the barrier layer moved closer toward the surface (30 m) and the barrier layer became correspondingly thinner (20–30 m), but showed stronger density stratification. Similar variations of the barrier layer during normal and El Niño conditions have been observed in the western equatorial Pacific by Ando and McPhaden (1997). The variations in the thickness of the barrier layer may potentially have an effect on the supply of nitrate into the surface layer, and therefore on the rates of new production in this part of the ocean.

The nitrate distributions showed that in the western region, the nutricline depth decreased compared to normal conditions, and therefore more nitrate was available for the

phytoplankton uptake in the well–lit surface layer. My observations agree with those of earlier studies carried out in equatorial Pacific (Rasmunson and Carpenter, 1982; Barber and Kogelschatz, 1989; McPhaden and Picaut, 1990; Philander 1990; Ando and McPhaden, 1997). In the central region, the nutricline depth increased during El Niño 1994/95, and the supply of nitrate in the euphotic zone also decreased.

New production, chlorophyll *a*, f-ratio

New production The integrated new production in the western equatorial Pacific during El Niño 1994/95 slightly increased compared to normal conditions. This observation is in agreement with my related study where the new production in the Warm Pool is estimated from the net surface heat fluxes and elemental ratios using a box model (see Chapter 4). Previous studies in the Warm Pool (Barber, 1990) have indicated an increase of 30–40 per cent in rates of total primary production during the 1987 El Niño. Since the estimates of new production were derived from those of the total production (Barber, 1990), it has been assumed that the rates of new production would increase as well. Results of my direct measurements during El Niño 1994/95 agree with such an expectation. My results suggest that the increase in new production during El Niño 1994/95 appears to be due to a higher supply of nitrate into the euphotic zone, associated with the observed shallowing of the nutricline. The new production in the upper surface layer remained low, although the barrier layer was thinner than under normal conditions. The mixing of nutrients to the upper surface layer as inferred from temperature may be restricted only to relatively infrequent periods of westerly wind bursts, when the mixed layer is deep enough to entrain the nitrate from the nutricline (Wijesekera and Gregg, 1996; Cronin and McPhaden, 1997).

The measured integrated nitrate uptake values (0.19 mmol m^{-2} d^{-1}) were lower than those (e.g., 1.4 mmol m^{-2} d^{-1}) observed by Rodier and Le Borge (1997) during October 1994 (El Niño conditions) at 167°E. Their values were comparable to my values measured in the central part during normal conditions. This observation is surprising since Rodier and Le Borge (1997) integrated chlorophyll was lower my observations (19 vs. 23.8 mg m^{-2}). The depth distribution of temperature from the TOGA-TAO buoy array show that

thermocline was slightly shallower during October 1994 than during December 1994, i.e., the time period of my observations. Therefore, the nutricline may also have been shallower during the October 1994. However, from the observed difference in the depth of the thermocline, it would be difficult explain almost an order of magnitude higher integrated new production in October 1994 compared to December 1994. Other possible reasons for the discrepancy between Rodier and Le Borge (1997) and my study may include methodological differences in ^{15}N measurements (e.g., *simulated in situ* vs. *in situ* incubation, amount of added isotope, incubation time, estimation of daily rates from hourly rates, integration depth), and difference in the time period of observations. The assessment of these differences was not possible since Rodier and Le Borge (1997) did not outline the details or the method.

In the central equatorial Pacific, the rates of new production during El Niño 1994/95 were markedly lower than during normal conditions, and similar to levels in the western Pacific. It is likely that the rates of new production were also limited by the availability of nitrate. The decrease in new production rates may be due to the lower nutrient supply associated with the increase of nutricline depth during the eastward expansion of the Warm Pool.

Chlorophyll *a* The integrated biomass in the western region did not change significantly during El Niño 1994/95 compared to normal conditions. As during normal conditions, the vertical distribution of chlorophyll *a* showed typical tropical structure. However, the maximum of chlorophyll *a* was closer to the surface, which may be related to the shallowing of the nutricline. In the central region, the integrated biomass was markedly lower than during normal conditions, and similar to levels in the west. The decrease in the integrated biomass rates may be due to the lower nutrient supply associated with the increase of nutricline depth during the eastward expansion of the Warm Pool.

f-ratio During El Niño 1994/95, the rates of total primary production in the western region decreased compared to normal conditions. This observation—in conjunction with the unchanged values of integrated chlorophyll *a* (i.e., the biomass)—implies that the rates of

regenerated production and values of the assimilation index (defined as primary production normalized by biomass) most likely decreased during El Niño 1994/95. Different values in the productivity index was observed in previous studies in the equatorial Pacific (Peña et al., 1990).

The estimated values of integrated primary production during El Niño 1994/95 suggest an f-ratio of 0.16 in the western region (Table 2.4), which agrees with previous studies (Rodier and Le Borgne, 1997). The f-ratio during El Niño 1994/95 is higher than that observed during normal conditions. It appears that the higher value of the f-ratio during El Niño 1994/95 resulted from lower primary production rather than higher new production. Variable f-ratios have been reported by previous studies in the equatorial Pacific (Peña et al., 1992). In the central region, the estimated f-ratio slightly increased during El Niño 1994/95 compared to normal conditions (Table 2.5) although the increase was not significant. Since the supply of nitrate in the euphotic zone was markedly lower during El Niño 1994/95 compared to normal conditions, I would expect that the proportion of new production to total production would be also lower during El Niño 1994/95.

2.4.3 Zonal and vertical fluctuation during strong El Niño 1997/98

Temperature and nutrient structure

As during El Niño 1994/95, the Warm Pool water expanded eastward during El Niño 1997/98, and, accordingly, the thermocline and nutricline were closer to the surface than during normal conditions.

New production and chlorophyll *a*

New production The integrated new production in the western equatorial Pacific during El Niño 1997/98 markedly increased (by ca. a factor of 10) compared to normal conditions. Rates of new production were comparable to those observed in the central Pacific region during normal conditions, where elevated nitrate concentration are observed at the surface due to the upwelling of subsurface water, and have never been observed in this normally

oligotrophic region.

In the western equatorial Pacific, the vertical structure of nitrate uptake showed that the increase in new production rates was most pronounced at depths from 50–100 m, while in the surface layer, the rates remained low. Since the depths 50–100 m corresponded to depths where the concentration of nitrate was significantly higher (up to 8 mmol m^{-3}) compared to normal conditions ($<$ 1 mmol m^{-3}), I may conclude that the increase in new production was primarily a result of higher supply of nitrate into euphotic zone associated with a decrease in nutricline depth. The high concentration of nitrate persisted in the euphotic zone, although both the light and temperature were favorable for phytoplankton growth. Possible reason may be that, similarly as in high-nutrient-low-chlorophyll region, other factors such as iron or grazing limited the biological production (Dugdale and Wilkerson, 1998; Cullen et al., 1992; Peña et al., 1990; Landry et al., 1997).

It has been suggested that iron concentrations are sufficient to support the phytoplankton production in the western equatorial Pacific, as a result of eolian iron supply from Asia (Barber and Chavez, 1991), and input of iron to surface waters from the Equatorial undercurrent (EUC), by advective and diffusive processes (Coale et al., 1996; Wells et al., 1999). Wells et al. (1999) reported the concentrations of iron in the upper portion of the EUC (100 m) at 145°E of ca. 0.35 nM. My observations of nitrate show concentrations of ca. 5 μM at these depths during normal conditions. During El Niño 1997/98, the nutricline rose compared to normal conditions, and the average nitrate at depth from 50 to 100 m was similar to that observed in the upper portion of the EUC during normal conditions (i.e., ca. 5 μM). Assuming the average Fe concentration in 50-100 m depth interval was ca. 0.35 nM, the ratio of nitrate relative to Fe supplied into the euphotic zone during El Niño 1997/98 was about 14,000:1. This is lower than the cellular N:Fe ratio (25,000:1-18,000:1) (calculated from the value of 167,000:1 for a molar C:Fe ratio for the open ocean phytoplankton (Coale et al., 1996) and 6.6-9.5 for molar C:N ratio (see Chapter 4)). The result suggests, that iron was supplied in excess of the demand, and hence it did not limit new production during El Niño 1997/98.

In the central equatorial Pacific, the integrated new production during El Niño 1997/98

was comparable to normal conditions. However, the depth distribution of new production differed from that during normal conditions. In normal conditions, I observed higher rates (> 0.02 mmol m^{-2} d^{-1}) of nitrate uptake in the surface layer (0–50 m) due to elevated nitrate concentrations that resulted from upwelling of subsurface nitrate. Below this layer, nitrate uptake was low (< 0.002 mmol m^{-2} d^{-1}). During El Niño 1997/98, the ^{15}N data showed an inverse pattern; nitrate uptake rates at the surface (0–40 m) where nitrate was depleted were low (< 0.002 mmol m^{-2} d^{-1}), but increased significantly (> 0.02 mmol m^{-2} d^{-1}) at depths from 40–70 m which again corresponded to higher concentrations of nitrate.

Chlorophyll *a* My study indicates that the integrated chlorophyll *a* in the western equatorial Pacific during El Niño 1997/98 remained relatively constant when compared to normal conditions in spite of a marked increase in the supply of nitrate into the euphotic zone and rates of new production. This observation differs from the results of Siegel et al. (1995) who observed 3-fold increase in biomass in the western equatorial Pacific due to the entrainment of nitrate-rich subsurface waters into the euphotic zone during westerly wind bursts. One of the possible reasons that the integrated biomass did not increase in the western equatorial Pacific during El Niño 1997/98 in spite of 9-fold increase in new production may be that grazing of zooplankton controls the biomass in this area (Cullen et al., 1992; Peña et al., 1990).

Another reason may be a shift in biomass community size structure to bigger cells. The phytoplankton biomass in the western equatorial Pacific is in general dominated by pico-plankton (0.2-1 μm) (Matsumoto, personal communication 1998). However, during El Niño 1997/98, a small increase in the contribution of netplankton 1- 10 μm was observed at depths of chlorophyll *a* maximum (60-100 m). The shift to bigger cells may be associated with increased nitrate concentrations compared to normal conditions and has been described earlier (Nielsen and Kiorboe, 1991). It has been suggested that the size structure of particulate matter influences the net loss of carbon from the surface waters, since large cells can be more easily transported from the euphotic zone to the deeper ocean by sinking (Michaels and Silver, 1988; Legendre and Le Ferve, 1989).

In the central region, the integrated biomass was significantly lower than during normal conditions, although the integrated new production was comparable to that observed during normal conditions. The possible reason for this phenomenon may be that grazing was able to compensate for higher new production and hence it modulated the dynamics of biomass (Cullen et al., 1992; Peña et al., 1990).

f-ratio During El Niño 1997/98, both the integrated primary and new production in the western region were higher than those observed during normal conditions, and the f-ratio was also higher (0.12). It was comparable to f-ratio observed during the moderate El Niño 1994/95, although the supply of nitrate in the euphotic zone was higher during El Niño 1997/98. In the central part the f-ratio did not change significantly between different conditions. The value of 0.16 is in agreement with low f-ratio reported in HNLC regimes (Rodier and Le Borge, 1997).

2.4.4 Similarities and differences between El Niño 1994/95 and El Niño 1997/98 and possible causes

Results during normal conditions were reproducible, while results from two El Niño events differed in some respects.

Similarities observed between the two El Niños were:

- The Warm Pool water expanded eastward, and the thermocline and nutricline rose in the western region and deepened in the central region.
- In the western region, the integrated new production increased compared to normal conditions, while the integrated biomass did not significantly change.
- In the central region, the integrated biomass was significantly lower than during normal conditions.
- Low f-ratios suggest that biological production was primarily supported by regenerated nitrogen.

- The depth of the nutricline may be an important factor in determining the rates of new production in the western and central equatorial Pacific on interannual time scales by regulating the supply of nitrate into the euphotic zone.

Differences between the two El Niño events:

- The expansion of the Warm Pool was more pronounced during El Niño 1997/98, and the thermocline and nutricline were closer to the surface.
- During the El Niño 1997/98 event the integrated new production in the western region was markedly higher than that observed during El Niño 1994/95.
- In the central region the integrated new production markedly decreased compared to normal conditions during the moderate event, while during the strong event, it was comparable to normal conditions.

2.4.5 Uncertainties in estimated rates of new production due to the effects of corrected nitrate profile, and ^{15}N isotope-enrichment

In my study, the measurements of ^{15}N isotope uptake were performed in the oligotrophic western equatorial Pacific where ambient nitrate concentrations were below analytical detection limits of the Autoanalyzer. These low nitrate concentrations may have potentially affected my results in several ways.

Firstly, when calculating the ^{15}N nitrate uptake (see Eq. 2.1), I assumed that the ambient nitrate concentration in surface waters equals zero when its value was below the detection limit of the Autoanalyzer (i.e., 0.1 mmol m^{-3}). The uptake rates may therefore be underestimated. To show the effect of the low nitrate profile on the mean values of integrated new production in the western and central equatorial Pacific, I determined nitrate concentrations in the surface water more accurately by the chemoluminescent method (Garside, 1967) for December 1995/January 1996, when low nitrate measurements were available. New production rates were then corrected using these measurements and compared to those calculated using nitrate concentrations obtained by the Autoanalyzer. In addition, I made a

correction for new production data measured in November/December 1994 assuming that average values of nitrate in the surface layer were similar to those observed in December 1995/January 1996. The results (see Appendix A) show that although the low-nitrate correction caused a moderate *increase* in the mean values of new production (up to 1.4 times in the western region during normal conditions), the differences between the corrected and measured values were often nonsignificant (e.g., during El Niño).

Secondly, an addition of the ^{15}N isotope in general disturbs the nitrate uptake system in surface waters where nitrate is low. As shown in the euphotic zone of the oligotrophic Atlantic ocean by Harrison and Harris (1997), the estimated nitrate uptake in the euphotic zone of the oligotrophic Atlantic ocean significantly increases (by a factor of 1.6) even when the amount of ^{15}N added to the seawater samples is a few nM. They proposed a correction method based on an empirically-derived correlation between the ambient concentration in the euphotic zone and the so-called "half-saturation" constant (see Appendix A). I anticipated that the measured nitrate uptake rates in my data may be overestimated because the euphotic-zone concentrations of in the oligotrophic western equatorial Pacific are below analytical detection limits; in addition, I added concentrations of the ^{15}N isotope (50 nM) that may be larger than the ambient concentrations (ca. 30 nM, see Table 2.1). These features indicate that the correction for the "enhancement" by isotope addition using the Harrison-Harris method may be required. Since, the measurements of nitrate uptake kinetics were not performed on our cruises, I assumed that they were similar to those measured in the oligotrophic Atlantic ocean (G. Harrison, personal communication 1998).

The isotope-enrichment correction (see Appendix A) caused a marked decrease in the integrated new production for all conditions. As expected, the relative reduction of the integrated new production was on average larger in the western part during normal conditions and in the entire region during El Niño conditions (3 times in both cases) than in the central part during the normal conditions (1.9 times). This reduction of new production may correspondingly decrease the value of estimated f-ratios in the western and central equatorial Pacific. Similar observations that the isotope-enrichment correction was more important in the areas with low nitrate (and small values of new production) were made

in the oligotrophic Atlantic ocean (Harrison, personal communication, 1998), although the reduction level averaged only 1.2–1.3 times.

Application of Harrison-Harris method to my data suggest that the measured rates of new production (and thus estimated f-ratios) in the western/central equatorial Pacific may be overestimated due to the added isotope. However, studies (Harrison et al., 1996) have shown spatial and temporal variations of kinetics parameters due to difference in physical and chemical environment (nutrient concentration, temperature, light), and species composition of phytoplankton (Goldman and Glibert, 1983). Therefore, measurements of kinetics parameters from western/central equatorial Pacific are required to confirm this conclusion.

2.5 Summary

My study presents an investigation of the variability in rates of new production during normal and El Niño conditions in the western (145°E to 165°E) and central (165°E to 165°W) equatorial Pacific in relation to changes in physical, chemical, and biological environment. This evaluation was based on direct measurements of the ^{15}N–nitrate uptake. Although several estimates of the rates of new production in the Warm Pool have been made using measurements of ^{15}N–nitrate uptake (Rodier and Le Borge, 1997) and indirect methods (Peña et al., 1994), no measurements have been performed so far during both El Niño and normal conditions. Four years of data are presented encompassing two years of normal conditions, and two levels of anomalous conditions: the moderate El Niño conditions (1994/95), and the El Niño in 1997/98, which is considered the strongest El Niño fluctuation in recent history.

While during normal conditions I did not observe significant differences in the zonal and vertical distributions of observed variables between two years, I have observed strong variations in the nature of El Niño. The summary of physical, chemical, and biological variables in the western and central equatorial Pacific for normal, moderate El Niño 1994/95, and strong El Niño 1997/98 are presented in Tables 2.7 and 2.8.

My results suggest that the depth of nitracline is an important factor in determining the

rates of new production in the western and central equatorial Pacific on interannual time scales by regulating the supply of nitrate into the euphotic zone. However, the magnitude of the variation in the supply of nitrate and therefore new production, depends on the strength of El Niño. Previous studies have observed a good correlation between the depth of the nitracline and the integrated primary production in the tropical Atlantic Ocean (Herbland and Voituriez, 1979).

Since new production sets also the scale for the export of organic carbon from the surface waters to the deep ocean (Eppley and Peterson, 1979), this results may have implications for the role of the western equatorial Pacific in the global carbon budget and climate variations. The western equatorial Pacific Warm Pool supports 70 per cent of the worlds annual tuna harvest (Lehodey et al., 1998). New production sets up the upper limit for the production that can be removed from the surface layer while maintaining the long-term integrity of the ecosystem. The information on new production rates and their interannual variation are thus important to predict the sustainable catch of tuna in the Warm Pool area, and to assess the future potential of this area for fisheries demands. However, more observations are needed to better understand the variations of new production on larger spatial and longer temporal scales. Since the direct measurements of new production are expensive, and limited in time in space, it is important to explore indirect methods that would allow us to monitor the spatial and the interanual variation of new production during El Niño and La Niña, and also fluctuations on short time scales such as westerly wind bursts. I describe a possible approach that would offer a solution to such a problem in Chapter 4. The correspondence of trends in physical and chemical variables on one hand, and biological variables on the other hand, suggests strong coupling between physical and biological processes in this particular region of Pacific.

2.6 Conclusions

Overall, the major findings of this study can be summarized as follows.

Western equatorial Pacific

Expected:

- The rates of new production during normal conditions were low; they were comparable to those observed in oligotrophic gyres.
- The low concentrations of nitrate may limit the rate of new production and biomass.
- The biological production is primarily supported by regenerated nitrogen.
- The integrated new production increased during El Niño.
- The variations in the rates of new production during El Niño were primarily determined by the variations in nitrate supply into the euphotic zone associated with the change of the nutricline depth during the well-known eastward expansion of the warm pool.
- The rate of increase in new production depends on the strength of El Niño (i.e., the depth of the thermocline/nutricline).

Unexpected:

- During El Niño 1997/98 the integrated new production increased by a factor 10 compared to normal conditions; it was higher than has ever been thought before.
- The integrated phytoplankton biomass did not significantly increase during El Niño 1997/98, although integrated new production was markedly higher.

Central equatorial Pacific

Expected:

- Differences between normal and El Niño conditions were evident in physical, chemical, and biological parameters.
- In normal conditions, nitrate was not a limiting factor, and some other mechanism, such as availability of iron or grazing of zooplankton, presumably controlled the new production and biomass.
- During El Niño 1994/95, the rates of new production and biomass markedly decreased compared to normal conditions.

Unexpected:

- During El Niño 1997/98, the integrated rates of new production were comparable to normal conditions, while biomass was markedly lower.
- The f-ratio did not vary significantly between normal and El Niño condition although the nitrate concentrations were markedly lower during El Niño.

Table 2.7. Summary of physical, chemical, and biological variables in the western equatorial Pacific-WEP (147^0E-165^0E) for normal, moderate El Niño 1994/95, and strong El Niño 1997/98.

	Physics	Chemistry	Biology
Normal conditions	Warm Pool (SST > 29^0C) Thermocline-20^0C (170m) SSS low (< 34 psu) Barrier layer thickness (40-50m)	Nitrate depleted (0-90m) 16 µM isopleth (250 m) Surface Si >2 µM Surface P < 0.2 µM	Surface Chl-a < 0.1 mg m^{-3} DCM at 90m Chl-a (25.9 mg m^{-2}) New production (0.15mmolN m^{-2} d^{-1}) Primary production (45.4 mmolC m^{-2} d^{-1}) f-ratio 0.02
Moderate El Niño 94/95	Warm Pool (SST > 29^0C) Thermocline-20^0C (150m) SSS low (< 34 psu) Barrier layer thickness (20-30m)	Nitrate depleted (0-80m) 16 uM isopleth (210m) Surface Si >2 µM Surface P < 0.2 µM	Surface Chl-a < 0.1 mg m^{-3} DCM at 75m Chl-a (23.8 mg m^{-2}) New production (0.19 mmolN m^{-2} d^{-1}) Primary production (7.7 mmolC m^{-2} d^{-1}) f-ratio 0.16
Strong El Niño 97/98	Warm Pool (SST > 29^0C) Thermocline-20^0C (120m)	Nitrate depleted (0-50m) 16 µM isopleth (180m)	Surface Chl-a < 0.1 mg m^{-3} DCM at 60 m Chl-a (25.5 mg m^{-2}) New production (1.16 mmolN m^{-2} d^{-1}) Primary production (62.2 mmolC m^{-2} d^{-1}) f-ratio 0.12

Table 2.8. Summary of physical, chemical, and biological variables in the central equatorial Pacific-CEP (165^0E-165^0W) for normal, moderate El Niño 1994/95, and strong El Niño 1997/98.

	Physics	Chemistry	Biology
Normal conditions	Cold tongue Upwelling SSS (> 34 psu)	Surface Nitrate 2-6 μM Surface Si > 2 μM Surface P > 0.2 μM	Surface Chl-a > 0.2 mg m^{-3} Chl-a (34.6 mg m^{-2}) New production (1.37mmol m^{-2} d^{-1}) Primary production (81.2 mmolC m^{-2} d^{-1}) f-ratio 0.11
Moderate El Niño 94/95	Warm Pool (SST > 29^0C) Thermocline-20^0C (150m) SSS low (< 34 psu) Barrier layer thickness (20-30m)	Nitrate depleted (0-80m) 16 uM isopleth (210 m) Surface Si < 2 μM Surface P < 0.2 μM	Surface Chl-a < 0.1 mg m^{-3} DCM at 75m Chl-a (21.2 mg m^{-2}) New production (0.19 mmolN m^{-2} d^{-1}) Primary production (8.7 mmolC m^{-2} d^{-1}) f-ratio 0.14
Strong El Niño 97/98	Warm Pool (SST > 29^0C) Thermocline-20^0C (120m)	Nitrate depleted (0-50m) 16 μM isopleth (180 m)	Surface chl-a < 0.1 mg m^{-3} DCM at 60 m Chl-a (24.9 mg m^{-2}) New production (1.25 mmolN m^{-2} d^{-1}) Primary production (51.8 mmolC m^{-2} d^{-1}) f-ratio 0.16

Chapter 3

Estimates of advective and diffusive fluxes and sources and sinks of carbon, nitrate and heat in the western equatorial Pacific

3.1 Introduction

The western equatorial Pacific is characterized by a vast pool of warm water, a weak or nonexistent upwelling, nutrient–depleted surface waters, and a strong coupling between atmosphere and ocean. The climatological biomass and biological production are low in this region, and the ocean is optically clear due to low absorption of solar radiation. It has been suggested that this area of the ocean plays an important role in seasonal to interannual climate variations (Rasmusson and Carpenter, 1982; Godfrey and Lindstrom, 1989) and in the global carbon cycle (Barber and Kogelschatz, 1989). A prerequisite for assessing the role of the western equatorial Pacific in the global carbon cycle, and climate variation, is an evaluation of heat, nitrate and carbon budgets.

The processes that regulate the distribution of heat, nitrate and carbon are related; the

heat budget components (net surface heat flux, penetrative irradiance, advective and diffusive fluxes) determine the sea surface temperature (SST), and the SST affects the distribution of pCO_2 in the surface waters, and thus the air-sea flux of carbon. The turbulent fluid motions which transport heat vertically also supply nitrate and dissolved inorganic carbon into the euphotic zone, where they may be taken up by phytoplankton. The rate of nitrate supply determines the rate of new production and therefore at steady-state, sets the upper limit to the rate of export of carbon into the deeper ocean. The variations in the phytoplankton biomass couple back into the heat budget of the upper surface layer through their influence on the radiative transfer through the upper ocean and the amount of light that is absorbed and converted to heat in the surface layer. By studying balances of heat, nitrate and carbon simultaneously, I attempted to determine what processes primarily govern the distribution of heat, nitrate and carbon in the western equatorial Pacific for the prediction of the role of this area of the ocean in climate and global biogeochemical cycles.

The surface layer heat balance in the western equatorial Pacific has been studied extensively before (Niiler and Stevenson, 1982; Enfield, 1986; Godfrey and Lindstrom; 1989; Cronin and McPhaden; 1997; Chen et al., 1994; Wijesekera and Gregg, 1996; Wang and McPhaden, 1997). It has been suggested that the regional net heat flux at the surface is balanced primarily by the vertical flux of heat at the bottom of the mixed layer (Niiler and Stevenson, 1982; Enfield, 1986; Wijesekera and Gregg, 1996) and penetrative irradiance through the base of the mixed layer (Lewis et al., 1990; Siegel et al., 1995). However, a few studies have indicated that advection might be important in the heat budget of the western equatorial Pacific (Cronin and McPhaden, 1997; Song and Friehe, 1997; McClain et al., 1999; Wang and McPhaden, 1997). The principal mechanisms responsible for maintaining the heat balance in this part of the ocean still remains unresolved due to lack of direct measurements (of turbulent mixing and vertical advection) and large uncertainties in the surface heat fluxes.

A complete study of the nitrate balance in the surface layer of the western equatorial Pacific has not yet been performed. A few studies have, however, estimated different

individual components of the nitrate budget. Peña et al. (1994) attempted to estimate indirectly turbulent fluxes of nitrate into the tropical Pacific Warm Pool area enclosed by the climatological 26° C isotherm from the net surface heat flux and the nitrate-temperature relationship. Using a general circulation model of the tropical Pacific (Philander et al., 1987), Peña et al. (1994) also estimated advective fluxes of nitrate in the Warm Pool, while Mackey et al. (1997) estimated zonal fluxes of nitrate in upper 300 m at 155°E on the equator, and Rodier and Le Borge (1997) performed ^{15}N uptake measurements at 167°E at the equator.

The evaluation of the carbon budget has been a focus of the US-JGOFS program. Studies of carbon balance have been conducted in the eastern equatorial Pacific (Quay, 1997), where upwelling is a relatively more important mechanism than vertical diffusive flux for the supply of nutrients, heat and dissolved inorganic carbon from deeper waters to the upper surface layer. In the western part of the equatorial band, individual components of the carbon budget, such as air-sea flux of CO_2 (Ishii and Inoue, 1995), primary productivity (Mackey et al., 1997; Rodier and Le Borge, 1997), and particulate organic export flux (Rodier and Le Borge, 1997) have been estimated. However, the complete study of carbon balance in the western equatorial region has not yet been done.

My study is the first attempt to evaluate the balances of heat, nitrate and carbon in the western equatorial Pacific. In this chapter, I evaluate the magnitudes of advective fluxes, diffusive fluxes, and sinks/sources of nitrate, dissolved inorganic carbon, and heat (or temperature) in the euphotic zone of the western equatorial Pacific (Fig. 3.1) using both direct measurements and values obtained by previous studies.

I test the hypothesis that vertical turbulent diffusion is the main mechanism for the supply of nutrients and dissolved inorganic carbon into the euphotic zone, and for the loss of heat. I also provide the basic assumptions which will be used in Chapter 4 for developing a one-dimensional model for estimating new production and air-sea exchange of CO_2.

The chapter is organized as follows. The governing equation for the distribution of nitrate, carbon and temperature in the upper surface layer is presented in Section 3.2. Section 3.3 outlines the methods and data that were used to estimate the magnitudes of advective

fluxes, diffusive fluxes, and sinks/sources of nitrate, dissolved inorganic carbon, and heat (or temperature) in the euphotic zone of the western equatorial Pacific. The heat, nitrate and carbon balances and the possible reasons for uncertainties are discussed in Section 3.4. The discussion focuses on the relative importance of the different processes as inferred from three balances, and possible variations of these processes on interannual scales associated with El Niño and fluctuations on shorter time scales, such as episodic events of westerly wind bursts (Section 3.5). The chapter ends by stating the implications of the conclusions, and their importance in developing a box model for estimating new production and air-sea exchange of CO_2 (Section 3.6).

3.2 Governing equation

The governing equation which describes the dynamics of nitrate, carbon and temperature in the upper ocean is the advection-diffusion equation for an incompressible medium (Batchelor, 1973). If the xy plane corresponds to the ocean surface, and the z axis is directed into the ocean's interior, then,

$$\frac{\partial X}{\partial t} = -u\frac{\partial X}{\partial x} - v\frac{\partial X}{\partial y} - w\frac{\partial X}{\partial z} + \frac{\partial}{\partial x}K_h\frac{\partial X}{\partial x} + \frac{\partial}{\partial y}K_h\frac{\partial X}{\partial y} + \frac{\partial}{\partial z}K_v\frac{\partial X}{\partial z} - S_x \,. \tag{3.1}$$

where the vector components u, v, and w are velocities along the x, y, and z axes, and the eddy diffusivity $\mathbf{K} = (K_x, K_y, K_z)$ is axially symmetric about the z axis (i.e., $K_x = K_y = K_h$, and $K_z = K_v$). In this expression, the scalar X corresponds to a given measurable quantity (i.e., concentration of nitrate, NO_3, or dissolved inorganic carbon DIC, or temperature, T).

The non-conservative term, S_x, is defined for nitrate, dissolved inorganic carbon, and temperature as net biological uptake of nitrate [mmolN m^{-3} s^{-1}], net biological uptake of dissolved inorganic carbon [mmolC m^{-3} s^{-1}], and absorption of solar radiation [W m^{-3}],

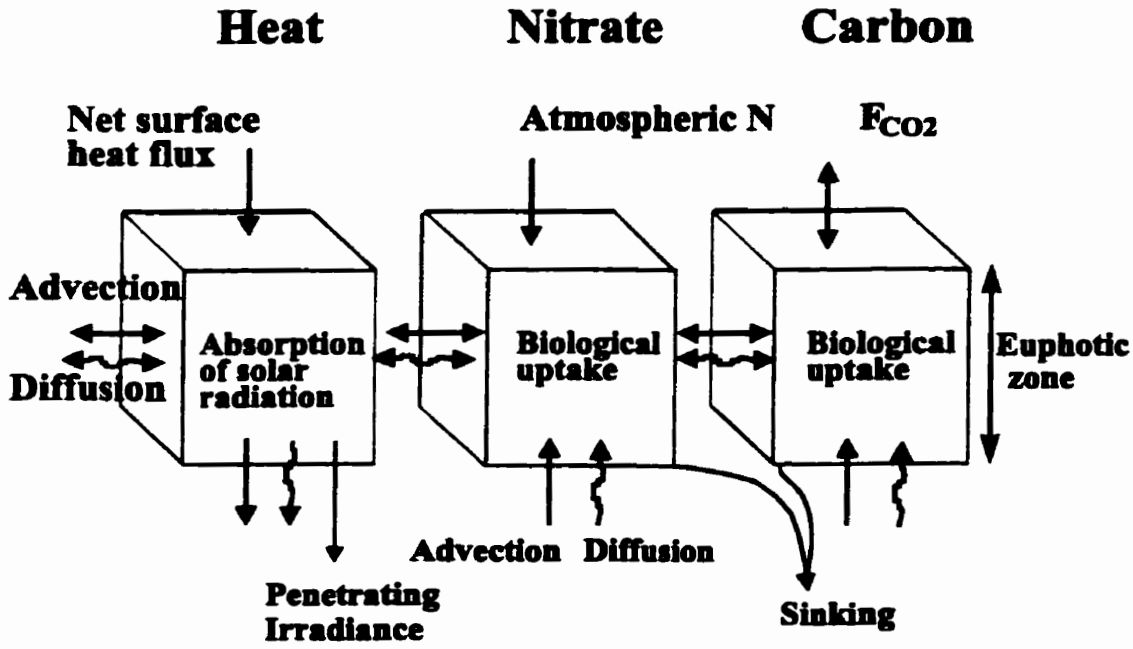

Figure 3.1: Heat, nitrate and carbon budgets in the western equatorial Pacific.

respectively, i.e.,

$$\begin{aligned} S_N &= p_N \, . \\ S_C &= p_C \, . \\ S_E &= -\frac{1}{c_p \rho} \nabla \cdot \mathbf{E} \approx -\frac{1}{c_p \rho} \frac{\partial E_z}{\partial z} \, , \end{aligned}$$

where $\mathbf{E} = (E_x, E_y, E_z)$ is the irradiance vector and $\partial E_x/\partial x, \partial E_y/\partial y \ll \partial E_z/\partial z$.

Since I am interested in the values of each term averaged over the depth of the euphotic zone D_{ez}, I integrate Eq. 3.1 to obtain the expression,

$$\begin{aligned} D_{ez}\overline{\frac{\partial X}{\partial t}} = & -D_{ez}\overline{u\frac{\partial X}{\partial x}} - D_{ez}\overline{v\frac{\partial X}{\partial y}} - w(\overline{X}_{D_{ez}} - \overline{X}_{D_{bc}}) + D_{ez}\overline{\frac{\partial}{\partial x}K_h\frac{\partial X}{\partial x}} + \\ & D_{ez}\overline{\frac{\partial}{\partial y}K_h\frac{\partial X}{\partial y}} + K_{vD_{ez}}\frac{\partial X}{\partial z}\Big|_{D_{ez}} - K_{v0}\frac{\partial X}{\partial z}\Big|_0 - D_{ez}\overline{S} \, . \end{aligned} \tag{3.2}$$

Definitions for the terms in the upper equation are summarized in Table 3.1. In Eq. 3.2, I have taken into account only the turbulent flux due to diapycnal mixing, thereby neglecting the vertical component of the isopycnal flux (Siegel et al., 1998). The vertical turbulent flux at the surface equals the sum of latent and sensible heat flux for temperature, the atmospheric sources for nitrate, and the air-sea flux of CO_2 for dissolved inorganic carbon.

In calculating the value of each term on the right-hand side of the Eq. 3.2, I estimated to first order the following parameters: the zonal and meridional velocities (u, v), horizontal eddy diffusivity coefficient (K_h) averaged over the euphotic zone, the vertical velocity (w), and the vertical eddy diffusivity coefficients $(K_{vD_{ez}})$ at the base of the euphotic zone. Secondly, I estimated the depth–averaged zonal $(\overline{\partial X}/\partial x)$, meridional $(\overline{\partial X}/\partial y)$, and vertical $(\overline{\partial X}/\partial z)$ gradients of nitrate, dissolved inorganic carbon, and temperature over the euphotic zone of the western equatorial Pacific. Thirdly, I determined the difference $\overline{X}_{D_{ez}} - \overline{X}_{D_{bc}}$ between the average nitrate and dissolved inorganic carbon concentrations, and average temperature in the the euphotic zone, and their values in the entrained water below the euphotic zone. Fourthly, I used the estimated values of velocity components, eddy diffusivities, and gradients, to calculate advective and diffusive fluxes, as shown in

Table 3.1: Expressions Used in Scaling analysis

Expression	Definition
D_{ez}	depth of the euphotic zone
$\overline{X}_{D_{ez}}$	depth–averaged value of X in the euphotic zone
$\overline{X}_{D_{bz}}$	average value of X entrained from beneath the base of the euphotic zone
$D_{ez}\overline{u\frac{\partial X}{\partial x}}$	depth–averaged zonal advective flux
$D_{ez}\overline{v\frac{\partial X}{\partial y}}$	depth–averaged meridional advective flux
$\overline{w(\overline{X}_{D_{ez}} - \overline{X}_{D_{bz}})}$	vertical flux due to entrainment across the base of the euphotic zone
$D_{ez}\overline{\frac{\partial}{\partial x}K_h\frac{\partial X}{\partial x}}$	depth–averaged zonal turbulent flux
$D_{ez}\overline{\frac{\partial}{\partial y}K_h\frac{\partial X}{\partial y}}$	depth–averaged meridional turbulent flux
$K_v D_{ez}\overline{\frac{\partial X}{\partial z}}\mid_{D_{ez}}$	vertical turbulent flux at the bottom of the euphotic zone
$K_{v0}\overline{\frac{\partial X}{\partial z}}\mid_0$	vertical turbulent flux at the surface

Eq. 3.2. Finally, I obtained the magnitudes of sink/source terms, S_x, by means of direct measurements.

The time rate of change of nitrate, dissolved inorganic carbon, and temperature in surface layer of the western equatorial Pacific depends on the time scale of interest. In estimating the balances of nitrate, dissolved inorganic carbon and heat, I used a steady state assumption in the Warm Pool for the annual average during normal conditions. The variations on interannual scales associated with El Niño and, fluctuations on shorter time scales, such as the episodic events of westerly wind bursts are addressed in the discussion. In the next section, I present methods and data that were employed in estimating components of the heat, nitrate and carbon balances in western equatorial Pacific.

3.3 Methods and data

Measurements that were used for the estimation of various terms in Eq. 3.2 were collected on the same cruises as those described in Chapter 2. Acoustic Doppler Current Profiler (ADCP) measurements were used to estimate horizontal components of the velocity (J.

Sildam, personal communication). Profiles of temperature, nitrate and dissolved inorganic carbon from the Warm Pool area were used for determining vertical and zonal gradients of these properties, and their average values at the depth of 100 m. To evaluate the magnitude of sink terms for nitrate and dissolved inorganic carbon, I used measurements of biological uptake of ^{15}N, presented in Chapter 2. Observations of meteorological variables and depth profiles of downwelling irradiance and upwelling radiance were used for the estimation of net surface heat flux and absorption of solar radiation in the water column (see Chapter 4).

Measurements for determining vertical velocity, eddy diffusivity coefficients, and meridional distributions of temperature, nitrate and dissolved inorganic carbon were not performed on our cruises. For these variables, I have used the typical values obtained from previous studies that were performed in the western equatorial Pacific. The rationale behind the choice of the particular set of values is discussed in more detail below.

I assumed the depth of the euphotic zone (defined as the depth at which the visible irradiance (400-700 nm) is reduced to approximately 1 per cent of surface PAR (Wilkerson and Dugdale, 1991)) to be $D_{ez} = 100$ m. This level was determined from measurements of downwelling irradiance and upwelling radiance performed by the SeaWiFS Multichannel Radiometer (Satlantic). In general, the term $\overline{X}_{D_{ez}} - \overline{X}_{D_{be}}$ is difficult to determine due to difficulties in determining the depth D_{be} from which water is entrained into the euphotic zone (Wyrtki, 1981; Hayes et al., 1991; Wang and McPhaden, 1997). Following Wang and McPhaden (1997), I defined the value $\overline{X}_{D_{be}}$ as the average X at a depth of 20 m below the depth of the euphotic zone.

3.3.1 Estimating horizontal advective and turbulent fluxes

Zonal and meridional velocities u and v.

Horizontal components of current velocity u (north) and v (east) were measured with a RDI Acoustic Doppler Current Profiler (ADCP) in December 1995 from 12 m to 500 m depth. Velocity measurements were averaged over 20-minute intervals and 8-m intervals in the vertical. Due to a misalignment angle of the ADCP orientation relative to the ship, only

data collected when the ship's speed was higher than 4.5 m s^{-1} were included in further analysis (J. Sildam, personal communication). Velocities were discretized into 0.5 degrees longitude points using the nearest-neighbor gridding method.

Results from the ADCP measurements during December 1995/ January 1996 are presented in Figs. 3.2 and 3.3 for the transect along the equator from 145°E to 165°E. Fig. 3.2 depicts the zonal component of velocity. I observed an eastward current at the surface layer from 0 to 70 m with an average speed of 0.2 m s^{-1}. Below this layer, i.e. at depths of 70–120 m, flow with average speeds of 0.3 m s^{-1} was toward the west. An Equatorial Undercurrent (EUC) was observed at depths 130–300 m with an eastward velocity of 0.3 m s^{-1}. Long–term climate records indicate that the zonal flow in the upper 120 m is westward during normal conditions, with average velocities of 0.2 m s^{-1} (McPhaden et al., 1992). The reversal of surface current at the time of our observations was associated with westerly winds. This phenomenon was observed by previous studies (Godfrey and Lindstrom, 1989; Sprintall and McPhaden, 1994; Cronin and McPhaden, 1997). In my study, I used the value of 0.2 ($\pm$0.1) m s^{-1} for average zonal velocity in the upper 100 m. This value is in agreement with velocity data from TOGA-TAO buoys in the western equatorial Pacific (McPhaden et al., 1998; Sprintall and McPhaden, 1994).

The meridional component of velocity (Fig. 3.3) was much smaller than the zonal component. I observed that the meridional velocity changed speed and direction along the equator: from 145°E to 156°E, it was pointing northwards (with values of 0.02 m s^{-1}), while west of 156°E it was directed southwards (with values of 0.01 m s^{-1}). Based on my results and previous observations (Wang and McPhaden, 1997), I used the value of 0.02 ($\pm$0.01) m s^{-1} for meridional velocity component.

Horizontal eddy diffusivity coefficient K_h.

There are no observationally-based estimates of horizontal eddy diffusivity available at the present time for the western equatorial Pacific. The value of 10^3 m^2 s^{-1} was obtained in the Atlantic Equatorial Undercurrent by means of experiments with clusters of drifting buoys (Farbach et al., 1986) and in North Atlantic ocean by the tracer release experiment NATRE

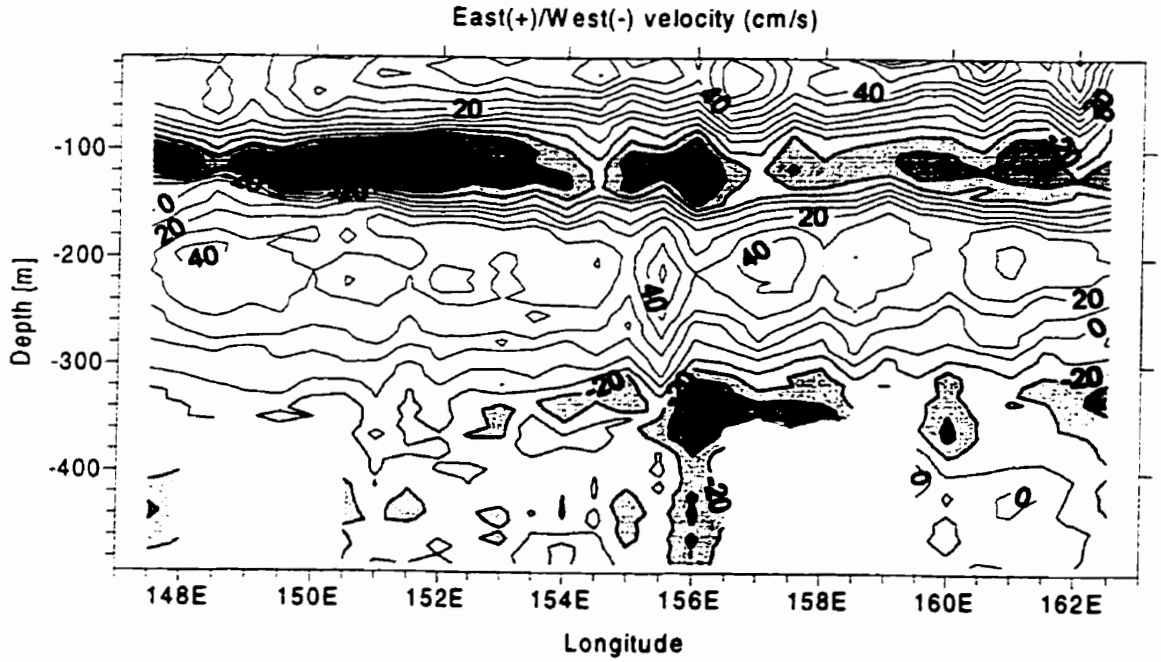

Figure 3.2: Zonal component of velocity [cm s^{-1}] on a transect along the equator from 147°E to 165°E during December 1995/ January 1996. Shaded (negative No.) areas indicate eastward current.

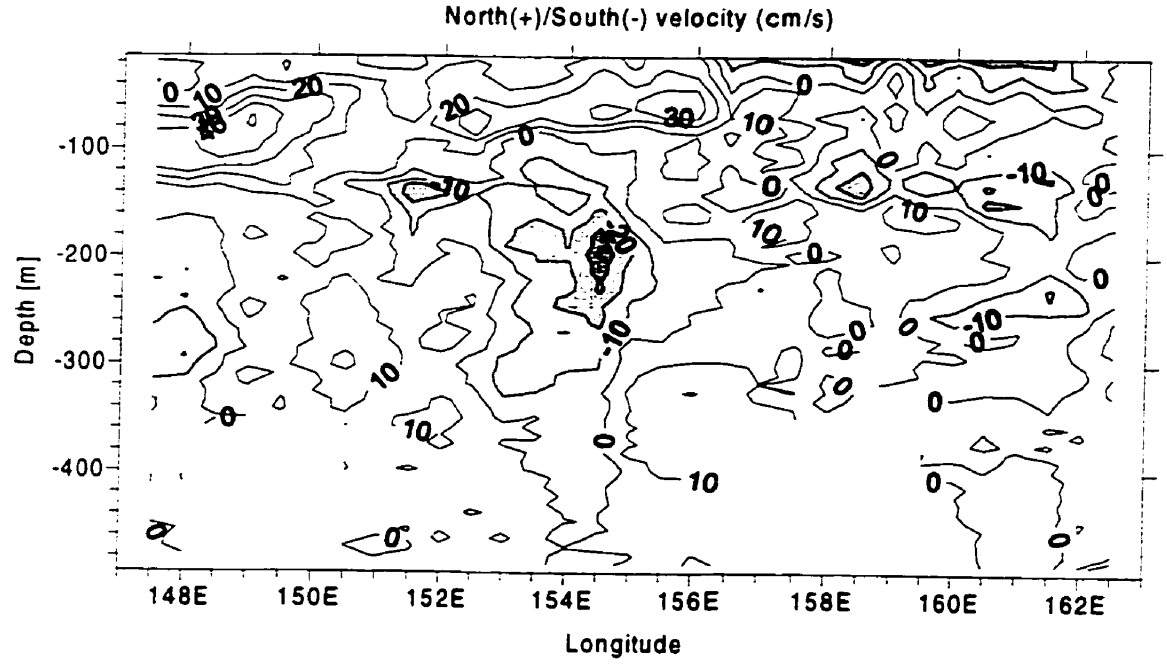

Figure 3.3: Meridional component of velocity [cm s^{-1}] on a transect along the equator from 147°E to 165°E during December 1995/ January 1996. Shaded areas (negative No.) indicate northward current.

(Sundermeyer and Price, 1996). It has been suggested that horizontal eddy fluxes in the upper 100 m in the central equatorial Pacific can be parameterized with an eddy diffusivity of order (0.01–1.4) $\cdot 10^3$ m^2 s^{-1} (Bryden and Brady, 1989). Typically, the values between 10^3 m^2 s^{-1} and 5 $\cdot 10^3$ m^2 s^{-1} are used in equatorial models (Bryden and Brady, 1989; Wacongne, 1989), and therefore the value (3 $\pm$2) $\cdot 10^3$ m^2 s^{-1} was adopted in my study.

Zonal gradients of nitrate, dissolved inorganic carbon, and temperature in the upper 100 m.

The zonal gradients of temperature, nitrate, and dissolved inorganic carbon were estimated at 10 m intervals over the upper 100 m in the western equatorial Pacific, from linear regression of data collected on our cruises. The average values ($\pm SE$ of the regression estimate) of these gradients in the upper 100 m are presented in Table 3.3. Measurements of temperature and nitrate (Figs. 2.4 and 2.5 in Chapter 2) show that these properties do not change significantly over the upper 100 m in the zonal ((3 $\pm$2) $\cdot 10^{-8}$ mmolN m^{-4} $\pm$ for nitrate, and (2 $\pm$1) $\cdot 10^{-8}$ K m^{-1} $\pm$ for temperature). These observations agree with zonal sections of annual nitrate concentrations (Levitus, 1994) and annual temperature (Levitus, 1994), and with those of previous studies carried out in the western equatorial Pacific (Ando and McPhaden, 1997; Barber and Chavez, 1991). Zonal sections of dissolved inorganic carbon in the western equatorial Pacific are shown in Fig 3.4. (Details on collecting the data are presented in Chapter 4). The observed gradients were (2 $\pm$1) $\cdot 10^{-7}$ mmolC m^{-4} which is in agreement with previous observations (Ishii and Inoue, 1995).

Meridional gradients of nitrate, dissolved inorganic carbon in the upper 100 m.

Measurements of temperature, nitrate and dissolved inorganic carbon along meridional transects in the western equatorial Pacific were not performed on our cruises. Previous studies of temperature (Levitus, 1994; Radenac and Rodier, 1996) and nitrate (Levitus, 1994; Barber and Kogelschatz, 1989; Mackey et al., 1995, Radenac and Rodier, 1996) indicated very small gradients in temperature and nitrate concentrations (ca. (1–5) $\cdot 10^{-7}$ K

m^{-1} for temperature, and ca. 10^{-7} mmolN m^{-4} for nitrate). No data on meridional distributions of dissolved inorganic carbon in the western equatorial Pacific are currently available. Measurements that have been performed in the central/eastern Equatorial Pacific (Goyet et al., 1996; Peltzer and Hayward, 1996; Wanninkhof et al., 1995; Feely et al., 1995) suggested gradients in the DIC distribution of order 10^{-5} mmolN m^{-4}. I expect these gradients to decrease in the western equatorial Pacific since the factors that primarily determine the distribution of dissolved inorganic carbon in surface waters (i.e., temperature, flux of CO_2 across the sea surface, nutrient concentrations and phytoplankton biomass through their effect on the uptake of DIC) have smaller gradients in the meridional direction in the western equatorial Pacific than in central/eastern part (Ishii and Inoue, 1995; Mackey et al., 1995; Radenac and Rodier, 1996). In my study I used a value of $(3\pm2)\cdot10^{-6}$ mmolN m^{-4} for the meridional dissolved inorganic carbon gradient.

The zonal components of velocity, the horizontal eddy diffusivity coefficient, and the horizontal gradients of nitrate, dissolved inorganic carbon, and temperature are given in Tables 3.2 and 3.3. These values were used for calculating the horizontal advective and diffusive fluxes, using expressions from Table 3.1.

Table 3.2: Selected Parameters for horizontal Velocities and Eddy Diffusivity Coefficients

Zonal velocity u	0.2 ± 0.1 m s^{-1}
Meridional velocity v	0.02 ± 0.01 m s^{-1}
Horizontal eddy diffusivity K_h	$(3 \pm 2)\cdot10^{3}$ m^2 s^{-1}

3.3.2 Estimating vertical advective and turbulent fluxes

Vertical velocity w at 100 m.

No direct measurements of equatorial vertical motion have yet been made. Based on numerical models (Philander et al., 1987; Wyrtki, 1981; Bryden and Brady, 1985; Enfield, 1986)

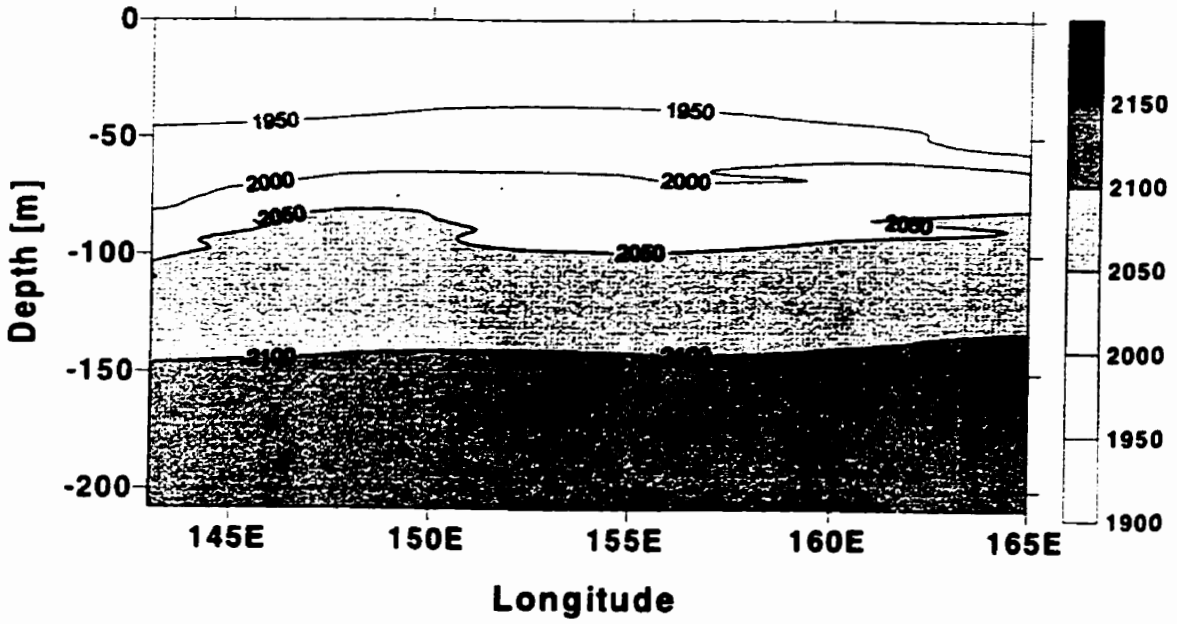

Figure 3.4: Dissolved inorganic carbon (mmolC m^{-3}) on the transect along the equator from 145° E to 165° E.

Table 3.3: Horizontal gradients of nitrate, dissolved inorganic carbon, and temperature. Uncertainties in zonal gradients refer to SE of the regression estimate.

Zonal nitrate gradient	$(3 \pm 2) \cdot 10^{-8}$ mmolN m^{-4}	this study
Meridional nitrate gradient	$(2 \pm 1) \cdot 10^{-7}$ mmolN m^{-4}	Radenac and Rodier, 1996
Zonal carbon gradient	$(2 \pm 1) \cdot 10^{-7}$ mmolC m^{-4}	this study
Meridional carbon gradient	$(3 \pm 2) \cdot 10^{-6}$ mmolC m^{-4}	Feely et al., 1995
Zonal temperature gradient	$(5 \pm 3) \cdot 10^{-8}$ K m^{-1}	this study
Meridional temperature gradient	$(3 \pm 2) \cdot 10^{-7}$ K m^{-1}	Radenac and Rodier, 1996

and computations of upwelling velocities from moored current measurements (Halpern et al., 1989), the magnitude of the vertical velocity is (1-3) $\cdot 10^{-5}$ m s^{-1} in central/eastern equatorial Pacific, a value which markedly decreases toward the west (Philander et al., 1987). Model results also predict that the vertical velocity has a maximum value at a depth of 40 to 80 m, and water that is upwelled to the surface at the equator comes from a depth of 100 m or less. In my calculations, I used the value $w = (1 \pm 2) \cdot 10^{-8}$ m s^{-1} which was determined at the depth of euphotic zone in the western equatorial Pacific (see Fig. 3.5, Philander et al., 1987; Halpern et. al, 1995). However, Fig. 3.5 indicates that the values of vertical velocities are negative at a depth of 100 m eastward from 155° E and positive westward. The net vertical advective transport may be therefore small when averaged over the western equatorial Pacific.

Vertical eddy diffusivity coefficient K_v.

Measurements of the rate of dissipation of kinetic energy, ϵ, performed in the western equatorial Pacific (Wijesekera and Gregg, 1996) have shown that the estimated values of vertical eddy diffusivity for density are of order 10^{-6} m^2 s^{-1} to 10^{-4} m^2 s^{-1} in the upper 200 m. In central/eastern Pacific (Peters et al., 1988; Gregg et al., 1985; Moum et al. 1989; Carr et al. 1992) values of the vertical eddy diffusivity for density are on average about 10^{-4} m^2 s^{-1} in the thermocline but can exceed 10^{-3} m^2 s^{-1} in the surface layer. Eddy

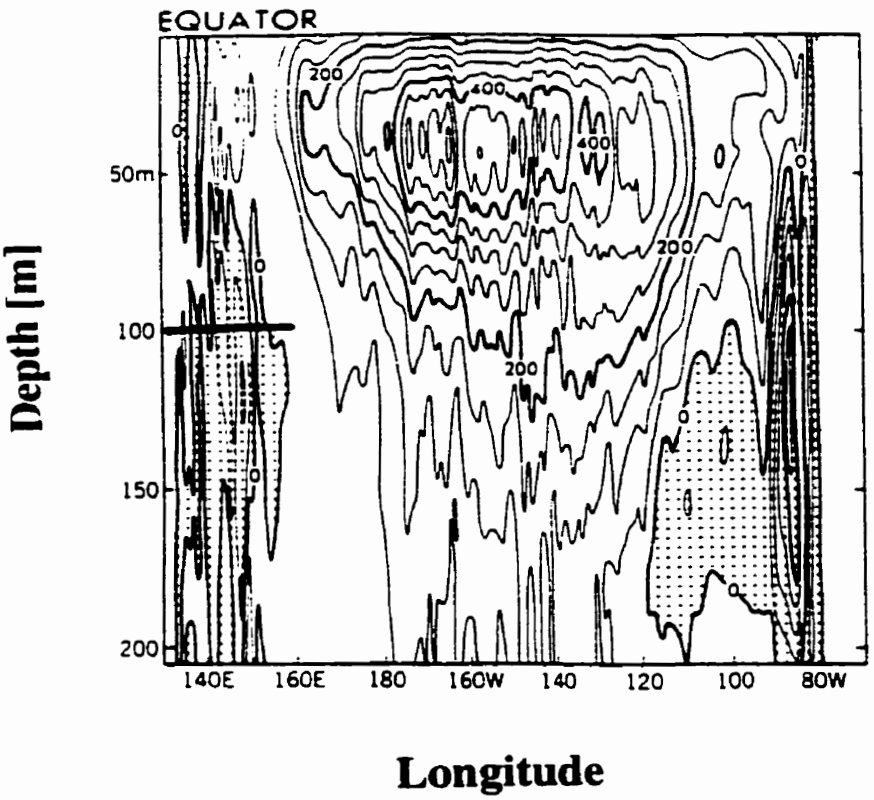

Figure 3.5: The annual mean vertical velocities [cm d^{-1}] as a function of depth in the equatorial Pacific from a General Circulation Model (Philander et al., 1987). Shaded areas indicate downwelling. The line at 100 m represents the depth at which irradiance is attenuated to 1 per cent of its surface value in the WEP (145° E to165° E). Figure is modified from (Philander et al., 1987).

diffusivities indirectly derived at the base of mixed layer (30 m) at 140° W from surface heat fluxes are of the order 5 $\cdot 10^{-3}$ m^2 s^{-1} (Bond and McPhaden, 1995). In my study, I made a rough estimation of K_v at the base of euphotic zone using the Pacanowski and Philander (1981) method. In this method the K_v is a function of the Richardson number, Ri, which is calculated as:

$$Ri = \frac{N^2}{(\partial u/\partial z)^2 + (\partial v/\partial z)^2}. \tag{3.3}$$

where the denominator is the squared velocity shear and N^2 is square of the buoyancy frequency. Velocity shear was obtained from ADCP measurements of zonal and meridional velocities binned into 8-m intervals in the vertical direction (see above). Previous studies have shown that velocity shear calculated using such averaged velocities may be underestimated (Toole et al., 1987). Good ADCP data was obtained from 0-200 m.

N^2 was calculated over 8 m intervals as,

$$N^2 = -\frac{g}{\rho_0}\frac{\partial \rho}{\partial z} \tag{3.4}$$

where g is the gravitational acceleration (g= 9.81 m s^{-2}) and ρ_0 is the average density of the sea water. The $\partial\rho$ / ∂z over 8 m intervals was computed from densities that were interpolated between stations where CTD measurements were collected.

Fig. 3.6 shows the Ri versus depth for the transect along the equator where our measurements were carried out. The average Richardson number at the depth of the euphotic zone (100 m) was of order 1. Using the Pacanowski and Philander (1981) expression, the calculated values of K_v were ca. (7 $\pm$3) $\cdot 10^{-5}$ m^2 s^{-1}. Pacanowski and Philander (1981) method is commonly used for parameterization of eddy diffusivity in the general circulation models. There is some doubt regarding the validity of the relationship described by Pacanowski and Philander (1981) (Gregg et al., 1985; Peters et al..1988; Carr et al., 1992); as a comparison, Wijesekera and Gregg (1996) estimated K_v values of 10^{-6} m^2 s^{-1} to 10^{-4} m^2 s^{-1} in the upper 200 m for the western equatorial Pacific during TOGA COARE. For my purposes I use the value derived from Pacanowski and Philander (1981) for subsequent

calculations, with estimated errors from the range of field observations i.e., $7 \pm 6 \cdot 10^{-5}$ m^2 s^{-1}.

I also attempted to estimate K_v from fine-scale CTD measurements using an indirect method presented in Appendix D. The method was however limited by the resolution of Satlantic CTD profiler.

Vertical gradients of carbon, and temperature, and their average concentrations in the upper 100 m.

Vertical gradients of nitrate, dissolved inorganic carbon, and temperature at 100 m were estimated from measured depth profiles of these quantities using least-squares linear regression (Sokal and Rohlf, 1995). The standard error of the slope of the regression line was calculated as shown in Appendix C. Data from December 1995/January 1996 were used for determining nitrate and temperature gradients. I calculated the DIC gradient from measurements collected in November/December 1994 and December 1997/January 1998. DIC measurements were not performed in December 1995/January 1996. The scatter diagrams of temperature versus depth, nitrate versus depth, and DIC versus depth are shown in Figs. 3.7, 3.8, and 3.9. Only data from approximately 100 to 200 m were used for determining the average vertical gradients at the bottom of the euphotic zone. Values of 0.11 mmolN m^{-4} (R^2=0.65), 1.0 mmolC m^{-4} (R^2=0.76), and 0.1° K m^{-1} (R^2=0.75), were obtained for nitrate, DIC and temperature gradients, respectively. Average ($\pm SE$) nitrate and dissolved inorganic carbon concentrations, and average temperature in the euphotic zone (0-100 m) and in the entrained water below the euphotic zone (120 m) were determined from the measured depth profiles of these properties.

Tables 3.4, 3.5, and 3.6 present the values of the vertical velocity and eddy diffusivity coefficients, vertical gradients of nitrate, dissolved inorganic carbon, and temperature, and the difference between upper layer nitrate, dissolved inorganic carbon, and temperature and that in the entrained water below. These parameters were used for calculations of vertical advective and diffusive fluxes of nitrate, dissolved inorganic carbon and heat.

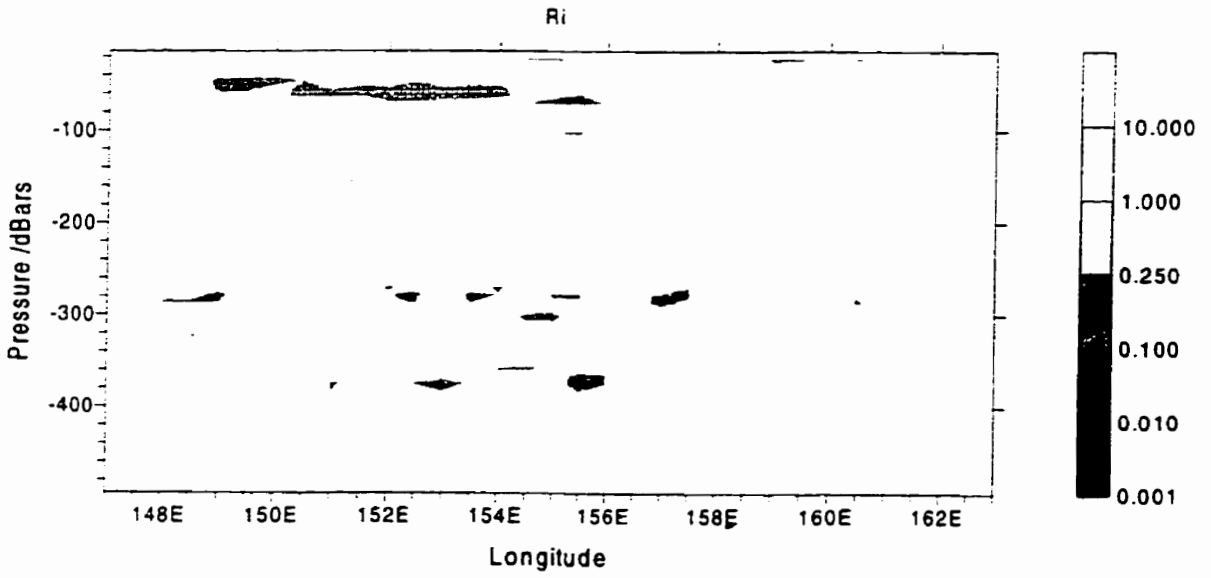

Figure 3.6: Gradient Richardson number as a function of depth on a transect along the equator from 147° E to 165° E in December 1995/ January 1996.

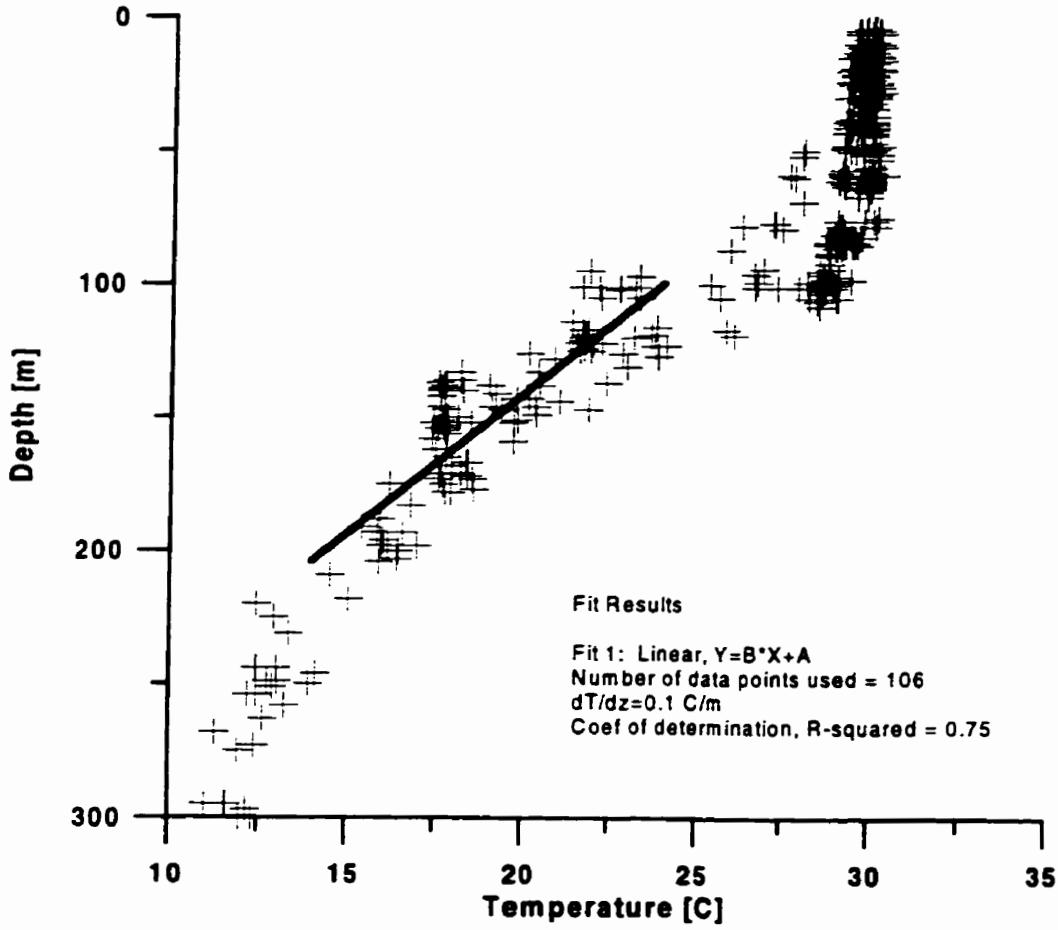

Figure 3.7: Scatter diagram of temperature [°C] versus depth [m]

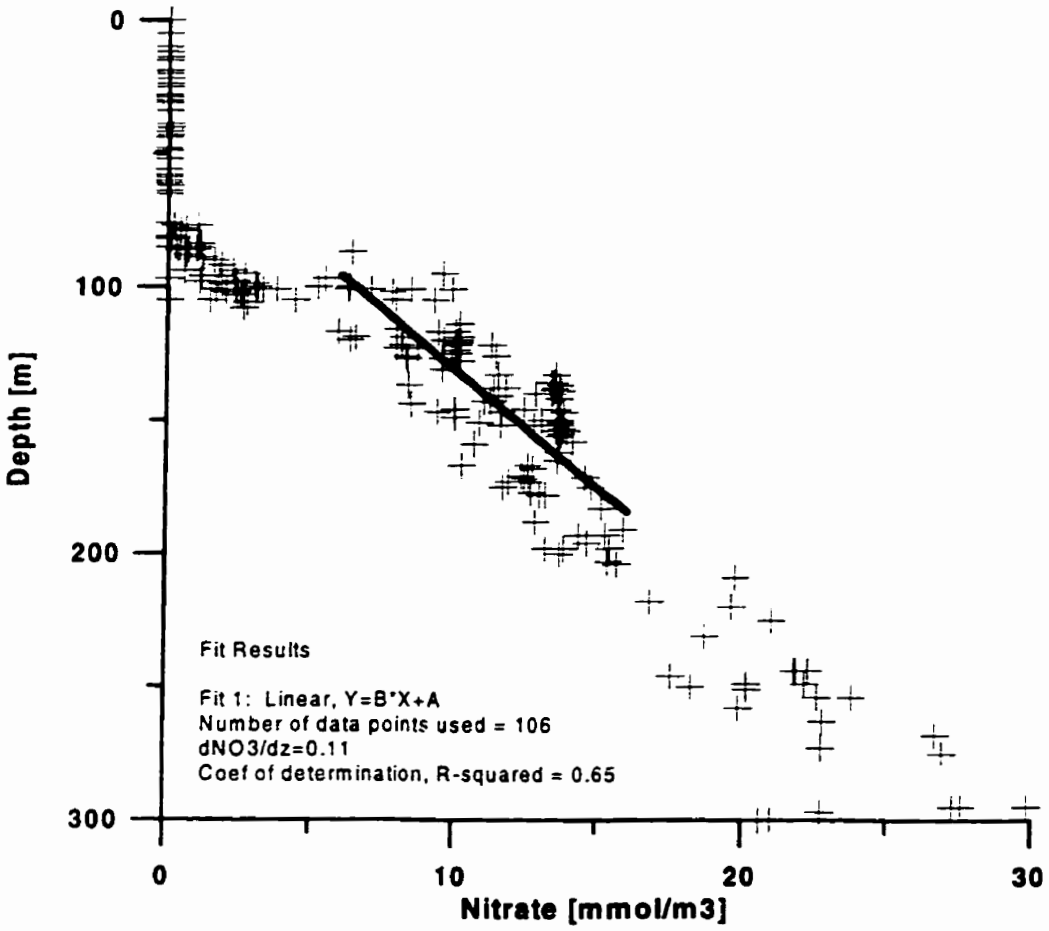

Figure 3.8: Scatter diagram of nitrate [mmolN m^{-3}] versus depth [m]

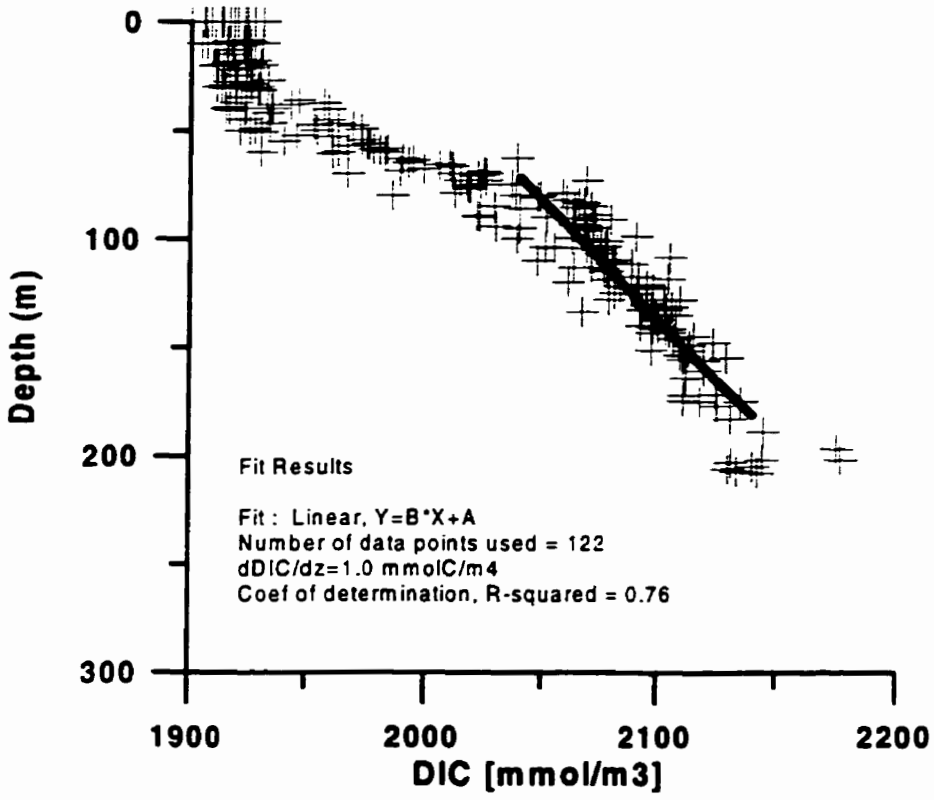

Figure 3.9: Scatter diagram of dissolved inorganic carbon [mmolC m^{-3}] versus depth [m]

Table 3.4: Selected Parameters for Velocities and Eddy Diffusivity Coefficients

Vertical velocity w at D_{ez}	$(1 \pm 2) \cdot 10^{-8}$ m s^{-1}
Vertical eddy diffusivity K_v at D_{ez}	$(7 \pm 6) \cdot 10^{-5}$ m^2 s^{-1}

Table 3.5: Average ($\pm SE$) Vertical Gradients of Nitrate, Dissolved Inorganic Carbon, and Temperature

Vertical nitrate gradient	(0.11 ± 0.02) mmolN m^{-4}	this study
Vertical carbon gradient	(1 ± 0.1) mmolC m^{-4}	this study
Vertical temperature gradient	(0.1 ± 0.01) K m^{-1}	this study

Table 3.6: Difference between Average Nitrate and Dissolved Inorganic Carbon Concentrations, and Average Temperature in the upper 100 m and in the Entrained Water from 120 m and their SE.

Nitrate concentration	(5 ± 1) mmolN m^{-3}	this study
Carbon concentration	(50 ± 5) mmolC m^{-3}	this study
Temperature	(5 ± 1) °C (298 K)	this study

3.3.3 Estimating source and sink terms, and boundary conditions

Biological uptake of nitrate and inorganic carbon.

Nitrate uptake in the western equatorial Pacific was measured as described in Chapter 2; average integrated rates of nitrate uptake measured at several stations along the equator ($\pm SE$) were, during normal conditions, about 0.15 mmolN/m^2/day ($\pm$0.05). The sink of dissolved inorganic carbon in the euphotic zone, i.e., the biological uptake of inorganic carbon associated with new production was obtained by multiplying the uptake of nitrate by the Redfield ratio (6.6 mol:mol). The average integrated biological uptake of inorganic carbon associated with nitrate uptake ($\pm SE$) was thus 1.0 mmolC m^{-2} d^{-1} ($\pm$0.35).

Air-sea flux of CO_2.

Studies of air-sea flux of CO_2 (Ishii and Inoue, 1995; Hisayuki et al., 1996) that have been performed in the western equatorial Pacific suggest that the flux of CO_2 in this area is ca. 1.0 mmolC m^{-2} d^{-1} ($\pm$0.5) from the ocean to the atmosphere.

Net surface heat flux and penetrative irradiance.

Net surface heat flux and penetrative irradiance through the depth of 100 m were estimated from measurements of meteorological parameters and downwelling and upwelling irradiance (see Section 2.2 for details). Average net surface heat flux over the western equatorial Pacific in normal conditions was 35 W m^{-2} ($\pm$15) (see Chapter 4) which agrees with the reported range of values (10 to 100 W m^{-2}) in the literature (Esbensen and Kushnir, 1981; Reed, 1985; Enfield, 1986; Gordon, 1989; Wijesekera and Gregg, 1996; Song and Friehe, 1997; Cronin and McPhaden, 1997; Wang and McPhaden, 1997). The uncertainty in net surface heat flux includes random errors due to the resolution of our instrument, and systematic errors associated with approximating the heat fluxes using the bulk formulas. The details on estimation of uncertainty in net surface heat flux are given in Chapter 4. The penetrative flux at 100 m depth was small, i.e., ca. 0.5 W m^{-2} (J. Sildam, personal communication).

Following the protocols discussed above, I estimated sources and sinks of nitrate, dissolved inorganic carbon, and temperature, and, as well, the boundary conditions (Table 3.7).

Table 3.7: Sources and Sinks of Nitrate, Dissolved Inorganic Carbon, and Temperature and the Boundary Conditions

Process	Average	Uncertainty	Reference
Nitrate uptake [mmolN m^{-2} d^{-1}]	0.15	±0.05	this study
Inorganic carbon uptake [mmolC m^{-2} d^{-1}]	1.0	±0.35	this study
Air-sea flux of CO_2 [mmolC m^{-2} d^{-1}]	1.0	±0.5	Ishii, 1995
Net surface heat flux [W m^{-2}]	35	±15	this study
Penetrative irradiance [W m^{-2}]	0.4	±0.4	this study

3.4 The nitrate, carbon and heat balances

Nitrate and carbon balances for the euphotic zone of the western equatorial Pacific were calculated as the differences between the net physical supply of nitrate or dissolved inorganic carbon into the euphotic zone and their respective sinks in the euphotic zone due to biological consumption. Similarly, the heat balance was estimated as the difference between heating rates from the net surface, and gains and losses from the upper layer by fluid transport of heat and penetrating irradiance. Uncertainties in advective and diffusive fluxes were calculated from uncertainties in velocities, eddy diffusivity coefficients, and gradients of nitrate, temperature and dissolved inorganic carbon using the expressions for propagation of errors (Bevington, 1969) shown in Appendix C.

3.4.1 The nitrate balance

To estimate the nitrate balance for the western equatorial Pacific region, the net physical rate of supply of nitrate was compared to biological consumption, i.e. integrated ^{15}N-labeled nitrate uptake over the depth of the euphotic zone (Wilkerson and Dugdale, 1992). Both

the estimates of production from measurements of net supply of nitrate into euphotic zone, and from ^{15}N-labeled nitrate uptake, represents a means of measuring the new production (Dugdale and Goering, 1967). I assume that ^{15}N-labeled nitrate incorporated into particles is quantitatively equivalent to the organic matter exported from the euphotic zone.

The results in Table. 3.8 and Figure 3.10 suggest that the dominant process for the supply of nitrate in the euphotic zone of the western equatorial Pacific is the vertical diffusive flux. Vertical advection and horizontal advective and diffusive fluxes appear to be less important components of the nitrate budget. The estimated net physical supply of nitrate in the euphotic zone (0.69 $\pm$0.60 mmolN m^{-2} d^{-1}) is not significantly different from the estimated biological consumption (new production) within the surface layer (0.15 $\pm$0.05 mmolN m^{-2} d^{-1}).

Possible reasons for uncertainties of the nitrate balance. One possible source of error may be in K_v and thus the vertical turbulent diffusive flux. Previous studies have estimated vertical turbulent flux of nitrate in the euphotic zone in the western equatorial Pacific: Mackey et al. (1995) determined the flux from eddy diffusivity obtained from an empirical relationship between K_v and gradient Ri, and from the measured nitrate gradient, and found a value of 0.2 mmolN m^{-2} d^{-1} (using K_v 10^{-5} m^2 s^{-1}). Peña et al. (1994) used net surface heat flux and the relationship between nitrate and temperatue to obtain the vertical turbulent flux of nitrate. They suggested values of order 0.2–0.3 mmolN m^{-2} d^{-1}, which corresponds to my measured values of new production. However, the vertical turbulent flux still remains to be determined accurately, since measurements of turbulent mixing are scarce and difficult to perform. The only direct measurements estimated K_v of 10^{-4} m^2 s^{-1} at the surface decreasing to 10^{-6} m^2 s^{-1} at 200 m. There is therefore, a large uncertainty in the vertical mixing rate.

Another source of error may be that the meridional advection transports nitrate away from the equator before it can be consumed by phytoplankton. In addition, the uncertainties associated with measuring biological uptake of ^{15}N–nitrate (e.g., underestimating due to nitrate uptake below 1% of surface light level (Clark, 1997), or overestimating due to tracer enrichment (see Chapter 2) may also contribute to error in nitrate balance.

I assumed that nitrate that is taken up by phytoplankton is exported from the euphotic zone to the deep ocean primarily in particulate form (PON), and therefore I do not take into account the export of dissolved organic nitrogen (DON) from the euphotic zone by advective and diffusive processes. DON was not measured on our cruises. However, recent studies have shown that new production in the oligotrophic ocean measured by ^{15}N-nitrate uptake can be underestimated up to 50 per cent when the production of DON is not taken into account (Bronk et al., 1994). Bronk et al. (1994) also suggested that the rates of DON production in the oligotrophic ocean are high (probably due to sloppy feeding and excretion by functional and dying cells). Using the upper asumption I may thus be underestimating the export of nitrogen from the euphotic zone. However, Flynn and Berry (1999) recently suggested that the loss of organic nitrogen during marine primary production may be significantly overestimated when using ^{15}N substrates.

Table 3.8: **The nitrate balance [mmolN m^{-2} d^{-1}]**

Process	Flux mmolN m^{-2} d^{-1}	Uncertainty	notes
Vertical diffusion	0.7	±0.6	probable upper bound
Vertical advection	0.005	±0.01	probable lower bound
Zonal advection	0.05	±0.04	this study
Meridional advection	−0.04	±0.03	probable lower bound
Horizontal diffusion	−0.03	±0.02	probable lower bound
Total physical flux	0.69	±0.60	
Biological uptake (new production)	−0.15	±0.05	this study
Net	0.54	±0.62	

In my analysis, I also assume that the atmospheric deposition of nitrogen is small compared to other sources of nitrate. Previous studies have suggested that atmospheric sources of nitrate from wet and dry deposition are small in the area where our observations were conducted (Duce et al., 1991). In addition, my vertical sections of nitrate distributions along the cruise track (Chapter 2) show that there is no observable nitrate gradient near the surface. My assumptions agree with studies of the nitrate balance in the Sargasso Sea that

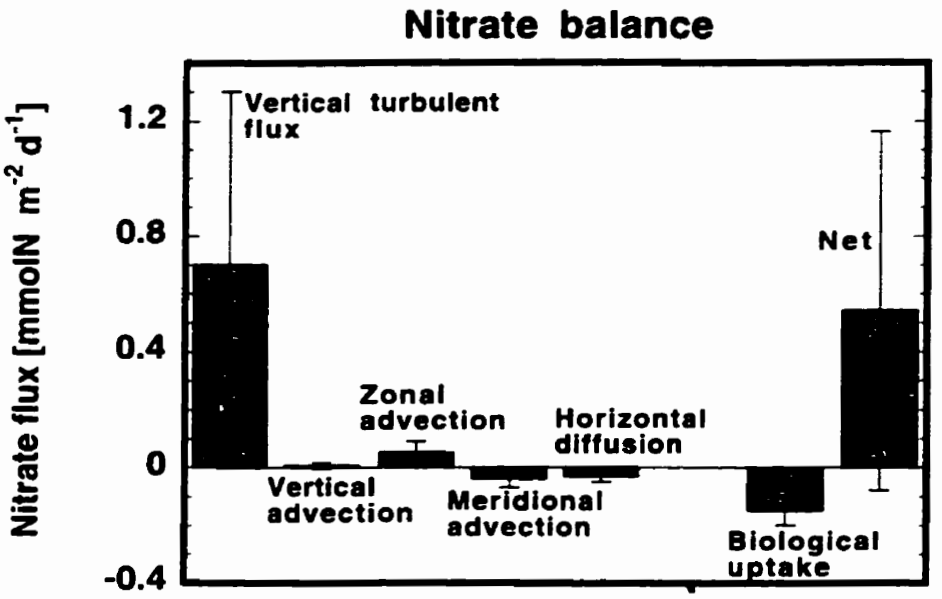

Figure 3.10: Nitrate balance in the western equatorial Pacific (mmolN m^{-2} d^{-1}). Net refers to sum of all the fluxes.

have shown the atmospheric deposition of nitogen is small and does not play an important role in the nitrogen cycle (Knap et al., 1986; Michaels et al. 1993; Siegel et al, 1998).

Another assumption employed in my study is that new production associated with fixation of nitrogen was small in the western equatorial Pacific and could thus be neglected. I am not aware of nitrogen fixation measurements in the western/central equatorial Pacific. It has been observed that in some parts of the ocean, nitrogen fixation can contribute significantly to new production (Capone and Carpenter, 1982; Carpenter and Romans, 1991; Karl et al., 1997). In the tropical southwestern Pacific, *Trichodesmium* blooms have been detected by satellite observations (Dupouy et. al, 1988). However, it has been suggested that *Trichodesmium* is unknown within the western equatorial Pacific region (Dupouy et al., 1988).

Comparison with other studies. The complete nutrient balance analysis for the western Pacific has not yet been performed. Previous studies have estimated different individual components of the nitrate budget. Peña et al. (1994) and Mackey et al. (1995) estimated vertical turbulent fluxes of order 0.2-0.3 mmolN m^{-2} d^{-1}. Rodier and Le Borge, (1997) measured ^{15}N uptake at 167°E.

3.4.2 The carbon balance

The results in Table 3.9 and Figure 3.11 suggest that dissolved inorganic carbon is primarily supplied into the euphotic zone by the vertical diffusive flux. As with nitrate, the net physical supply of dissolved inorganic carbon is comparable (4.5 $\pm$5.2 mmolC m^{-2} d^{-1}) to the losses from the euphotic zone due to biological uptake (-1.0 $\pm$0.35 mmolC m^{-2} d^{-1}).

Possible reasons for uncertainties in carbon balance. Again as with nitrate, the possible reasons for the error in carbon balance include errors in K_v and the consequent vertical turbulent flux. Another reason may be the uncertainties in estimated air-sea exchange of CO_2. In addition, I may be underestimating the export of carbon from the euphotic zone due to the following reasons:

Firstly, I assume that dissolved inorganic carbon and nitrate are taken up by phytoplankton and exported out of the euphotic zone in Redfield ratio (i.e., new production in carbon units was calculated by multiplying nitrate uptake by 6.6 mol:mol). Previous studies have indicated that using the Redfield ratio to convert new (nitrate) production to carbon may lead to significant underestimation of organic export from the euphotic zone (Sambrotto et al., 1993). In addition, POC:PON ratio in suspended matter in the euphotic zone measured on our cruises (see Chapter 4) was also higher (9.5mol:molN) than the nominal Redfield ratio (6.6 mol:mol). Using that ratio the estimated uptake of dissolved inorganic carbon would be higher (1.4 vs. 1.0 mmolC m^{-2} d^{-1}).

Secondly, I neglected the export of dissolved organic carbon (DOC) and particulate inorganic carbon ($CaCO_3$), from the euphotic zone, as well as the export due to vertical migration of zooplankton. Recent modeling efforts suggest that a significant portion of the new production can be removed as DOM (Toggweiler, 1989). Studies in the central equatorial Pacific (Quay, 1997), where biological production is higher than in the western region, suggest that DOC export from the surface layer is ca. 4-8 mmolC m^{-2} d^{-1}. I expect this export to be smaller in the western equatorial Pacific. However, the measurements of DOC were not performed on our cruises, and therefore I could not estimate the significance of this term in carbon export from the euphotic zone.

Thirdly, I also neglected the consumption of DIC in the euphotic zone associated with other sources of nitrogen (atmospheric nitrogen, dinitrogen fixation (Karl et al., 1997; Walsh, 1996), which may increase the export of carbon from the euphotic zone.

Comparison with other studies Studies of carbon balance have been conducted in the eastern equatorial Pacific (Quay, 1997), where upwelling is more important mechanism than diffusion. The balance was achieved within 30–50 per cent. In the western part of the equatorial band, individual components of the carbon budget have been estimated, such as air-sea flux of CO_2, (Ishii and Inoue, 1995–used in our study), primary productivity (Mackey et al., 1997; Rodier and Le Borge, 1997), and export flux of POC (Rodier and Le Borge, 1997). However, I am not aware that the carbon budget analysis in the western equatorial Pacific has been performed so far, and therefore the comparison with previous

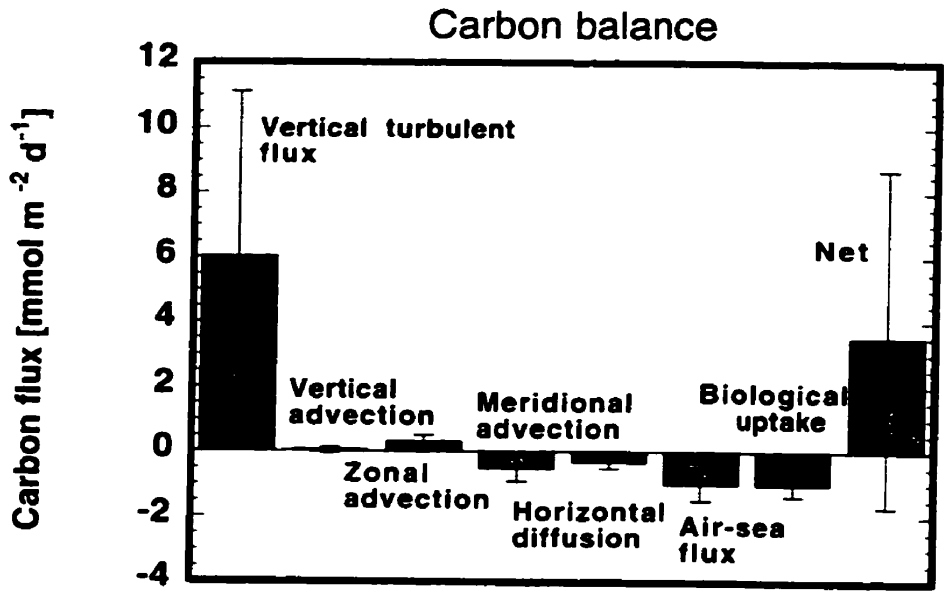

Figure 3.11: Carbon balance in the western equatorial Pacific (mmolC m^{-2} d^{-1}).

Table 3.9: **The carbon balance [mmolC m^{-2} d^{-1}]**

Process	Flux mmolC m^{-2} d^{-1}	Uncertainty	Notes
Vertical diffusion	6.0	±5.1	probable upper bound
Vertical advection	0.04	±0.08	probable lower bound
Zonal advection	0.3	±0.2	this study
Meridional advection	−0.5	±0.4	probable lower bound
Horizontal diffusion	−0.3	±0.2	probable lower bound
Air-sea exchange	−1.0	±0.5	Ishii, 1995
Total physical flux	4.5	±5.2	
Biological uptake (new production)	−1.0	±0.35	this study
Net	3.5	±5.2	

studies was not possible.

3.4.3 The heat budget

Table 3.10: **The heat balance [W m^{-2}]**

Process	Flux W m^{-2}	Uncertainty	Notes
Vertical diffusion	−28.2	±24.3	
Vertical advection	−0.2	±0.4	probable lower bound
Zonal advection	−4.0	±3.1	this study
Meridional advection	2.4	±2.0	probable lower bound
Horizontal diffusion	−1.5	±0.5	probable lower bound
Penetrative irradiance	−0.5	±0.3	this study
Total flux	-32.0	±24.6	
Net surface heat flux	35	±15	this study
Net	3.0	±28.8	

My study indicates that the vertical diffusive flux, and the net surface heat flux, are the largest components of the heat balance of the western Pacific Warm Pool (see Table

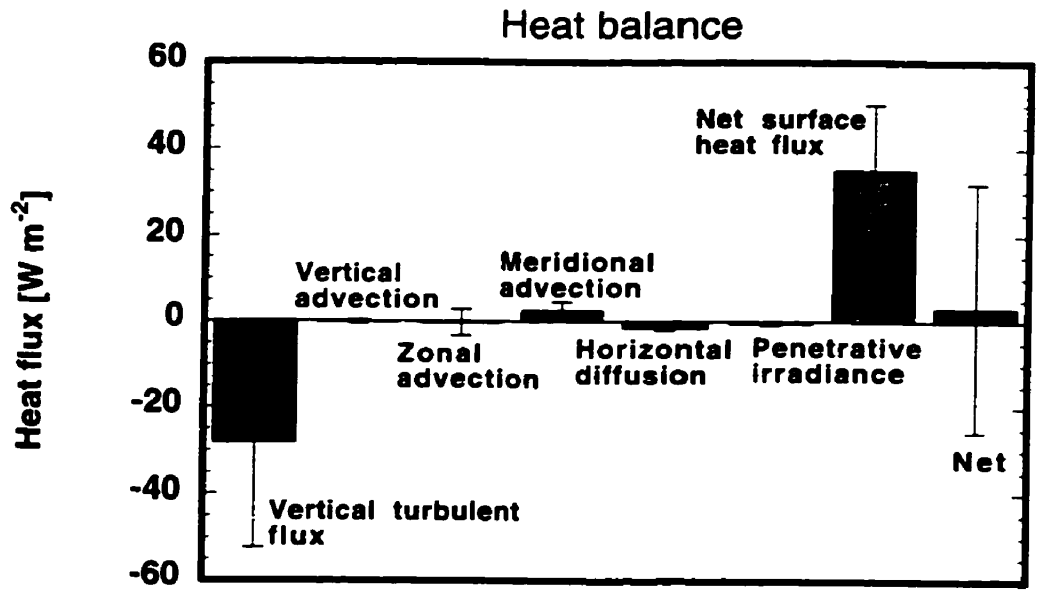

Figure 3.12: Heat balance in the western equatorial Pacific (W m^{-2}).

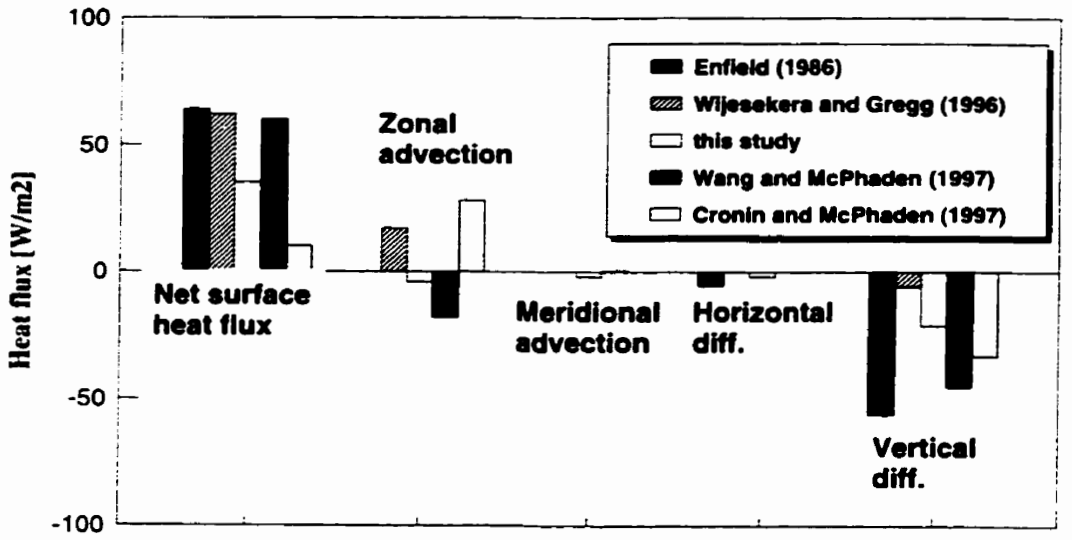

Figure 3.13: Comparison of heat balance components estimated by studies performed in the western equatorial Pacific.

3.10 and Figure 3.12), which is in agreement with previous studies of surface layer heat balance in the equatorial Pacific (Niiler and Stevenson, 1982; Enfield, 1986; Wijesekera and Gregg, 1996). Wang and McPhaden (1997) have suggested that zonal advection may play important role in cooling the upper surface layer in the Warm Pool area. However, their measurements were conducted at 165° E which is on the edge of the area that I define as the Warm Pool during normal conditions (i.e., $T > 29$°C). The turbulent flux of heat at the bottom of the euphotic zone (when using $K_v = 7 \cdot 10^{-5}$ m^2 s^{-1}) equals 28 W m^{-2} and is comparable to the net surface heat flux of 35 W m^{-2}. Unlike nitrate and dissolved inorganic carbon, a higher eddy diffusivity would be required to balance the net surface heat flux. The possible reason for this discrepancy may be in overestimating the net surface heat flux due to instrumental errors, errors associated with using bulk formulas, and due to short time and space scales of our observations. These errors will be addressed in more detail in the next chapter. All the components of the heat budget are in agreement with previous observations in the western equatorial Pacific (Enfield, 1986; Wijesekera and Gregg, 1996; Cronin and McPhaden; 1997; Wang and McPhaden, 1997). A comparison between different studies is presented in Fig. 3.13.

3.5 Discussion

My study presents the first attempt to evaluate balances of nitrate, carbon and heat in the western equatorial Pacific Warm Pool. The purpose of the study is to determine the relative importance of the processes that are responsible for distributions of nitrate, temperature and dissolved inorganic carbon. The evaluation is based on both direct measurements and values obtained by previous studies.

My study indicates that horizontal gradients of temperature, nitrate and, dissolved inorganic carbon are much smaller than the vertical ones in the euphotic zone in the western equatorial Pacific (as is true for most of the ocean); horizontal advective and diffusive fluxes are also small relative to vertical diffusive fluxes and can thus be neglected. The advective flux in the vertical direction is also smaller than the corresponding diffusive flux for nitrate,

temperature and dissolved inorganic carbon. It thus appears that the turbulent diffusion is the main mechanism for supply of nitrate and dissolved inorganic carbon into the euphotic zone in the western equatorial Pacific and for the loss of heat.

The reason why advection is relatively less important than diffusion can be conceptually explained as follows. Upwelling velocities in the equatorial Pacific are associated with the divergence of Ekman flow at the equator which is confined only to the upper ocean layer (40–80 m) (Wyrtki, 1981; Philander et al., 1987; Barber and Kogelschatz, 1989). Below this layer, there is a geostrophic flow toward the equator due to the general east-west slope of sea level along the equator; the convergence of this flow at the equator causes downwelling. For upwelling to bring nitrate–rich and cold water to the surface layer, cold and nutrient rich water must thus be available at depths of 40–80 m. In the western equatorial Pacific, the nutricline (i.e. the gradient that separates the nutrient-depleted the deep water nutrient reservoir) and the thermocline are 90–150 m deep (Barber and Kogelschatz, 1989; Chapter 2) and the water that is upwelled comes to the surface layer from above the thermocline/nutricline. Therefore, vertical advection does not significantly contribute to the supply of nitrate into the euphotic zone in the western equatorial Pacific and the loss of heat. The same conclusion can be made for dissolved inorganic carbon.

However, in the central equatorial Pacific, upwelling becomes relatively more important for the supply of heat, nitrate, and dissolved inorganic carbon into the euphotic zone than in the western part. Vertical velocities increase eastward of the date line, the thermocline and the nutricline shoals, and therefore upwelling may bring colder and nutrient-rich water to the surface.

My results show that the supply of nitrate and dissolved inorganic carbon into the euphotic zone of the western equatorial Pacific is higher than the losses due to biological consumption and air-sea flux of CO_2. The possible reason may be overestimating the eddy diffusivity coefficient K_v and nitrate and dissolved inorganic carbon fluxes at the bottom of the euphotic zone. (values for K_v that would balance the nitrate and carbon consumption are approximately 1-2 $\cdot 10^{-5}$ m^2 s^{-1}, which is smaller than the value used above, (i.e., 7 $\cdot 10^{-5}$ m^2 s^{-1}) In contrast, the gain of heat due to net surface heat flux was larger than the

loss associated with vertical turbulent flux. The imbalance of fluxes at the bottom of the euphotic zone and the biological uptake is of concern, since it questions my assumption that the turbulent flux of nitrate at the bottom of the euphotic zone equals new production. However, the factors responsible for this phenomenon are not well understood. One of the ways to further elucidate this phenomenon is by estimating K_z by means of independent methods (e.g., Thorpe, 1977). Another possible reason are uncertainties in estimated biological uptake of nitrate and dissolved inorganic carbon, that were addressed above.

The nitrate, carbon and heat budgets were estimated for normal conditions in the western equatorial Pacific. However, the relative importance of individual components in supplying heat, nitrate and carbon in the euphotic zone may vary on interannual scales associated with El Niño, and during higher frequency events such as westerly wind burst (Delcroix et al., 1993; Hemantha and Gregg, 1996). It has been shown that during El Niño conditions, the nutricline and the thermocline shoal in the western part of the equatorial Pacific (Barber and Kogelschatz, 1989; Radenac and Rodier, 1996; Chapter 2), and as a consequence, the supply of nitrate and dissolved inorganic carbon in the euphotic zone increases. In addition, variations in the rates of biological uptake (see Chapter 2), air-sea exchange of CO_2 (Ishii and Inoue, 1995), surface currents, and net surface heat flux (Chapter 4) were observed during El Niño compared to normal conditions. Mackey et al. (1997) also observed increased flow of nitrate to the east in upper 300 m at 155°E on the equator during El Niño.

In addition, the variation of different processes during higher frequency events, such as westerly wind bursts (Delcroix et al., 1993; Hemantha and Gregg, 1996), have been observed in the western equatorial Pacific. Westerly wind bursts are pulses of anomalous westerly surface winds in the western equatorial Pacific that last 6–10 days and have speeds of 5 to 20 m s^{-1} (McPhaden et al., 1992). They reverse the zonal surface current direction, reduce the warm pool heat content due to increased latent heat losses, and increase the subsurface entrainment flux of cold and nutrient richer subsurface water into the euphotic zone (Delcroix et al., 1993; Hemantha and Gregg, 1996). It has also been observed that chlorophyll *a* concentration within the mixed layer increases following westerly wind bursts in

the western equatorial Pacific by nearly a factor of 3 (Siegel et al., 1995). Higher phytoplankton pigment biomass enhances the mixed layer heating by trapping more solar energy in the surface layer (Lewis et al., 1990), which may potentially affect the heat content of the upper surface layer. It has been hypothesized that the increase of chlorophyll *a* concentration that follows the westerly wind bursts is due to the entrainment of nitrate-rich subsurface waters into the euphotic zone (Siegel et al., 1995). It has been recognized that such injections of nutrients may affect the rate of new production (Eppley and Renger, 1988; Marra et al., 1990). Since as many as a dozen westerly wind events occur within a year (McPhaden et al., 1992; Harrison and Giese, 1991) in the western equatorial Pacific, these may potentially affect the annual rate of nitrate uptake in this area.

A possible extension of my study would be to use satellite and buoy observations to determine interannual and higher frequency variations of different budget components. The international TOGA Tropical Atmosphere-Ocean (TAO) buoy array in the equatorial Pacific consists of approximately 70 ATLAS thermistor chain moorings (Hayes et al., 1991) that measure surface wind speed, air temperature, SST, relative humidity and subsurface temperature at 10 depths in the upper 500 m, and a smaller number of PROTEUS moorings (Hayes et al., 1991) that in addition to meteorological variables, measure upper ocean currents and incoming shortwave radiation. These meteorological data (i.e., surface wind speed, air temperature, SST, relative humidity) and incoming shortwave radiation from those buoys that were located in the western equatorial Warm Pool can be used to calculate the variations in the surface heat flux. In addition, meteorological data, depth profiles of temperature, and currents can be used to detect the high frequency phenomena such as westerly wind burst events, and to evaluate the relative role of these events on heat fluxes. Through nitrate-temperature and nitrate-dissolved inorganic carbon relationships (see Chapter 4), the buoy data can also be potentially used for asessing the variations of nitrate and dissolved inorganic carbon fluxes during westerly wind burst events, and their role in annual new production and air-sea exchange of CO_2.

3.6 Implications for developing a 1-D model

Based on the results summarized in Tables 3.8, 3.9, and 3.10, the horizontal components of advective and diffusive terms, and the vertical advection in Eq. 3.1 are small relative to the vertical turbulent flux and the source/sink terms. Consequently, they can be neglected and Eq. 3.1 becomes a one-dimensional diffusion reaction equation

$$\frac{\partial \overline{X}}{\partial t} = K_v \frac{\partial^2 \overline{X}}{\partial z^2} - S_x \,. \tag{3.5}$$

where K_v is the vertical eddy diffusivity and S_x is sink/source. For nitrate ($\overline{X} = NO_3$), the sink term equals the uptake of nitrate by the phytoplankton; the Neumann (no flux) boundary condition ($\partial NO_3/\partial z = 0$) is applied at the air-sea surface, and the Dirichlet boundary condition ($NO_3 = NO_{30}$) is assumed at the base of the euphotic zone. For temperature ($\overline{X} = T$), at the air-sea surface, $\partial T/\partial z$ is assumed to be proportional to the net surface heat flux; at the base of the euphotic zone, the Dirichlet boundary condition ($T = T_0$) is assumed. For the dissolved inorganic carbon ($\overline{X} = DIC$), at the air-sea surface, $\partial DIC/\partial z$ is assumed to be proportional to the air-sea flux of carbon dioxide; at the base of the euphotic zone, the Dirichlet boundary condition ($DIC = DIC_0$) is assumed.

Eq. 3.5—subjected to the appropriate boundary conditions—describes the local rates of change in the distribution of a given scalar quantity $\overline{X}$, providing the local values of K_v, and S_x are known. Because the measurements of these physical quantities are so demanding, such an approach can be applied only at a discrete measurement sites and for a limited measuring time.

I used the assumption that in the western equatorial Pacific, nitrate, heat and dissolved inorganic carbon were primarily supplied into the euphotic zone by vertical turbulent diffusion in developing the idealized one-dimensional model for estimating new production and air-sea exchange of carbon dioxide in this area (Chapter 4).

3.7 Summary and Conclusions

My study presents the first attempt to simultaneously evaluate balances of nitrate, carbon and heat in the western equatorial Pacific. The purpose of the study was to determine the relative importance of the processes that are responsible for the distributions of nitrate, temperature and dissolved inorganic carbon. The evaluation is based on both direct measurements and values obtained by previous studies. Observations include horizontal components of the velocity, profiles of temperature, nitrate and dissolved inorganic carbon, measurements of biological uptake of nitrate and dissolved inorganic carbon, and observations of meteorological variables and absorption of solar radiation in the water column. Values for the vertical velocity, eddy diffusivity coefficients, meridional distributions of temperature, nitrate and dissolved inorganic carbon, and air-sea flux of CO_2 were obtained from previous studies that were performed in the western equatorial Pacific.

I conclude that in normal conditions, the vertical turbulent diffusion is primarily responsible for the supply of nitrate and dissolved inorganic carbon in the euphotic zone and for the loss of heat in the western equatorial Pacific. Vertical advection, and horizontal advective and turbulent fluxes appear to be less important components. The estimated supply of nitrate and dissolved inorganic carbon into the euphotic zone of the western equatorial Pacific was larger than the estimated losses due to biological consumption, and the air-sea flux of CO_2, while the loss of heat associated with vertical turbulent flux was smaller than the gain due to net surface heat flux. The possible reasons for these imbalances may be uncertainties in quantifying different components (net surface heat flux, air-sea exchange of CO_2, biological uptake, turbulent mixing) and lack of direct measurements (vertical advection).

The heat, nitrate and carbon balances were estimated for normal conditions in the western equatorial Pacific. However, the relative importance of individual components may vary on interannual scales associated with El Niño and La Niña, and during higher frequency events in the western equatorial Pacific, such as westerly wind burst. Further studies will be needed to investigate these variations. TOGA-TAO buoy and satellite observations can provide a mean to achieve this goal.

The results of my study may have implications for the prediction of the role of the western equatorial Pacific in biogeochemical cycles and climate variations, and for modeling efforts in this area of the ocean since they suggest that a 1-D case may be used to model nitrate and carbon fluxes, and consequently new production and air-sea exchange of CO_2 in this area of the ocean (see Chapter 4).

Chapter 4

Model for estimating new production and air-sea exchange of carbon in the western equatorial Pacific Warm Pool

4.1 Introduction

In the western equatorial Pacific Warm Pool, the climatological biomass and new production are low (Peña et al., 1994; Radenac and Rodier, 1996; Mackey et al., 1995). However, recent studies in this area have suggested pronounced interannual variability in new production during El Niño oscillations (see Chapter 2) and large variability in phytoplankton biomass associated with wind burst events (Siegel et al. 1995). Given the large size of the Warm Pool area, and this variability, the Warm Pool may markedly contribute to global new production. It has also been suggested that the equatorial Pacific may have a profound effect on global atmosphere CO_2 concentrations since it is potentially a strong oceanic source of CO_2 (Keeling and Revelle, 1985; Tans et al., 1990). As with new production, the flux of CO_2 across the sea surface undergoes interannual variations associated with El Niño conditions (Inoue and Sugimura, 1992; Feely et al., 1995; Inoue et al., 1996). It is thus important to estimate the variability in new production and air-sea exchange of CO_2

over the large spatial scales represented by the Warm Pool, and over time-scales consonant with the El Niño oscillations.

The new production can be determined by different methods, such as measuring ^{15}N–nitrate uptake (Dugdale and Goering, 1967; see Chapter 2), collecting sinking particles in sediment traps, or estimating the net flux of nitrate into the euphotic zone (see Chapter 3). The air-sea CO_2 flux can be estimated from measurements of the partial pressure difference of CO_2 across the air-sea interface and the coefficient of gas exchange. However, these methods are expensive and difficult to perform, and limited in both time and space. It is thus of interest to investigate methods that would allow one to estimate the new production and air-sea exchange of CO_2 from other parameters for which more frequent observations with better spatial resolution are available. Remote observations, coupled with suitable models, provide means to accomplish this goal.

Recently, Lewis (1992) and Peña et al. (1994) developed an idealized model for estimating the new production in terms of the net surface heat flux and nitrate-temperature correlation. Peña et al. (1994) used this model in estimating the mean annual integrated rate of new production in the warm pool area enclosed by the climatological 26°C contour and land boundaries; however, because they used the annual climatological data for surface heat fluxes, only large scale average values could be estimated. In this chapter, I present an initial validation of an advanced version of the model that couples both the new production and air-sea exchange of CO_2 with the net surface heat flux via nitrate-temperature and DIC-nitrate relationships. I used direct measurements of the surface heat flux components to estimate the new production and air-sea exchange of carbon. I defined the western Pacific Warm Pool as waters where $T > 29$°C. During normal conditions, the Warm Pool covered the western part of the Equatorial band (147°E–165°E), while during El Niño, the Warm Pool water ($T > 29$°C) expanded eastward over a much larger region (147°E–165°E) (see Chapter 2).

4.2 Coupling of nitrate and heat fluxes

In my study, I have concluded from scaling analysis (see Chapter 3) that in the western equatorial Pacific, nitrate, heat and inorganic carbon were primarily supplied to the euphotic zone by vertical turbulent diffusion. This conclusion on the importance of vertical processes was used in developing an idealized one-dimensional model for estimating new production and air-sea exchange of carbon dioxide in this area. To determine the interannual changes of new production or air-sea exchange of CO_2 over the entire western Pacific Warm Pool (T > 29°C), I adopted a more idealized model than that represented by Eq. 3.5. Firstly, the steady-state condition was assumed. Secondly, Eq. 3.5 was integrated over the entire euphotic zone to obtain the expression for the corresponding flux of a scalar quantity X at the base of the euphotic zone. This formalism was applied to the nitrate, heat and carbon fluxes in developing a one-dimensional model for estimating new production and air-sea exchange of CO_2 in the western equatorial Pacific.

Under the assumptions presented in more detail in Chapter 3, and further assuming that atmospheric sources of nitrate, dinitrogen gas fixation and chemoautotrophic nitrification are negligible in the euphotic zone of the western equatorial Pacific, the turbulent flux of nitrate, NO_3, at the base of the euphotic zone is determined by the expression,

$$K_v \frac{dNO_3}{dz} |_{z_d} = -\int_0^{z_d} S\, dz = P_n \,. \tag{4.1}$$

where P_n represents the new production or uptake (sink) of the nitrate integrated over the depth z_d of the euphotic zone.

The turbulent heat flux at the base of the euphotic zone is balanced by the difference between the net surface heat flux Q_n and penetrative irradiance Q_p (Lewis et al., 1990) at the base of the euphotic zone (Lewis, 1992; Peña et al., 1994)

$$K_v \frac{dT}{dz} |_{z_d} = \frac{Q_n - Q_p}{c_p \rho} \,. \tag{4.2}$$

where c_p is the specific heat of seawater and ρ is the seawater density.

Temperature and the nitrate concentrations are correlated in deeper water (Kamykowski and Zentara, 1986; Fig. 4.2) and, therefore, their vertical fluxes from the deeper ocean to

the euphotic zone are also related (Lewis, 1992; Peña et al., 1994). Using Eqs. 4.1 and 4.2, and assuming that eddy diffusivities for heat and nitrate are equal, the new production P_n can be then expressed as a function of the nitrate-temperature slope dNO_3/dT, and the heat fluxes (Lewis, 1992),

$$P_n = \frac{dNO_3}{dT} \frac{Q_n - Q_p}{c_p \rho} . \tag{4.3}$$

Since dNO_3/dT is relatively well documented (Zentara and Kamykowski, 1977; Fiedler et al., 1991; Peña et al., 1994; Halpern and Feldman, 1994), one can potentially determine the new production from satellite or buoy observations of the surface heat fluxes and therefore substantially improve the spatial and temporal coverage of the area.

4.3 Coupling of nitrate, heat, and carbon fluxes

Applying the same assumptions that were used for nitrate and heat fluxes to the flux of dissolved inorganic carbon (DIC), we obtain the expression

$$K_v \frac{dDIC}{dz} + F_{CO_2} = -\int_0^{z_d} S\, dz = P_c . \tag{4.4}$$

where the first term represents the vertical turbulent flux of DIC at the base of the euphotic zone, the second term is the air-sea flux of CO_2, and P_c is the new production expressed in carbon units.

The new production in carbon units can be expressed as $P_c = RP_n$, where R is the carbon to nitrogen ratio of the organic matter exported from the euphotic zone to the deep ocean. Assuming eddy difusivities for nitrate and carbon are equal, and using the expression for coupling of nitrate and heat fluxes (Eq. 4.3) we can calculate the air-sea flux of CO_2 as a function of the heat fluxes (Lewis, 1992),

$$F_{CO_2} = \frac{Q_{net} - Q_p}{c_p \rho} \frac{dNO_3}{dT} \left(R - \frac{dDIC}{dNO_3}\right) . \tag{4.5}$$

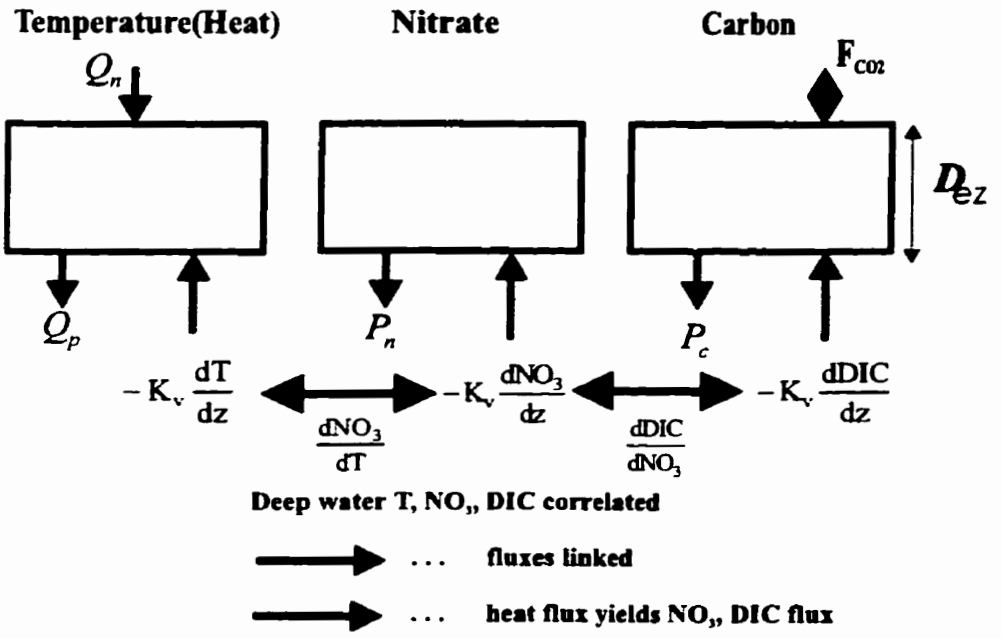

New production

$$P_n = \frac{Q_n - Q_p}{C_p \rho} \frac{dNO_3}{dT}$$

Air-sea exchange of CO2

$$F_{CO_2} = \frac{Q_n - Q_p}{C_p \rho} \frac{dNO_3}{dT} \left(R - \frac{dDIC}{dNO_3} \right)$$

Figure 4.1: Schematic diagram for coupling of heat (temperature), nitrate and carbon.

where $dDIC/dNO_3$ is the ratio of the vertical gradients in dissolved inorganic carbon and nitrate at the base of the euphotic zone. The schematic for coupling of temperature (heat), nitrate and carbon is presented in Fig. 4.1. Since heat fluxes can be obtained from satellite (Liu and Gautier, 1990; Jourdan and Gautier, 1994) or buoy observations (Wang and McPhaden, 1997; Lee, 1997), this model can facilitate evaluating the air-sea exchange of CO_2 over the larger area of western equatorial Warm Pool and over longer periods of time.

4.4 Methods and data

Data presented in this chapter were collected on the cruises which were described in more detail in Chapter 2. CTD observations, and measurements of nitrate and inorganic carbon were used to determine elemental ratios, while measurements of particulate organic nitrogen (PON) and particulate organic carbon (POC) were used to obtain the carbon to nitrogen ratio in suspended organic matter in the euphotic zone. POC:PON ratio was assumed to represent the C:N ratio of organic matter exported from the euphotic zone. Meteorological observations, and measurements of vertical profiles of downwelling irradiance and upwelling radiance were performed to estimate net surface heat flux and penetration of solar radiation. Elemental ratios, POC:PON ratios, net surface heat fluxes, and penetrative irradiance represented the parameters for calculating the new production and air-sea exchange of CO_2 via the coupling model.

4.4.1 Elemental ratios

In addition to collecting CTD and nutrient data, we also measured total inorganic carbon at each station at 18 sampling depths from 0 to 300 m. Vertical profiles of total inorganic carbon were obtained by automated colourmetric analysis (Ishii and Inoue, 1995). From the measured data, I generated two scatter diagrams of nitrate concentration as a function of temperature, and dissolved inorganic carbon concentration versus nitrate concentration. I calculated the average slopes of the nitrate-temperature relationship, and dissolved inorganic carbon-nitrate relationship by means of a linear regression (Sokal and Rohlf, 1995). These average values were obtained using only the data from below the euphotic zone (approximately 100–250 m), i.e., in the depths where the nitrate concentrations and temperature distribution are well correlated.

4.4.2 POC:PON ratio

Particulate organic nitrogen (PON) and particulate organic carbon (POC) were measured to determine the ratio of carbon to nitrogen (C:N) in the suspended organic matter in the

euphotic zone. Water samples for determining biological uptake of ^{15}N-labeled nitrate and ^{13}C-labeled carbon were collected at six fixed depths at each station. Samples were incubated as described in Chapter 2. PON and POC for incubated samples were determined using mass spectrometric analysis (Owens, 1988). For each water sample the POC:PON ratio was calculated. The average POC:PON in the euphotic zone for all samples was assumed to represent the C:N ratio in the organic matter exported from the euphotic zone. The uncertainties associated with this assumption are discussed in more detail in Section 4.5.4.

4.4.3 Net surface heat flux and penetrative irradiance through the base of euphotic zone

The net surface heat flux is defined as (Gill, 1982),

$$Q_n = Q_i - Q_b - Q_s - Q_l \ . \tag{4.6}$$

where Q_i is the shortwave solar radiation, Q_b is the net longwave radiation, Q_s is the sensible heat flux, and Q_l is the latent heat flux; these four terms were computed using bulk formulas (Gill, 1982).

The shortwave radiation is calculated as,

$$Q_i = Q_{i0}(1 - \alpha) \ . \tag{4.7}$$

where Q_{i0} is the solar radiation above the sea surface and α is surface albedo. Q_{i0} was measured by an Eppley precision pyranometer (PSP), and α was assumed to be equal 0.06 (Gill, 1982). The net longwave radiation is given by

$$Q_b = 0.985\sigma T_s^4(0.39 - 0.05{e_a}^{0.5})(1 - 0.7n_c) \ . \tag{4.8}$$

where $\sigma(5.67 \cdot 10^{-8}$ W m^{-2}K$^{-4})$ is the Stefan-Boltzmann constant, T_s is sea surface skin temperature, e_a is the water vapor pressure and n_c is the fraction of sky covered by cloud. T_s was measured by an EGG Heinmann KT19.85 infra-red instrument, and observations of n_c were reported in tenths from visual observations. Water vapor pressure, e_a, was calculated

from atmospheric pressure and air temperature, measured by an Setra SBP270, and relative humidity, R_h, measured by Vaisala HMP35C-L, (see Appendix B).

The latent and sensible heat fluxes are computed from the following bulk formulas.

$$Q_l = \rho_a L C_e (q_s - q_a) u_w \ . \tag{4.9}$$

$$Q_s = \rho_a c_{pa} C_h (T_s - T_a) u_w \ . \tag{4.10}$$

where ρ_a is air density, c_{pa} (J Kg^{-1} K^{-1}) is the specific heat of air, $L = 2.5 \cdot 10^6$ (J Kg^{-1}) is the latent heat of vaporization, and C_e ($1.5\ 10^{-3}$) and C_h ($0.83\ 10^{-3}$) are turbulent exchange coefficients for latent and sensible heat, respectively (Smith, 1980). T_a represents the temperature of air, measured by Vaisala HMP35C-L, q_s is saturation humidity, and u_w is wind speed. Specific humidity at saturation, q_s, is a function of saturation vapor pressure, ϵ_s, atmospheric pressure, p, and mixing ratio ϵ (see Appendix B).

Incoming solar radiation, barometric pressure, air temperature and humidity, wind velocity, and sea surface skin temperature were measured on board R/V Kaiyo and R/V Mirai. Hourly averages were used for the calculation of the components of the net surface heat flux. Finally, I calculated the mean values of the net surface heat flux averaged over the warm pool during normal and during two El Niño events.

The penetrating flux of visible radiation through the base of euphotic zone is defined by

$$Q_P = \int_{350}^{700} E_d(0^-, \lambda) \epsilon^{-\int_{0^-}^{D_{eu}} K(z,\lambda) dz} d\lambda \tag{4.11}$$

where $E_d(O-, \lambda)$ is the spectral irradiance just below the surface, and $K(z, \lambda)$ is the spectral attenuation coefficient. The downwelling irradiance $E_d(0-, \lambda)$ was measured using an upward-looking spectral irradiance sensor (Satlantic). The attenuation coefficient $K(z, \lambda)$ was obtained from vertical profiles of the spectral distribution of downwelling irradiance and upwelling radiance that was measured with a high precision profiling spectroradiometer (Satlantic) at each station; it was then interpolated between stations.

4.4.4 New production and air-sea exchange of CO_2

Integrated rates of new production, and air-sea flux of CO_2 were calculated from surface heat fluxes, elemental ratios, and C:N ratio of the organic matter sinking from the euphotic zone as presented in Sections 4.2 and 4.3. New production values predicted by the model were compared to integrated ^{15}N uptake over the depth of the euphotic zone (Chapter 2) that were measured on the same cruises as model parameters. Values of the air-sea flux of CO_2 were compared to the values found in literature (Ishii and Inoue, 1995).

4.5 Results

4.5.1 Model parameters

Nitrate-temperature relationship

The scatter diagram of nitrate versus temperature is presented in Fig. 4.2. I used data from the Warm Pool area during both normal (December 1995/January 1996) and El Niño events (November/December 1994 and December1997/January 1998). The average slope of the nitrate-temperature relationship was calculated using those data from the region below the euphotic zone (approximately 100–250 m, $T > 15°C$)., i.e. below the depth where biological processes (nitrate uptake and absorption of solar radiation by phytoplankton) significantly influence the nitrate and temperature distributions. At these depths, changes in nitrate and temperature were well correlated ($r^2 = 0.90$). The average slope value ($\pm$ SE) was -1.04 ± 0.02 mmol m^{-3} $°C^{-1}$ (with the 95 per cent confidence interval between -1.08 and -1.00 mmol m^{-3} $°C^{-1}$).

As can be seen from Fig. 4.2, nitrate and temperature in the surface layer of the Warm Pool were poorly correlated (the nitrate concentration was virtually zero), and thus surface temperature could not be used as a reliable predictor for nitrate as has been attempted before (Dugdale et al., 1989; Sathyendranath et al., 1991). In the region below 250 m ($T < 15°C$), the temperature was nearly constant, while the nitrate concentrations increased from 20 to 35 mmol m^{-3}.

Dissolved inorganic carbon-nitrate relationship

The scatter diagram of dissolved inorganic carbon (DIC) versus nitrate (NO_3) is shown in Fig. 4.3. I used data from the Warm Pool area during both normal (December 1995/January 1996) and El Niño conditions (November/December 1994 and December 1997/January 1998). As above, I calculated the average slope of the dissolved inorganic carbon-temperature relationship using only the data in the region below the euphotic zone (approximately 100–250) where dissolved inorganic carbon and nitrate were well correlated

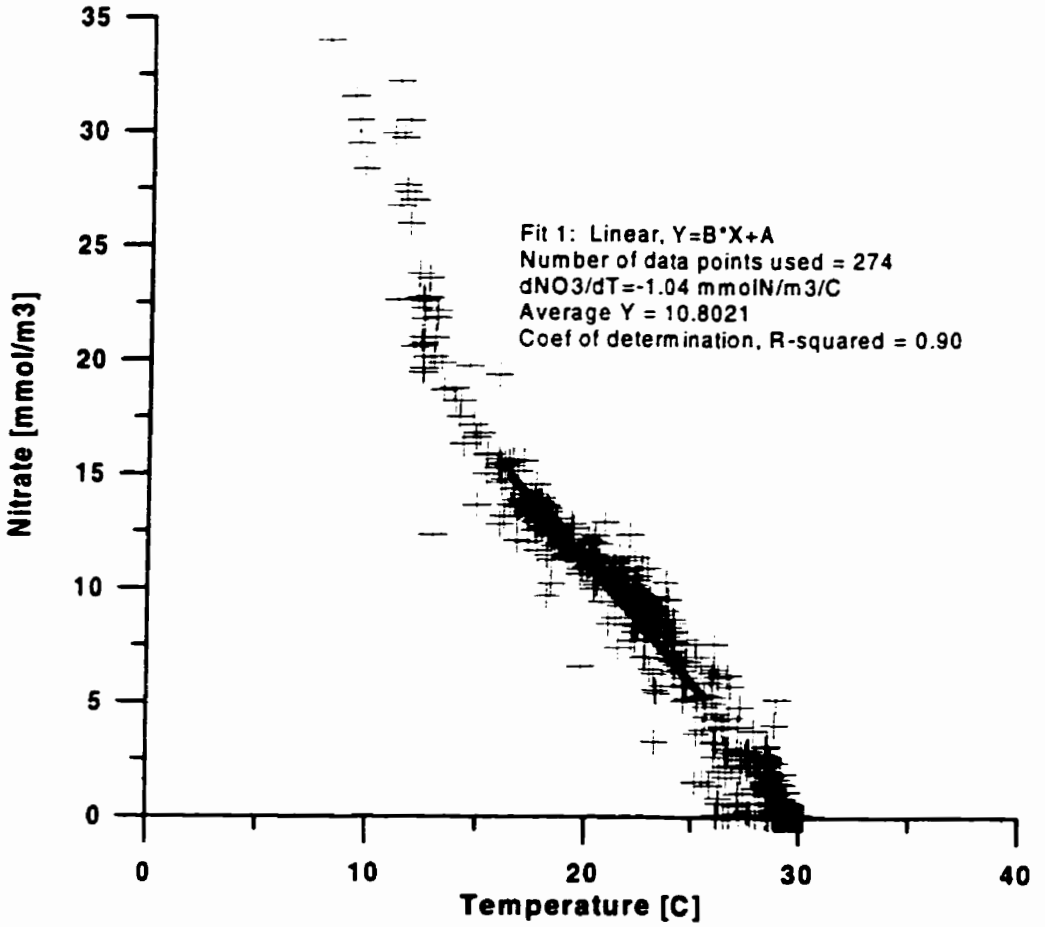

Figure 4.2: Scatter diagram of nitrate concentration [mmol m^{-3}] versus temperature [°C]. Data from the Warm Pool area during both normal (December 1995/January 1996) and El Niño conditions (November/December 1994 and December 1997/January 1998) are presented.

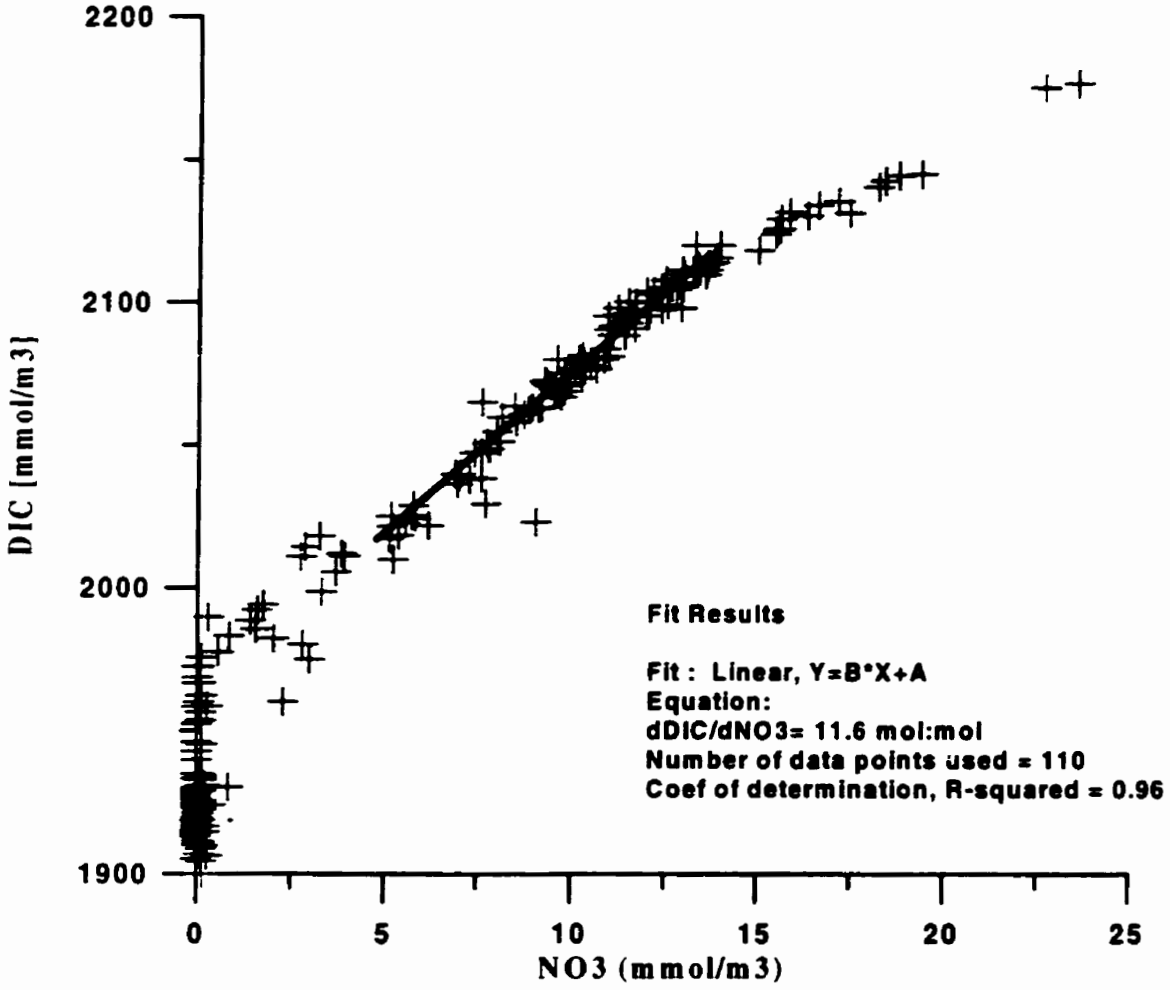

Figure 4.3: Scatter diagram of dissolved inorganic carbon [mmol m^{-3}] versus nitrate concentration [mmol m^{-3}]. Data from the Warm Pool area during both El Niño conditions (November/December 1994 and December1997/January 1998) are presented. During normal (December 1995/January 1996) data were not awailable.

($r^2 = 0.96$). The average slope value ($\pm$ SE) was 11.6 $\pm$0.2 mol:mol (with the 95 per cent confidence interval between 11.1 and 12.0 mol:mol) and was substantially higher than the Redfield ratio (6.6 mol:mol). Fig. 4.3 shows that nitrate and dissolved inorganic carbon in the surface layer of the Warm Pool were poorly correlated; nitrate concentration was virtually zero, while DIC concentration was decreased in the upper surface layer due to outgassing of CO_2 from the ocean to the atmosphere, and biological uptake. In the region below 250 m ($NO_3 > 15$ mmol m^{-3}), the average value of the slope ($\pm$ SE) of the dissolved inorganic carbon-temperature relationship was 6.5 $\pm$0.1 mol:mol.

POC:PON ratio

Depth distributions of POC:PON ratio for water samples collected in the Warm Pool area during both normal and El Nino conditions are presented in Fig. 4.4. Results show that the mean value of POC:PON ratio was higher than the nominal Redfield ratio for all depths. The average value ($\pm$ SE) in the euphotic zone was 9.5 ($\pm$0.1) mol:mol. SE was calculated as SD/$\sqrt{n}$ for all POC:PON values in the euphotic zone. I used this value to approximate the C:N ratio of organic matter exported from the euphotic zone for calculating the air-sea exchange of CO_2.

Net surface heat flux and penetrative irradiance through the base of euphotic zone

Table 4.1 shows the values of the surface heat flux components averaged over the Warm Pool during normal (December 1995/January 1996) and El Niño conditions (November / December 1994 and December 1997/January 1998), and their climatological values (Oberhuber, 1988). The net surface heat flux was dominated by the loss of latent heat and by input of solar radiation which is in agreement with previous studies from this area (Cronin and McPhaden, 1997, Song and Friehe, 1997). The value of the net surface heat flux slightly increased during El Niño 1994/95 (from 33 to 36 W m^{-2}) although this increase was not statistically significant. During El Niño 1997/98, the net surface heat flux was markedly higher (by a factor of 3) compared to normal conditions, primarily due to an increase in solar radiation. My values of surface heat fluxes during normal and El Niño 1994/95 event

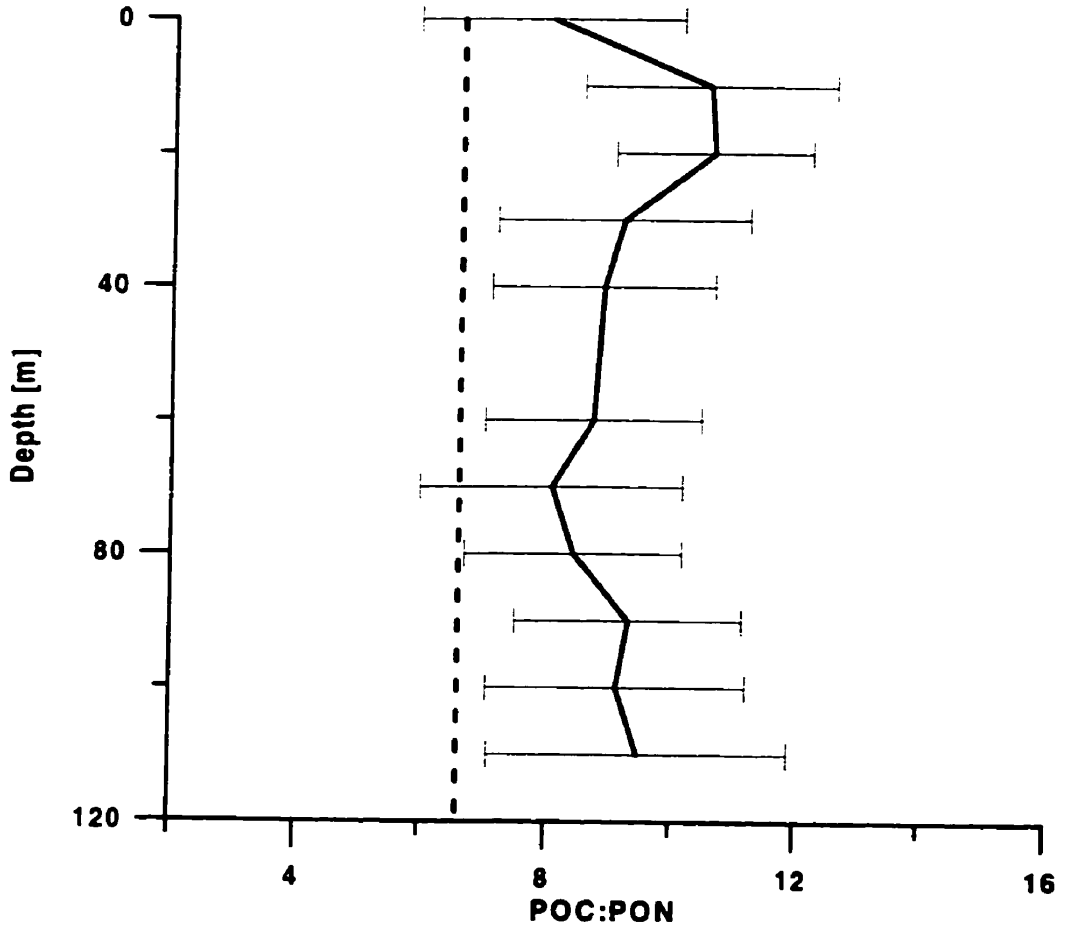

Figure 4.4: Depth distribution of particulate organic carbon to particulate organic nitrogen ratio [mol:mol] in the western Pacific Warm Pool. Data from the Warm Pool area during both normal (December 1995/January 1996) and El Niño conditions (November/December 1994 and December1997/January 1998) are presented. Dashed line represents Redfield ratio. Error bars represent SD of POC:PON measured at 18 stations.

are in agreement with climatological data. However, during the El Niño 1997/98 event the latent heat flux and solar radiation were higher than their climatological values.

Measured vertical profiles of photosynthetically available radiation (PAR) in the western equatorial Pacific showed that at the bottom boundary of the model (100 m), (PAR) was small (ca. 1 %) during both normal conditions and El Niño events (J. Sildam, personal communications). Little longitudinal and interannual variability of this profile was observed in the Warm Pool region (J. Sildam, personal communications).

Table 4.1: **Mean values of the surface heat flux components [W m^{-2}] in the Warm Pool during normal (December 1995/January 1996) and El Niño conditions (November/December 1994 and December 1997/January 1998), and their climatological values (Oberhuber, 1988).**

	Normal Dec95	El Niño 1994/95	El Niño 1997/98	Oberhuber climatology
Q_l	−97	−105	−126	−120 − 80
Q_s	9	5	2	0 − 10
Q_b	−44	−55	−49	−50 − 40
Q_i	184	201	272	150 − 210
Q_n	33	36	99	10 − 50

4.5.2 New production and air-sea flux of CO_2

Model parameters used for estimating the new production and air-sea flux of CO_2 are summarized in Table 4.2. The integrated rate of new production and their uncertainties (see Appendix C) in the western Warm Pool estimated from the model were 0.73 ±0.36 mmol m^{-2} d^{-1} during the normal conditions, 0.79 ±0.38 mmol m^{-2} d^{-1} during El Niño 1994/95 conditions, and 2.19 ±1.08 mmol m^{-2} d^{-1} during El Niño 1997/98 conditions, respectively. Table 4.3 shows the comparison of model results with integrated rates of ^{15}N biological uptake that were measured on the same cruises (see Chapter 2). Uncertainties in direct measurements represent SE of new production measured at several stations. Model predictions were, during both normal and El Niño conditions, larger than the average values

obtained by direct measurements (during normal and El Niño 1994/95 approximately by a factor of five, and during El Niño 1997/98 approximately by a factor of two). Computed values of the flux of CO_2 from the ocean to the atmosphere were, during normal conditions, El Niño 1994/95 and El Niño 1997/98, -1.5 $\pm$0.75, -1.66 $\pm$0.83 and -4.5 $\pm$2.25 mmol m^{-2} d^{-1}, respectively. Both new production and air-sea flux of CO_2 were larger during El Niño 1997/98 than during normal conditions.

Table 4.2: **Model parameters used for estimating the new production and air-sea flux of CO_2.**

nitrate-temperature slope	-1.04 mmol m^{-3} $^{o}C^{-1}$
DIC-nitrate slope	11.6 mol:mol
POC:PON ratio	9.5 mol:mol
net surface heat flux Q_n	33, 36 and 99 W m^{-2}

Table 4.3: **Mean values of integrated new production [mmol m^{-2} d^{-1}] and their uncertainties in the Warm Pool during normal and El Niño conditions. Uncertainties in model predictions were estimated as shown in Appendix C. Uncertainties in direct measurements represent SE of new production measured at several stations.**

	Normal	El Niño 1994/95	El Niño 1997/98
Model	0.73 ± 0.36	0.79 ± 0.38	2.19 ± 1.08
^{15}N uptake	0.15 ± 0.05	0.19 ± 0.05	1.16 ± 0.19

4.5.3 Errors in estimating model parameters

Contribution by errors in the net surface heat flux

The errors in estimating surface heat fluxes include systematic errors, random errors, and errors due to inadequate spatial and temporal data sampling (Hsiung, 1986). Systematic errors in data observations due to such factors as calibration stability and heating exposure

of instruments are difficult to estimate and were not assessed in my study; however, rigorous attention was paid to absolute calibration and minimization of these sources of error, and it can thus be expected that they were small by comparison to other sources. Another source of systematic errors was associated with approximating the heat fluxes using the bulk formulas. Several investigators have shown that under idealized measuring conditions (no errors in observations), the uncertainty in the net surface heat flux when using bulk formulas is in the range of 10 per cent (Hsiung, 1986; Wijesekera and Gregg, 1996).

Random errors resulted mainly from instrument resolution and spatial and temporal sampling errors. In this assessment, I considered only those random errors due to the resolution of our instruments (summarized in Table 4.4). Corresponding uncertainties in determining the four components of the surface heat flux were calculated using the expressions for propagation of errors (Bevington, 1969), as shown in Appendix C.

The four components of the net surface heat flux were computed from measured meteorological variables (Table 4.4) using Eqs. 4.7 to 4.9. Assuming that these components are not correlated, I estimated the uncertainty of the surface heat flux components due to random errors in measurements of meteorological variables using the expression for propagation of errors shown in Appendix C. The errors for Q_i, Q_b, Q_l, and Q_s, were 2 W m^{-2}, 15 W m^{-2}, 6 W m^{-2}, and 1 W m^{-2}, respectively. These values agree well with those (5 W m^{-2}, 20 to 30 W m^{-2}, 10 W m^{-2}, and 1-2 W m^{-2}) of previous studies of surface heat fluxes in the Equatorial Pacific (Zhang and McPhaden, 1995; Kessler and McPhaden, 1995). Using the estimated values of random errors, I obtained an uncertainty in the net surface heat flux of 15 W m^{-2}, which agrees with estimates of Cronin and McPhaden (1997) (15 W m^{-2}) and Wijesekera and Gregg, (1996) (10 W m^{-2}).

Since our shipboard measurements were performed only on a narrow cruise track on the equator and for a short period of time, I could not determine the spatial and temporal variation of the net surface heat flux from our data. The complete analysis of the spatial and temporal variation of net surface heat flux in the western equatorial Pacific has yet to be performed, however, some previous studies at least partially addressed interannual and interseasonal variations of different components of surface heat flux in the western

Table 4.4: **Instrument resolution.**

Measured variable	Instrument type	Instrument resolution
SST	EG&G Heinmann KT19.85	0.5°C
Air temperature T	Vaisala HMP35C-L	0.1°C
Humidity q	Vaisala HMP35C-L	2 per cent
Atmospheric pressure p	Setra SBP270	0.6 mB
Wind speed u	Young 05106	0.3 m/s
Solar radiation Q_t	Eppley PSP	1 per cent

equatorial Pacific (Weare, 1981; Wang and McPhaden, 1997; Ando and McPhaden, 1997; Lee, 1997).

Annual climatological data of the net surface heat flux in the tropical Pacific (Esbensen and Kushnir, 1981; Weare, 1981; Oberhuber, 1988) indicated the absence of marked changes in the net surface heat flux in the zonal direction over the western equatorial Pacific area, while the net flux varies meridionaly about 10 to 20 W m^{-2} from 10°N to 10°S. Wang and McPhaden (1997) observed a prominent seasonal variation (from 20 to 100 W m^{-2}) of net surface heat flux at 165° on the equator using TOGA-TAO buoy data. Lee (1997) also used TOGA-TAO data for the time period from 1992-1996 to estimate spatial and temporal variation of latent heat flux in the tropical Pacific. They concluded that in a meridional direction (from 8° S to 8° N), latent heat flux varies seasonally from 70 to 110 W m^{-2} in the western equatorial Pacific. In addition, higher frequency variations of net surface heat flux associated with westerly wind bursts have been observed in the western equatorial Pacific (Wijesekera and Gregg, 1996; Cronin and McPhaden, 1997; Song and Friehe, 1997). It follows from these observations that a large number of observations are necessary to capture the fluxes over longer periods of time and to reduce aliasing due to high frequencies, such as westerly wind bursts.

To estimate spatial and temporal variability in surface heat fluxes in more detail, one can use satellite (e.g., Liu and Gautier, 1990) or buoy data. In the western equatorial Pacific there is an array of 17 TOGA-TAO buoys which report the vector wind, SST, air

temperature, and relative humidity (Lee, 1997). Meteorological variables are collected each hour and from these values, daily averages are computed. By using buoy data, one can determine zonal and meridional variations of surface heat flux components over the western equatorial Pacific. Temporal variation of different surface heat flux components can also be estimated from buoy data using harmonic analysis (Wilks, 1995).

Contribution by errors in the nitrate-temperature, DIC-nitrate relationship, and POC:PON ratio

Slopes of the nitrate-temperature relationship and dissolved inorganic carbon-nitrate relationship were obtained by least-squares linear regression of measured data (Sokal and Rohlf, 1995). The standard error of the slope of the regression line was calculated as shown in Appendix C. The standard errors of the slope of the nitrate-temperature and dissolved inorganic carbon-nitrate relationship were ± 0.02 mmol $m^{-3}N\ {}^{\circ}C^{-1}$ (2%) and ± 0.2 mol:mol (3%), respectively.

The POC:PON ratio was obtained as the average ratio for all collected samples in the euphotic zone. The estimated standard error (Glantz, 1977) was ± 0.1 mol:mol (1 %). There may be an error associated with assumption that the POC:PON ratio in suspended organic matter is equal to C:N ratio of sinking flux. In my calculations I use the value of POC:PON ratio of 9.5, with estimated error of ± 1.5 (15 %). from the range of field observations of C:N ratio in sediment traps (Murray, 1989, Rodier an Le Borge, 1997). If sinking flux had a higher or lower C:N, my estimate of new production would be overestimated or underestimated accordingly.

Uncertainty in estimated new production and air-sea flux of CO_2

Based on data presented above, it appears that inaccuracies in the values of the net surface heat flux and C:N ratio dominate the estimation of the new production and air-sea flux of CO_2 via an idealized model. Errors in net surface heat flux, elemental ratios, and POC:PON ratio were propagated to the new production and air-sea flux of CO_2 using Eq. C.5 (Appendix C) and assuming that these parameters are not correlated.

Using values in Table 4.5, the estimated errors in the new production and air-sea flux of CO_2 are about 50 per cent (i.e., mmolN m^{-2} d^{-1} for new production, and $\sigma_{F_{co2}}$=0.8 mmolC m^{-2} d^{-1} for air-sea flux of CO_2). Results for the new production rates from direct measurements suggest that the difference in the rate of new production between El Niño 1994/95 and normal conditions is of order 0.04 mmolN m^{-2} d^{-1} ($< \sigma_{P_n}$=0.37), and 1.01 mmolN m^{-2} d^{-1} ($> \sigma_{P_n}$=0.37) between El Niño 1997/98 and normal conditions.

Table 4.5: **Selected parameters for error analysis.**

	Average	Uncertainty	Per cent
Q_n	35 W m^{-2}	±15	45
$b_{N,T}$	1.04 mmol m^{-3}N $°C^{-1}$	±0.02	2
$b_{C,N}$	11.6 mol:mol	±0.2	3
R	9.5 mol:mol	±1.5	15

4.6 Discussion

My study represents an attempt to estimate the integrated rates of new production and air-sea flux of CO_2 in the western equatorial Pacific Warm Pool, and to investigate their interannual variability associated with El Niño conditions. I used an integrated model to estimate new production and air-sea flux of CO_2 in terms of the following parameters: the surface heat fluxes; the relationships between nitrate and temperature; the relationships between nitrate and dissolved inorganic carbon; and the C:N ratio of the organic matter sinking from the euphotic zone. Since heat fluxes can be potentially obtained from satellite (Liu and Gautier, 1990; Jourdan and Gautier, 1995) or buoy observations (Wang and McPhaden, 1997; Lee, 1997), this model can be used to evaluate the new production and air-sea exchange of CO_2 over a large area of the western equatorial Warm Pool and over longer periods of time than is currently possible with my data.

Comparison with other studies. Peña et al. (1994) used this model for estimating the new production in terms of the net surface heat flux and the nitrate-temperature correlation in the warm pool area enclosed by the climatological 26°C and land boundaries; however, because they used the annual climatological data for surface heat fluxes, only large scale average values could be estimated. Previous studies have attempted to estimate the new production from satellite measurements of SST and the relationship between nitrate and temperature (Dugdale et al, 1989, Sathyendranath, 1991). However, my study (see Section 4.5.1) indicated that the surface temperature cannot be used as a reliable predictor for nitrate in the western equatorial Pacific; therefore these methods are not applicable. The air-sea flux of CO_2 has been previously estimated from satellite observations of SST and statistical relationships between measured pCO_2 and temperature (Stephens et al., 1995). Such an approach is limited since it requires the ship observations of pCO_2 that are expensive and provide inadequate spatial and temporal sampling. The advantage of my model is that it does not require the ship observations of pCO_2 and biological variables that are expensive and limited in both time and space.

4.6.1 Main findings

Nitrate-temperature relationship. In my study, I have observed a trimodal structure of the vertical profile of nitrate-temperature relationship in the western equatorial Pacific (i.e., 0–100 m nitrate was depleted and temperature was nearly constant; 100–250 m nitrate and temperature were well correlated; below 250 m the temperature was nearly constant, while the nitrate concentrations increased from 20 to 35 mmol m^{-3}). This is consistent with previous studies (Peña, 1994). The average (± SE) slope value of the relationship between 100–250 m (–1.04 ±0.02 mmol $m^{-3}N\ °C^{-1}$) agrees with those obtained in other studies in the equatorial Pacific (Pena, 1994; Halpern and Feldman, 1994). My findings thus corroborate earlier observations (see Chapter 2) that at the depths below the euphotic zone (100 m), nitrate uptake and absorption of solar radiation by phytoplankton do not significantly influence the temperature and nitrate distributions. These distributions are therefore primarily controlled by the mode of the water transport (i.e., turbulence in the

western equatorial Pacific).

Nitrate- dissolved inorganic carbon relationship. The value of the slope of the nitrate-dissolved inorganic carbon relationship below the euphotic zone (100–250 m) was higher than the nominal value of the Redfield ratio (11.6 vs. 6.6 mol:mol). Ratios of DIC to NO_3 that exceed Redfield ratio have been reported by previous studies (Laws, 1991; Sambrotto, 1993; Banse, 1994) in the surface waters of different parts of the world's ocean. The possible reason for the high value of the DIC: NO_3 ratio below the euphotic zone may be that organic matter exported out of the euphotic zone (and remineralized in the water column below the euphotic zone) is enriched in carbon. This is in agreement with high the C:N ratio (9.5 mol:mol) of the suspended organic material observed in the euphotic zone (see below). In addition, a fraction of organic matter may be exported from the euphotic zone as DOM, which is relatively nitrogen poor, and may thus also be responsible for an increase in the DIC:NO_3 ratio below the euphotic zone. Export of carbon from the the euphotic zone associated with other sources of nitrogen (atmospheric nitrogen, dinitrogen fixation (Walsh, 1996) may also increase the DIC: $NO_3 ratio$.

C:N ratio of the suspended organic matter. My study showed that the C:N ratio of the suspended organic matter in the euphotic zone (9.5 mol:mol) was higher than the nominal Redfield ratio. This is in agreement with previous studies that have reported high C:N ratios of suspended organic matter in the euphotic zone in the equatorial Pacific (8.9 mol:mol: Murray et al., 1989). Also, the C:N ratio can markedly vary in response to changes in nutrient and light limitation (Longhurst and Harrison, 1989; Goldman, 1986), with high ratios (up to > 17) observed in nitrate limited environments (Goldman, 1986; Dauchez et al, 1995). It is important to note that nitrate is depleted in surface waters of the western equatorial Pacific and it is therefore reasonable to expect C:N ratios that exceed the nominal Redfield ratio. In addition, some previous studies have indicated that carbon-nitrogen ratios in particulate matter exported from the euphotic zone may be markedly higher than nominal Redfield ratio (Laws, 1991; Sambrotto, 1993). In the equatorial Pacific, Rodier and Le Borge (1997) observed C:N ratios (6.9 mol:mol) in the sediment trap material at the base of

the euphotic zone close to the nominal Redfield ratio, while Murray et al. (1989) reported high C:N ratios (about 10 mol:mol). The possible reasons Rodier and Le Borge (1997) suggest for their observation of low C:N ratios include high abundance of bacteria (which have low C:N) on marine snow or feces (Karl et al., 1988); and a presence of feces with low C:N ratio, which are excreted by carnivorous diet on zooplankton.

Evidence for a net upward flux of carbon from deeper ocean into the euphotic zone. Lower C:N ratios (9.5 mol:mol) of sinking organic matter compared to DIC:NO_3 (11.6 mol:mol) suggest a net upward flux of carbon from the deeper ocean into the euphotic zone of the western equatorial warm pool. In the absence of horizontal export of DIC from the euphotic zone (see Chapter 3), the steady-state condition can be reached only with a non-zero flux of carbon from the euphotic zone across the sea surface. This agrees with the conclusion that the western Warm Pool is a source of CO_2 to the atmosphere (Ishii and Inoue, 1995).

Heat flux across the sea surface. The findings of my study indicate that the flux of heat across the sea surface is dominated by the loss of latent heat and by inputs of solar radiation which agrees with previous studies (Cronin and McPhaden, 1997). My data showed the following trends in changes of the surface heat flux components during El Niño: the solar radiation increased due to lower cloud cover over the warm pool, latent heat flux increased mainly due to higher wind speed, long wave radiation increased because of the increased SST, and sensible heat flux decreased due to smaller differences between the air temperature and SST. The net surface heat flux slightly increased during the moderate El Niño 1994/95 (from 33 to 36 W m^{-2}) although this increase was not statistically significant. In the extraordinary El Niño 1997/98, the net surface heat flux was markedly higher (by factor 3) than during normal conditions. The increase was primarily due to higher solar radiation. The values of the net surface heat flux agree with those (range 20–100 W m^{-2}) of previous studies (Esbesen and Kushnir, 1981; Weare et al., 1981; Hsiung, 1986; Reed, 1985; Wijesekera and Gregg, 1996).

New production and air-sea carbon flux. My model predicts that both the integrated rate of new production and the flux of CO_2 from the ocean to the atmosphere are larger during El Niño than during normal conditions in the western equatorial Pacific. The increase in new production during El Niño is in qualitative agreement with direct measurements of ^{15}N-nitrate uptake (see Chapter 2). My results in Chapter 2 suggest that the increase in new production during El Niño appears to be due to a higher vertical supply of nitrate into euphotic zone that is associated with observed shallowing of the nutricline. The higher air-sea flux of CO_2 during El Niño is also in agreement with previous studies that estimated CO_2 flux in the western Pacific from direct measurements of pCO_2 in the air and in the sea (Inoue et al., 1996). They postulate that the increase during El Niño may be a result of enhancement of vertical mixing.

Factors affecting the air-sea exchange of carbon. Positive correlation between new production and sea to air flux of CO_2 during El Niño is surprising for the following reason: The air-sea flux of CO_2 is in general determined by the partial pressure difference of CO_2 between the water and atmosphere, and the coefficient of gas exchange. The partial pressure of CO_2 in the ocean is controlled by temperature, salinity, total alkalinity, and DIC. DIC can vary due to phytoplankton production, and water transport. The net uptake of DIC associated with phytoplankton production decreases the partial pressure of CO_2 in the surface waters. In the Warm Pool area, the partial pressure of CO_2 in the water is higher than that in the air. I would thus expect that higher uptake of DIC by phytoplankton observed during El Niño (see Chapter 2) would decrease the partial pressure difference of CO_2, and therefore the flux of CO_2 from ocean to the atmosphere. In contrast to this expectation, the model results show an increase in sea to air flux of CO_2 during El Niño. The reason is lower C:N ratio (9.5 mol:mol) of downward organic flux compared to upward inorganic flux (11.6 mol:mol). During El Niño the upward flux of both nitrate and dissolved inorganic carbon into the upper surface layer increased. Assuming that nitrate limits new production and system is in steady-state, higher upward flux of subsurface nitrate-rich water into the euphotic zone increases new production and therefore downward flux of particulate organic nitrogen and carbon. However, carbon and nitrate are supplied into the euphotic zone in a

higher ratio than that exported, thus the net upward flux of dissolved inorganic carbon in the upper surface layer increase during El Niño. In absence of horizontal export of DIC from the euphotic zone for the steady-state condition to be reached, the flux of CO_2 from the ocean to the atmosphere must therefore increase during El Niño. The increase in new production and sea to air flux of CO_2 agree with direct measurements.

Model predictions vs. direct measurements. The predicted values of the CO_2 air-sea exchange during normal and El Niño 1994/95 are of the same order of magnitude as the those estimated by previous studies from direct measurements of partial pressures of CO_2 in the air and in the sea (Ishii and Inoue, 1995). The model values during El Niño 1997/98 are, however, significantly higher. This observation is in agreement with preliminary results of pCO_2 measurements collected during the same cruise tracks (Ishii, personal communication) that suggest that during El Niño 1997/98 the surface water was supersaturated with CO_2, and pCO_2 (sea) was higher than normally observed in this region. The magnitude of the new production predicted by the model are higher (by approximately a factor of 5) than those obtained by my direct measurements (Chapter 2).

4.6.2 Limitations of the model

Possible reasons for discrepancy between the model predictions and measurements are:

- errors in estimating the model parameters,
- uncertainties associated with model assumptions, and
- uncertainties in evaluation of ^{15}N biological uptake.

Errors in estimating the model parameters. The errors in estimating the model parameters consist of three potential sources: errors in the net surface heat flux, errors in estimating the nitrate-temperature and dissolved inorganic carbon-nitrate slopes, and errors associated with the interpretation of C:N ratio of organic matter exported from the euphotic zone. I have shown that the dominant source of error are uncertainties in estimating

the net surface heat flux. Possible reasons for potential overestimation of net surface heat flux include systematic errors, random errors, and the errors due to inadequate spatial and temporal sampling. These errors were explained in more detail in Section 4.5.3.

Uncertainties associated with model assumptions. Assumptions of my model were discussed in detail in Chapter 3. In my study, I did not evaluate possible covariance among the model parameters; Peña et al. (1994) observed that the variations of the surface heat flux and the nitrate-temperature relationship were not correlated. Due to lack of dissolved inorganic carbon measurements, I could not validate this assumption for correlation between heat flux and dissolved inorganic carbon-nitrate relationship. I would expect that similarly to the nitrate-temperature relationship, the dissolved inorganic carbon-nitrate relationship is not correlated with the surface heat flux. For the same reason I could not evaluate the possible covariance between DIC-nitrate relationship and POC:PON ratio in suspended organic matter, however, I am aware that they may be correlated.

When estimating the new production and air-sea exchange of CO_2, I neglected vertical and horizontal advection, horizontal diffusion, vertical component of the isopycnal flux. the atmospheric inputs of nitrate and nitrogen fixation. Scaling analysis in Chapter 3, however, showed that these assumptions are valid for the western equatorial Pacific. Results in (Chapter 3) show that I may have overestimated the supply of nitrate and inorganic carbon into euphotic zone by approximately 10 per cent since I did not include transports due to vertical and horizontal advection, and horizontal diffusion.

In my model, I assumed that the bottom boundary of the box model is at 100 m. Measured depth profiles of PAR reveal that in the western equatorial Pacific, this depth corresponded to approximately 1 per cent of surface light levels. Although the net growth at this light intensity (i.e., ca. 0.5 W m^{-2}) is still possible (Geider et al., 1986), no significant biological uptake was observed below this depth during normal and moderate El Niño conditions (see Chapter 2). Nitrate uptake below 100 m was however observed during strong El Niño 1997/98 conditions.

I also assumed that POC:PON ratio measured in the suspended organic matter (i.e., samples captured water bottles) in the euphotic zone represented the carbon to nitrate ratio

in organic matter that was exported out of the euphotic zone in the deeper ocean. This assumption may have potentially affected my result for air-sea flux of CO_2 in several ways.

Firstly, the C:N ratios measured in natural samples may be biased due to the detrital and heterotrophic material in the samples (e.g., presence of zooplankton (Rodier and Le Borge, 1997) and bacteria may decrease the C:N ratio (Karl et al., 1988), while presence of old detrital material may increase the C:N ratio).

Secondly, the C:N ratio of suspended matter may be different than that of sinking particles (i.e., collected by sediment traps). Karl and Knauer, (1984) observed higher C:N ratios in suspended matter compared to the sediment trap material in the northeast Pacific, while (Raimbault et al., 1999) reported lower C:N ratios of suspended material in the central Pacific south of equator. It has been sugested that the quantity and the composition of sinking material are strongly dependent on size distribution of phytoplankton and on the structure of the food web (Michaels and Silver, 1987). In the western equatorial Pacific the phytoplankton biomass is dominated by small cells (Rodier and Le Borgne, 1997). Most of this material is recycled in the euphotic zone and only small portion is exported out of the surface layer (Michaels and Silver, 1987, Legendre and Le Fevre, 1989). Particulate matter that is sinking out of the upper surface layer consists mainly of large phytoplankton, fecall pellets and marine snow (Legendre and Le Fevre, 1989). Is has been sugested that larger cells are less efficient in assimilating nitrogen than smaller cells (Kristiansen et al., 1994), and therefore have higher carbon content relative to nitrogen (Daly et al., 1999). In addition, faster remineralization of nitrogen in the water column (Christian et al., 1997) may also cause higher C:N ratio of the material collected by sediment traps. On the other hand, higher nitrogen content of zooplankton fecal pellets (Rodier and Le Borge, 1997) and high abundance of bacteria on marine snow or feces may lead to lower C:N ratio of sinking material (Karl et al., 1988) compared to suspended matter.

Thirdly, I assumed that most of the organic matter exported from the euphotic zone was transported by sinking particles (Eppley and Peterson, 1979), and therefore I neglected transport of dissolved organic matter (DOM) and the active transport of organic matter by vertical migrators. Measurements of DOM concentrations were not performed during our

cruises. Recent modeling efforts suggest that a significant portion of the new production can be removed as DOM (Togweiler, 1989) However, previous studies in the equatorial Pacific (Quay, 1997; Rodier and Le Borge, 1997) suggest that DOM export from the surface layer is small, and organic matter is exported from the euphotic zone primarily as POM. Significant export of relatively nitrogen poor DOM would potentially increase the C:N ratio of organic matter exported from the euphotic zone and therefore decrease the estimated air-sea flux of CO_2.

Finally, the assumption of steady-state was employed over the time interval of each cruise (ca. one month). Measurements of temperature, nitrate and dissolved inorganic carbon show this assumption is valid. The assumption of steady-state may be problematic over longer periods, since during wind burst events the distribution of temperature, nitrate and dissolved inorganic carbon in the upper surface layer change over the period of few days due to the entrainment of cold-nutrient rich subsurface water.

It is important to note that my model accounts for variations in air-sea flux of pCO_2 during El Niño due to changes in vertical supply of subsurface pCO_2-rich water to the euphotic zone (inferred from surface heat flux), and for variations in biological activity (alow for variable POC:PON ratio). It does not take into account the changes in pCO_2 flux that results from changes in SST during El Niño conditions since the the steady-state conditions are assumed.

Uncertainties in evaluation of ^{15}N biological uptake. Finally, the uncertainties in estimation of biological uptake of ^{15}N-nitrate may be a reason for discrepancy between model predictions and measurements. Recent studies have shown that new production in the oligotrophic ocean measured by ^{15}N-nitrate uptake can be underestimated up to 50 per cent when the production of DON is not taken into account (Bronk et al., 1994). In addition, methodological errors (see Chapter 2), and bias due to spatial and temporal variability can also contribute to discrepancies. Since my measurements were performed only on a narrow cruise track on the equator at discrete locations and discrete sampling depths, and for a short period of time, I could not evaluate the effect of variation of higher frequency events, such as westerly wind bursts (Delcroix et al., 1993; Hemantha and Gregg, 1996) on new

production. These events may potentially increase the annual rate of nitrate uptake in the western equatorial Pacific (see Chapter 3).

4.6.3 Summary

It appears that my model may be useful in predicting the new production and air-sea exchange of CO_2 using short-term observations at discrete locations. A better estimate of net surface heat flux and C:N ratio of organic matter exported from the upper surface layer are necessary to reduce the error in estimating both new production and air-sea exchange of CO_2. The primary advantage of this model is that one can potentially determine both the new production and CO_2 flux from satellite or buoy observations of the surface heat fluxes. The simplifying assumptions used in the model permit parameterization of the biogeochemical fluxes in terms of quantities that are able to be observed remotely for use in prediction of role of the Western Pacific region in global carbon cycles and climate variation.

4.7 Conclusions

Overall, the major findings of my study presented in this chapter can be summarized as follows:

- The vertical profile of the nitrate-temperature relationship showed trimodal structure in the Warm Pool region. Nitrate and temperature were well correlated at depths of 100–250 m.
- Dissolved inorganic carbon and nitrate were supplied from deep water in the euphotic zone in a ratio higher that the nominal value of the Redfield ratio.
- C:N ratio of the suspended organic matter in the euphotic zone was also higher that the nominal value of the Redfield ratio, although less than the supply ratio.

- Flux of heat across the sea surface was dominated by the loss of latent heat and by gains due to solar radiation.
- The net surface heat flux increased during El Niño events compared to normal conditions, primarily due to increase in solar radiation.
- The model predicted the increase in integrated rates of new production and the sea to air flux of CO_2 during El Niño compared to normal conditions, which is in agreement with direct measurements.
- The predicted values of the new production were larger than those obtained by direct measurements (during normal and El Niño 1994/95 by a factor of ca. 5, and during El Niño 1997/98) by a factor of ca. 2). The predicted values of the CO_2 flux were also higher that the literature values (ca., by a factor of ca. 2).
- The dominant sources of error were uncertaintes in estimating the net surface heat flux and uncertaintes in C:N ratio of organic matter exported from the upper surface layer.
- The simplifying assumptions used in the model permit parameterization of the biogeochemical fluxes in terms of quantities that are able to be observed remotely for use in prediction of role of the Western Pacific region in global carbon cycles and climate variation.

Chapter 5

Conclusions

This thesis research is an interdisciplinary attempt to consider together the physical, biological and chemical processes that influence the biological production and air-sea exchange of CO_2 in the warm waters of the western equatorial Pacific during normal and El Niño conditions. The main objective was to quantify identifiable differences in the rate of new production and air-sea carbon exchange between normal and El Niño conditions, and to parameterize these processes in terms of quantities that can be observed remotely by satellite or buoys for use in prediction of the role of the Western Pacific region in climate variation and global biochemical cycles.

Physical patterns in the western and central Pacific during normal and Niño conditions have been extensively described by previous studies. Although we know the changes in physical environment can have a significant effect on biogeochemical processes, these processes are still insufficiently understood since direct measurements are scarce. In this study, biogeochemical processes in the western Pacific Warm pool were quantified using an interdisciplinary approach which combines both direct measurements and a box model. Direct measurements included shipboard observations on four cruises. Data were collected during two years of normal conditions, and two years of anomalous conditions (the moderate El Niño event in 1994/95, and the strong El Niño event in 1997/98). Direct measurements of the rate of nitrate uptake (new production) along the equator are the first measurements of new production in the western and central Pacific performed so far during both El Niño and

normal conditions.

The null hypothesis tested in my thesis was that there were no quantitatively identifiable differences in the rate of heat storage, new production and air-sea carbon exchange between normal and El Niño conditions. I rejected this hypothesis by the following findings of my study:

- New production and air-sea exchange of CO_2, and net surface heat flux in the western Pacific Warm Pool increase during El Niño events.
- The magnitude of this increase strongly depends on the nature of El Niño (moderate vs. strong event).
- Variations in new production in the western and central equatorial Pacific on inter-annual time scales correlate well with the change of the nutricline depth during the eastward expansion of the Warm Pool.
- Simultaneous study of nitrate, carbon and heat budgets in the western equatorial Pacific suggest that the vertical turbulent diffusion is the main mechanism for the supply of nutrients and dissolved inorganic carbon into the euphotic zone, and for the loss of heat during normal conditions.
- Based on this conclusion on the importance of vertical processes, I developed a box model for indirectly estimating the rates of new production and air-sea CO_2 exchange in the Warm Pool from the net surface heat flux, elemental ratios, and the C:N ratio of the organic matter sinking from the euphotic zone.
- It appears that at the present time, the large inaccuracies in measurements of the heat fluxes allow only qualitative estimation of trends of the rates of new production during normal conditions and El Niño. The method may, however, provide means for estimating both the new production and air-sea flux of CO_2 from remotely-sensed observations for use in prediction of role of the Western Pacific region in global carbon cycles and climate variation.

- Further studies will be needed to estimate the relative importance of higher frequency events on biogeochemical processes in the western equatorial Pacific, such as westerly wind bursts. TOGA-TAO buoy and satellite observations can provide a means to achieve this goal.

Appendix A

The effects of corrected nitrate profile, and ^{15}N isotope-enrichment correction on the rates of new production

Tables A.1 and A.2 summarizes the effect of low-nitrate and isotope-enrichment corrections on the mean values of integrated (0-120 m) ^{15}N uptake (new production) in the western and central equatorial Pacific for two cruises; November/December1994 (El Niño (left) and December 1995/January 1996 (normal conditions). The results are shown for the measured uncorrected data, for data derived from the corrected nitrate profile (concentrations obtained by using chemoluminescence method applied in surface waters), and for the data corrected for the ^{15}N enrichment. The ^{15}N isotope-enrichment correction was computed using Harrison and Harris (1997) method (see below).

A.1 Harrison and Harris (1997) correction method

Harrison and Harris (1997) proposed a correction method based on an empirically-derived correlation between the ambient concentration, N_a, in the euphotic zone and the so-called

Table A.1: Mean (± SD) integrated new production [mmol m^{-2} d^{-1}] in WEP (147°E–165°E) obtained using the nitrate measured by Autoanalyzer and using low-nitrate measured by chemoluminescence method.

	Autoanalyzer	low nitrate
Normal (Dec 95/Jan 96)	0.15 ± 0.05	0.21 ± 0.08
El Niño (Nov/Dec 94)	0.19 ± 0.10	0.20 ± 0.09

Table A.2: Mean (± SD) integrated new production [mmol m^{-2} d^{-1}] in WEP (147°E–165°E) and CEP (165°E–165°W) obtained using the uncorrected data and using data corrected for isotope-enrichment.

	WEP Corrected	WEP Uncorrected	CEP Corrected	CEP Uncorrected
Normal (Dec 95/Jan 96)	0.15 ± 0.05	0.05 ± 0.07	1.37 ± 0.52	0.74 ± 0.31
El Niño (Nov/Dec 94)	0.19 ± 0.10	0.06 ± 0.03		

"half-saturation" constant (k_s), i.e.,

$$k_s = 15.44 + 1.21\,N_a\ . \tag{A.1}$$

where N_a is ambient nitrate concentration.

The value of the estimated half-saturation constant is used to determine the relative uptake at ambient nitrate concentration U_a and at the nitrate concentration after the addition of the ^{15}N isotope U_{a+t} as

$$U_a = \frac{N_a}{k_s + N_a}. \tag{A.2}$$

and

$$U_{a+t} = \frac{N_a + {}^{15}N}{k_s + N_a + {}^{15}N}. \tag{A.3}$$

The ratio of the two uptakes (i.e., the enhancement factor $E = U_{a+t}/U_a$) can be used to correct the experimentally measured uptake rate (G. Harrison, personal communication),

$$p_N^{corr} = \frac{p_N^{meas}}{E}\ . \tag{A.4}$$

Appendix B

Estimation of water vapor pressure, specific humidity at air temperature, and specific humidity at saturation

To estimate surface heat fluxes from meteorological measurements we calculated water vapor pressure, specific humidity at air temperature, and specific humidity at saturation, as presented bellow (Gill, 1982).

Water vapor pressure Water vapor pressure, e_a, was calculated as,

$$\frac{e_a}{p} = \frac{q_a}{(\epsilon + (1+\epsilon)q_a)} . \tag{B.1}$$

where q_a is the specific humidity at air temperature, p is the atmospheric pressure, measured by an Setra SBP270, and ϵ=0.62167 is a mixing ratio. The term q_a was obtained using Eq. B.6.

Specific humidity at saturation Specific humidity at saturation, q_s, is a function of saturation vapor pressure, e_s, atmospheric pressure, p, and mixing ratio ϵ;

$$\frac{e_s}{p} = \frac{q_s}{(\epsilon + (1+\epsilon)q_s)} . \tag{B.2}$$

therefore,

$$q_s = \left(\frac{1}{\epsilon}\left(\frac{p}{\epsilon_s} - 1\right) + 1\right)^{-1} . \tag{B.3}$$

and ϵ_s is,

$$\epsilon_s = 0.98 f_w 10^{\frac{(0.7859+0.3477T_a)}{(1+0.00412T_a)}} , \tag{B.4}$$

where 0.98 is a correction for salinity, and f_w is given by,

$$f_w = 1 + 10^{-6} p(4.5 + 0.0006{T_a}^2) . \tag{B.5}$$

Specific humidity at air temperature Specific humidity at air temperature, q_a, was obtained as,

$$q_a = \left(\frac{1}{R_h q_s} - \frac{1}{R_h} + 1\right)^{-1} .$$

to

(B.7)

where R_h is relative humidity measured by Vaisala HMP35C-L.

Appendix C

Statistics

C.1 Estimation of the slope of regression line and standard error of the slope

Slopes of temperature vs. depth, nitrate vs. depth, and dissolved inorganic carbon vs. depth (Chapter 3), and the nitrate-temperature relationship and dissolved inorganic carbon-nitrate relationship (Chapter 4) were obtained by least-squares linear regression of measured data (Sokal and Rohlf, 1995). The slope of the regression line b was calculated as

$$b = \frac{n(\Sigma XY) - (\Sigma X)(\Sigma Y)}{n(\Sigma X^2) - (\Sigma X)^2} \quad . \tag{C.1}$$

where X and Y are the independent and dependent variables, respectively and n is number of points in the sample. The standard error of the slope of the regression line, σ_b was calculated as (Glantz, 1977),

$$\sigma_b = \frac{1}{\sqrt{n-1}} \frac{\sigma_{x,y}}{\sigma_x} \quad . \tag{C.2}$$

where the variability about the regression line $\sigma_{x,y}$ was obtained as follows (Glantz, 1977),

$$\sigma_{x,y} = \sqrt{\frac{\Sigma(Y - (a + bX))^2}{n-2}} \quad . \tag{C.3}$$

C.2 Propagation of errors

Uncertainties in determining advective and diffusive fluxes in heat, nitrate, and carbon budgets (Chapter 3), and different components of the surface heat flux, new production, and air-sea flux of CO_2 (Chapter 4) were calculated using the expressions for propagation of errors (Bevington, 1969) as follows. Briefly, if the quantity, x, we wish to derive is a function of measured variables u, v,..., i.e.,

$$x_i = f(u_i, v_i, \ldots) . \tag{C.4}$$

the variance in the derived quantity σ_x can be calculated as (Bevington, 1969),

$$\sigma_x^2 = \sigma_u^2(\frac{\partial x}{\partial u})^2 + \sigma_v^2(\frac{\partial x}{\partial v})^2 + 2\sigma_{u,v}^2(\frac{\partial x}{\partial u})(\frac{\partial x}{\partial u})\ldots] , \tag{C.5}$$

where σ_u and σ_v are variances of u and v respectively, and $\sigma_{u,v}$ is the covariance.

C.3 Uncertainty in estimated new production and air-sea flux of CO_2

Errors in net surface heat flux and elemental ratios, and POC:PON ratio were propagated to the new production and air-sea flux of CO_2 using Eq. C.5 and assuming that these parameters are not correlated.

Since Q_p is negligible (see Chapter 3), Eqs. 4.3 and 4.5 can be rewritten as

$$P_n = \frac{Q_n}{c_p \rho} b_{N,T} , \tag{C.6}$$

$$F_{CO_2} = \frac{Q_n}{c_p \rho} b_{N,T} (R - b_{C,N}) , \tag{C.7}$$

where $b_{N,T}$ is the slope of nitrate-temperature relationship, $b_{C,N}$ is the slope of inorganic carbon-nitrate relationship, and R is C:N ratio of organic matter exported from euphotic zone to the deeper ocean.

The relative error in the new production is,

$$\frac{\sigma_{P_n}}{P_n} = \sqrt{\frac{\sigma_{Q_n}{}^2}{Q_n{}^2} + \frac{\sigma_{b_{N.T}}{}^2}{b_{N.T}{}^2}} \,. \tag{C.8}$$

and the relative error in air-sea flux of CO_2 is,

$$\frac{\sigma_{F_{co2}}}{F_{co2}} = \sqrt{\frac{\sigma_{Q_n}{}^2}{Q_n{}^2} + \frac{\sigma_{b_{N.T}}{}^2}{b_{N.T}{}^2} + \frac{\sigma_{b_{C.N}}{}^2}{(R - b_{C.N})^2} + \frac{\sigma_{b_R}{}^2}{(R - b_{C.N})^2}} \,. \tag{C.9}$$

Appendix D

Estimating the eddy diffusivity from fine-scale CTD measurements in the western equatorial Pacific

D.1 Introduction

Information about time and space scale of variability in turbulent fluxes of nutrients and heat in the euphotic zone is important for addressing ocean's role in biogeochemical processes and climate variation. To estimate turbulent fluxes of nutrients and heat, quantitative evaluation of the eddy diffusivity coefficient K_v is required. Since such evaluations are at present limited in time and space, values of K_v over larger ocean regions are often chosen somewhat arbitrarily or are adjusted in numerical models so as to force agreement of the simulated and the observed density and velocity fields (Gregg, 1987). A method which could estimate K_v over extensive oceanic regions would offer a means for indirectly estimating the new production and air-sea carbon exchange from the vertical fluxes of nitrate and inorganic carbon, respectively, at the bottom of the euphotic zone.

The eddy diffusivity coefficient K_v can be obtained directly by measuring the spread of tracer (Burke, 1994; Ledwell et al., 1993). The drawback of this method is that it is very

expensive since the tracer has to be monitored at specific depths and locations to provide an accurate estimate for K_v. An alternative approach is to evaluate eddy diffusivity from dissipation rates of turbulent kinetic energy using microstructure models (Gregg, 1987; Osborn 1980; Osborn and Cox, 1972; Hamilton et al., 1989; McDougall and Ruddick, 1992; Oakey, 1982; Oakey, 1988). Such direct microstructure measurements are still scarce due to high costs of instrumentation and cumbersome procedures (Gargett et al., 1993). Another possibility is to estimate the eddy diffusivity coefficient indirectly using fine-scale CTD measurements which are commonly available. When using indirect methods, the microscale dissipation is inferred from larger scale properties such as overturning lengths. Even when providing only a rough estimation of mixing, the indirect methods can offer enormous potential for widening our global base of dissipation estimates. The specific purpose of the study presented here was to investigate whether the rate of mixing can be inferred from CTD measurements that were performed in the western equatorial Pacific using SeaWiFs Profiling Multichanel Radiometer System (Satlantic Inc.). An additional purpose was that I wanted to estimate K_v independently from the methods I used in Chapter 3.

D.2 Theory

Here, I adopted the Osborn dissipation model (Osborn, 1980) in which the eddy diffusivity coefficient for density is defined as

$$K_v = \frac{\Gamma \epsilon}{N^2}, \tag{D.1}$$

where N is buoyancy frequency, Γ is a parameter denoting mixing efficiency and ϵ is the rate of dissipation of kinetic energy. Buoyancy frequency can be obtained from CTD measurements, and mixing efficiency is assumed to be constant. In my calculations, I set Γ=0.25; this value was estimated by means of measurements (Oakey, 1985) as well as theoretical calculations (Osborn, 1980).

The key component in the Osborn model is the estimation of the rate of dissipation of kinetic energy ϵ. In this study, I estimated the microscale dissipation ϵ from overturning

(often called Thorpe) length scales L_t (Thorpe, 1977). The Thorpe scale empirically defines the overturn thickness; it can be estimated from the density inversions that overturn creates in the stratified water column (Thorpe, 1977). If a measured density profile is reordered into a gravitationally stable profile—that is, a profile with density monotonically increasing with depth—then the vertical distance that the parcel of water has to be moved in order to achieve a gravitationally stable profile determines the Thorpe displacement as a function of depth. The Thorpe scale is then calculated as the root-mean-square (rms) value of Thorpe displacements over the depth span enclosing the overturn. It has been indicated (Dillon 1982; Peters et al., 1988) that the Thorpe scale is directly proportional to the Ozmidov scale L_o (Ozmidov, 1965) which represents the size of the largest isotropic eddy in stratified fluid,

$$L_o = \sqrt{\frac{\epsilon}{N^3}} \tag{D.2}$$

In the open ocean, the Ozmidov scale L_o and the Thorpe scale L_t are approximately equal (Dillon, 1982). Using Eqs. D.1 and D.2, K_v can be written as a function of Thorpe scale,

$$K_v = \Gamma L_t^2 N \ . \tag{D.3}$$

As noted above, both N and L_t can be obtained from the fine-scale CTD measurements. This is potentially advantageous since, in this way, microscale mixing rates are estimated from measurements of density that are routinely obtained using free-fall profilers. The method offers an attractive possibility to provide extensive spatial and temporal monitoring of small scale turbulence. On the other hand, the detection of overturns is limited by the density resolution of the instrument and its sampling rate. The method is also sensitive to instrument noise or systematic errors (e.g. mismatch in time response of temperature and conductivity sensors) which may result in artifactual detection of the overturn and thus incorrect values of mixing rates.

D.3 Methods

D.3.1 Resolving power of the instrument

A preliminary step was to estimate the minimum eddy diffusivity which can be resolved with a Satlantic CTD instrument. Table D.1 summarizes the specifications of a Satlantic CTD profiler used in my measurements. The vertical resolution δ_z and density resolution δ_ρ of the instrument are given in Table D.2. The minimum overturn rate L_{min} detectable by the experiment was estimated as five times the vertical resolution (Galbraith and Kelley, 1996). The resolution for rate of dissipation of kinetic energy, ϵ_{min}, was determined using the expression proposed by Galbraith and Kelley (1996), $\epsilon_z = 25\delta_z^2 N^3$. The minimum resolvable eddy diffusivity was calculated using Eq. D.3.

Table D.1: Specifications of a Satlantic CTD Profiler

Sampling rate	6 Hz
Falling speed	1 m s^{-1}
A/D converter	16 bits
Calibration range for T	0°–30° C
Calibration range for conductivity	0–60 mS
Calibration range for pressure	0–300 dbar
Precision for T	0.00046° C/bit
Precision for conductivity	0.0091 mS/bit
Precision for pressure	0.0046 dbar/bit

Results in Table D.2 show that we are only able to resolve overturns thicker than 1.0 m and dissipation rates greater than 10^{-6} m^2 s^{-3}. The limiting factor in both overturning thickness and dissipation rates is the depth resolution of Satlantic instrument δ_z. Minimum resolvable eddy diffusivities are of order 10^{-4} m^2 s^{-1}. However, values of K_ρ estimated at the base of euphotic zone (100 m) in the western equatorial Pacific from microstructure measurements of ϵ are of order 10^{-6} m^2 s^{-1} to 10^{-4} m^2 s^{-1} (Gregg et. al, 1985, Wijesekera and Gregg, 1996). The CTD profiler may thus detect only very large mixing events.

Table D.2: Resolution of Parameters

Vertical resolution δ_z	0.2 m
Density resolution δ_ρ	0.0029 kg m^{-3}
Overturn resolution L_{min}	1 m
Dissipation resolution ϵ_{min}	10^{-6} m^2 s^{-3}
Eddy diffusivity resolution K_v	10^{-4} m^2 s^{-1}

As pointed out before, the instrument noise or systematic errors in CTD measurements may result in artifactual detection of the overturning. I used an algorithm developed by Gargett (personal communication) to correct for instrument noise in density measurements and to calculate Thorpe scale over the reordering regions that are found in my data.

D.3.2 Gargett approach

In an algorithm proposed by Gargett (personal communication), the effect of noise is considered only for the density measurements. Mismatches in time response of temperature and conductivity sensors are neglected. The CTD profiler was falling with speed of 1 m s^{-1}; for this speed the response of temperature and conductivity sensors were matched). The principle idea employed in the algorithm is that the measured density profile stays in its original order provided that the absolute difference of density values between two neighboring measurement points is less than the noise level δ. In the first step, the algorithm identifies those values of density ("hinge" values) that differ more than δ with respect to their neighboring measurement points. In the second step, all those density values that differ less than δ with respect to their neighbors are rejected; to these measurement points, the nearest hinge value of density is assigned. This step thus establishes a modified density profile which is then—in the third step—sorted following the standard sorting procedure. In the fourth step, the Thorpe displacement is calculated from the sorted profile and the regions of possible overturning are identified; all those regions thinner than five times the vertical resolution (approximately 1 m) were rejected. In the fifth step, the Thorpe lengths

defined as the rms value of Thorpe displacement over each overturning region are calculated. In the sixth step, for each overturning region, the T-S diagram is visually inspected and all those regions with "loops" in T-S diagrams (where for a given temperature, the salinity is not uniquely defined) are rejected. Finally, K_v is calculated in each overturning region using Eq. D.3.

To test whether the algorithms successfully corrected for instrument noise in density measurements, I added uniformly distributed random noise on the intervals (-0.003 kg m^{-3}, 0.003kg m^{-3}) and (-0.001 kg m^{-3}, 0.001kg m^{-3}) to the measured density profiles, and then estimated Thorpe scales using the Gargett (personal communication) method. I compared the estimated values with those obtained from measured profile of density.

D.4 Results and Discussion

The major findings of my study can be summarized as follows.

Satlantic CTD profiler could potentially resolve mixing events with $K_v > 10^{-4}$ m^2 s^{-1}. Since microstructure measurements in the western equatorial Pacific (Gregg et. al, 1985, Wijesekera and Gregg, 1996) have suggested the values of K_v at the base of euphotic zone of order 10^{-6} m^2 s^{-1} to 10^{-4} m^2 s^{-1}, I may be able to detect only very large mixing events.

Between these events K_v could be estimated using two approaches.

In the first approach, the turbulent flux, given by

$$F = -K_v d\rho/dz \tag{D.4}$$

from K_v and density gradient can be obtained at those regions where I identified overturning. It is reasonable to assume that the flux F is constant over the euphotic zone and that no horizontal flux occurs. Then, K_v can be calculated between the overturning regions using Eq. D 4 and the measured profile of the density gradient. Finally, K_v at the base of the euphotic zone is estimated as the average of those values for K_v that are obtained on the depth interval $[z_d - \zeta, z_d + \zeta]$ where ζ was set to 50 m.

In the second approach ϵ can be calculated using Eq. D.2. Next, assuming that ϵ is approximately lognormally distributed in the ocean one can predict those values of ϵ which

can not be resolved by our instrument. Finally, K_v can be obtained using Eq. D.1. Again, K_v at the base of the euphotic zone can be estimated as the average of those values for K_v that are obtained on the depth interval $[z_d - \zeta, z_d + \zeta]$ where ζ was set to 50 m.

Figs. D.1 depict histograms of ϵ, and K_v obtained for all overturns that were found on sigma-t profiles using Gargett (personal communication) method, on the interval from 100 to 200 m for 12 stations in the western equatorial Pacific ϵ and K_v for each overturn were computed using Eq. D.1 and Eq. D.1. Thorpe scale was obtained using the Gargett (personal communication) computational algorithm, and N^2 for each overturning region was calculated from reordered profile of sigma-t. Histograms of ϵ show approximately lognormal distribution. This is in agreement with estimates of dissipation parameters in the ocean (Baker and Gibson, 1987; Oakey, 1985; Osborn and Lueck, 1985)

The comparison of Thorpe displacements calculated from the measured profile of sigma-t with those estimated from two modified profiles of sigma-t with added uniformly distributed random noise suggest that the Gargett (personal communication) algorithm corrects for instrumental noise in density measurements. During our observations the falling speed of instrument was between 0.6 m s^{-1} and 1.0 m s^{-1}. Few spikes can be found on the sigma profiles that might be due to the mismatch when falling speed deviated from 1 m/s. The Gargett algorithm does not correct for density spikes that can lead to high Thorpe displacements and thus an artificial signal of overturn. I have rejected all the overturns that include less than four measuring points. This should remove the majority of spikes on density profile since spikes usually include only one or two measuring points.

In conclusion, the approach used in my study may potentially offer the possibility to provide the estimate of mixing rates from CTD measurements, which can be obtained using free-fall profilers. However, due to the resolution of the Satlantic instrument this approach was not possible in the low mixing environment of the western equatorial Pacific.

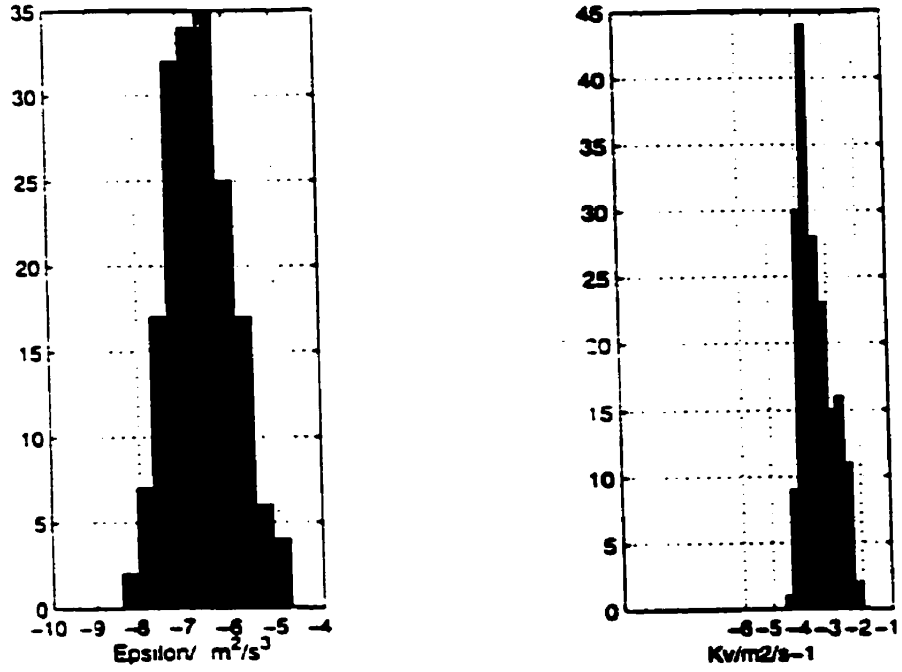

Figure D.1: Histograms of ϵ ($m^2\ s^{-3}$) and K_v ($m^2\ s^{-1}$) for 12 stations in the western equatorial Pacific for reordering regions found on the density profiles using Gargett (personal communication) approach.

References

Ando, K. and McPhaden, M.J (1997). Variability of surface layer hydrography in the tropical Pacific Ocean, *J. Geophys. Res.*, 102:23,063-23,078.

Antoine, D. and Morel, A. (1995). Modeling the seasonal course of the upper ocean pCO_2 (I). Development of a one-dimensional model, , 47B:103-121.

Baker, M.A. and Gibson, C.H. (1987). Sampling turbulence in the stratified ocean: Statistical consequences of strong intermittency, *J. Phys. Oceanogr.*, 17:1,817-1,836.

Banse, K. (1994). Uptake of inorganic carbon and nitrate by marine plankton and the Redfield ratio, *Global biogeochem. Cycles*, 8:81-84.

Barber, R.T. and Chavez, F.P. (1983). Biological consequences of El Niño, *Science*, 222:1203-1210.

Barber, R.T. and Kogelschatz, J.E. (1989). Nutrients and productivity during 1982/1983 El Niño. In: P.W. Glynn (editor), *Global ecological consequences of the 1982-83 El Niño-Southern oscillation*, Elsevier, Amsterdam, pp. 21-53.

Barber, R.T. (1990). Ocean productivity and global carbon flux. In: *Preprint Volume of the Symposium on Global Change Systems*, American Meteorological Society, pp. 18-21.

Barber, R.T. and Chavez, F.P. (1991). Regulation of primary productivity rate in the equatorial Pacific, *Limnol. Oceanogr.*, 36:1,803-1,815.

Batchelor, G.K. (1973)*An introduction to fluid dynamics*. Cambidge University Press, Cambridge, UK.

Bevington, P.R. (1969).*Data reduction and Error Analysis for the physical Sciences*, McGraw-Hill, New York. 336 pp.

Bond, N.A. and McPhaden, M.J. (1995). An indirect estimate of the diurnal cycle in upper ocean turbulent heat fluxes at the equator, 140°W, *J. Geophys. Res.*, 100:18,369-18,378.

Bronk, D.A., P.M. Glibert, and B.B. Ward (1994). Nitrogen uptake, Dissolved organic nitrogen release, and new production, *Science*, 265:1843-1846.

Bryden, H.L. and Brady, E.C. (1989). Eddy momentum and heat fluxes and their effects on the circulation of the equatorial Pacific, *J. of Marine Res.*, 47:55-79.

Bryden, H.L. and Brady, E.C. (1985). Diagnostic model of the three-dimensional circulation in the upper equatorial Pacific, *J. Phys. Oceanogr.*, 15:1255-1273.

Burke, J.F. (1994). Analysis of microstructure data from the north Atlantic tracer release experiment, *Ph.D. Thesis*, Dept. of Oceanography, Dalhousie University.

Capone, D.G. and Carpenter, E.J. (1982). Nitrogen fixation in the marine environment, *Science*, 217:1,140-1,142.

Carpenter, E.J. and Romans, K. (1991). Major role of the cyanobacterium *Trichodesmium* in nutrient cycling in the north Atlantic ocean, *Science*, 254:1,356-1,358.

Carr, M.E., N.S. Oakey, B. Jones, and M.R. Lewis (1992). Hydrographic patterns and vertical mixing in the equatorial Pacific along 150°W, *J. Geophys. Res.*, 97:611-626.

Carr, M.E., M.R. Lewis, and D.E. Kelley (1995). A physical estimate of new production in the equatorial Pacific along 150°W, *Limnol. Oceanogr.*, 40(1):138-147.

Chavez, F. P. and Barber, R.T. (1985). Plankton production during El Niño, *WCRP Publications series*, 4:23-31.

Chavez, F.P. and Barber, R.T. (1987). An estimate of new production in the equatorial Pacific, *Deep-Sea Res.*, 34:1229-1243.

Chen, D., A.J. Busalacci, and L.M. Rothstein, (1994). The roles of vertical mixing, solar radiation, and wind stress in a model simulation of the sea surface temperature seasonal cycle in the tropical Pacific ocean, *J. Geophys. Res.*, 99:20,345-20,359.

Christian, J.R., M.R. Lewis, and D.M. Karl (1997). Vertical fluxes of carbon, nitrogen, and phosphorus in the North Pacific Subtropical Gyre near Hawaii, *J. Geophys. Res.*, 102:15,667-15,677.

Clark, D.G. (1997). Physical and biological sources and sinks of nitrate in the Canary Basin, *MSc. Thesis*, Dept. of Oceanography, Dalhousie University.

Coale, K. H., S.E. Fitzwater, R.M. Gordon, K.S. Johnson, and R.T. Barber (1996). Control of community growth and export production by upwelled iron in the equatorial Pacific, *Nature*, 379:621-624.

Craig, H., W.S. Broecker, and D.W. Spencer (1982). *GEOSECS Pacific Expedition: Section and profiles*, U.S. Government Printing Office, Washington, D.C., 4: 251.

Cronin, M.F. and McPhaden, M.J. (1997). The upper ocean heat balance in the western equatorial Pacific warm pool during September-December 1992, *J. Geophys. Res.*, 102:8533-8553.

Cullen, J. J. (1982). The Deep Chlorophyll Maximum: Comparing Vertical Profiles of Chlorophyll a, *Can. J. Fish. Aquat. Sci.*, 39:791-803.

Cullen, J. J. (1991). Hypothesis to explain high-nutrient conditions in the open sea, *Limnol. Oceanog.*, 36:1578-1599.

Cullen, J. J., M.R. Lewis, C.O. Davis, and R.T. Barber (1992). Photosynthetic characteristics and estimated growth rates indicate grazing is the proximate control of primary production in the equatorial Pacific, *J. Geophys. Res.*, 97:693-654.

Cullen, J. J. (1995). Status of the iron hypothesis after the Open-Ocean Enrichment Experiment, *Limnol. Oceanog.*, 40:1336-1343.

Curran, P.J. (1988). The semivariogram in remote sensing, An introduction. *Remote Sensing of Environment*, 24:493-507.

Dauchez, S., Legendre L., and Fortier L. (1995). Assessment of simultaneous uptake of nitrogenous nutrients (^{15}N) and inorganic carbon (^{13}C) by natural phytoplankton populations. *Mar. Biol.*, 123:651-666.

Daly, K.L., D.W.R. Wallace, W.O. Smith. Jr., A. Skoog, R. Lara, M. Gosselin, E. Falck, and P.L. Yager (1999). Non-Redfield carbon and nitrogen cycling in the Arctic: Effects of ecosystems structure and dynamics, *J. Geophys. Res.*, 104:3,185-3,199.

Delcroix, T. and Henin, C. (1991). Seasonal and interannual variation of sea surface salinity in the tropical Pacific Ocean, *J. Geophys. Res.*, 96:22,135-22,150.

Delcroix, T., G. Eldin, M. Radenac, J. Toole, and E. Firing (1992). Variation in the western equatorial Pacific Ocean, 1986-1989, *J. Geophys. Res.*, 97:5423-5445.

Delcroix, T., G. Eldin, M. McPhaden, and A. Morliere (1993). Effect of westerly wind bursts upon the western equatorial Pacific Ocean, February-April 1991, *J. Geophys. Res.*, 93:16,379-16,385.

Delcroix, T. and Picaut, J. (1998). Zonal displacement of the western equatorial Pacific fresh pool, *J. Geophys. Res.*, 103:1087-1098.

Dillon, T.M. (1982). Vertical overturns: A comparison of Thorpe and Ozmidov length scales, *J. Geophys. Res.*, 87:9601-9613.

Duce R.A., P.S. Liss, J.T. Merrill, P. Buar-Menard, B.B. Hicks, J.M. Miller, J.M. Prospero, R. Arimoto, T.M. Church, W. Ellis, J.N. Galloway, L. Hanson, T.D. Jickells, A.H. Knapp, K.H. Rienhart, B. Schneider, A. Soudine, J.J. Tokos, S. Tsunogai, R. Wollast, and M. Zhou (1991). The atmospheric input of trace spieces to the world ocean, *Global Biogeochemical Cycles*, 5:193-259.

Duce, R.A. and Tindale, N.W. (1991). Atmospheric transport of iron and its deposition in the ocean, *Limnol. Oceanogr.*, 36:1,715-1,726.

Dugdale, R.C. and Goering, J.J. (1967). Uptake of new and regenerated forms of nitrogen in primary production, *Limnol. Oceanogr.*, 12:196-206.

Dugdale, R.C., A. Morel, A. Bricaud, and F.P. Wilkerson (1989). Modeling new production in upwelling centers: A case study of modeling new production from remotely sensed temperature and color, *J. Geophys. Res.*, 94:18,119-18,132.

Dugdale, R.C., F.P. Wilkerson, R.T. Barber, and F.P Chavez (1992). Estimating new production in the equatorial Pacific Ocean at 150°W, *J. Geophys. Res.*, 97:681-686.

Dugdale, R.C. and Wilkerson, F.P. (1998). Silicate regulation of new production in the equatorial Pacific upwelling, *Nature*, 391:270-273.

Dupouy, C., M. Petit, and Y. Dandonneau (1988). Satellite detected cyanobacteria bloom in the southwestern tropical Pacific: implication for oceanic nitrogen fixation, *Int. Remote Sens.*, 9: (3) 389-396.

Enfield, D.B. (1986). Zonal and seasonal variability of the equatorial Pacific heat balance, *J.Phys. Oceanogr.*, 16:1,038-1,054.

Eppley, R.W. and Peterson, B.J. (1979). Particulate organic matter flux and planktonic new production in the deep ocean, *Nature*, 282:677-680.

Eppley, R.W. and Renger, E.H. (1988). Nanomolar increase in surface layer nitrate concentration following a small wind event, *Deep-Sea Res.*, 35:1,119-1,125.

Esbensen, S.K. and Kushnir, Y. (1981). The heat budget of the global ocean, *An atlas based on estimates from marine observations*, Climate Research Institute, Oregon State University, Corvallis, Report No. 29.

Fahrbach, E., C. Brockmann, and J. Meincke (1996). Horizontal mixing in the Atlantic Equatorial Undercurrent estimated from drifting buoy clusters, *J. Geophys. Res.*, 91:10,557-10,565.

Feely, R.A., R. Wanninkhof, C.E. Cosca, P.P. Murphy, M.F. Lamb, and M.D. Steckley (1995). CO_2 distributions in the equatorial Pacific during the 1991-1992 ENSO event, *Deep-Sea Res*, 42:365-386.

Flynn, K.J. and Berry, L.S. (1999). The loss of organic nitrogen during marine primary production may be significantly overestimated when using ^{15}N substrates, *Proc. R. Soc. Lond. B.*, 266:641:647.

Fiedler, P.C., V. Philbrick, and F.P. Chavez (1991). Oceanic upwelling and productivity in the eastern tropical Pacific, *Limnol. Oceanogr.*, 36:1834-1850.

Galbraith, P.S. and Kelley, D.E. (1996). Identifying overturns in CTD profiles, *J. Atmospher. Ocean. Techn.*, 13:688-702.

Gargett, A., T. Granata, C. Marrase, P. Nival, A. Robinson, and H.Y. Yamazaki (1993). Instruments and methods, *U.S. Globec*, 5.

Garrett, C. (1991). Marginal mixing theories, *Atmosphere-Ocean*, 29:313-339.

Garside, C. (1967). A chemiluminescent technique for the determination of nanomolar concentrations of nitrate and nitrite in seawater, *Marine Chemistry*, 11:159-167.

Geider, R.J., B. Osborne, and J.A. Raven (1986). Growth, photosynthesis and maintenance metabolic cost in the diatom *Phaeodactylum tricornutum* at very low light levels, *J. Phycol.*, 22:39-48.

Gent, P. (1991). Heat budget of the TOGA-COARE domain in an ocean model. *J. Geophys. Res.*, 96:3,323-3,330.

Glantz, S.A. (1977). *Primer of Biostatistics*, McGraw-Hill, New York.

Gill, A.G. (1892). *Atmosphere-Ocean Dynamics*, New York: Academic Press.

Godfrey, J.S. and Lindstrom, E.J. (1989). The heat budget of the equatorial Western Pacific surface mixed layer, *J. Geophys. Res.*, 94:8,007-8,017.

Goldman, J.C. and Glibert, P.M. (1983). Kinetics of inorganic nitrogen uptake by phytoplankton, In: E.J. Carpenter and D.G. Capone (eds), *Nitrogen in the marine environment*, Academic Press. pp. 233-274.

Goldman, J.C. (1986). On phytoplankton growth rates and particulate C:N:P ratios at low light, *Limnol. Oceanogr.*, 31(6):1358-1363.

Gordon, C. (1989). Comparison of the surface fluxes in the tropical Pacific Ocean derived from and atmospheric general circulation model and from climatology, *Tropical Ocean-Atmosphere Newsletter*, 51:1-4.

Goyet, C., P.R . Guenther, C.D. Keeling, and L.D. Talley (1996). Carbon Dioxide, Hydrographic, and Chemical Data Obtained During the Thomas Washington Cruise Tunes-3 in the Equatorial Pacific Ocean (WOCE Section P16C), Environmental Sciences Division, Publication No. 4606.

Gregg, M.C., H. Peters, J.C. Wesson, N.S. Oakey, and T.J. Shay (1985). Intensive measurements of turbulence and shear in the equatorial undercurrent, *Nature*, 318:140-144.

Gregg, M.C. (1987). Diapycnal mixing in the thermocline: a review, *J. Geophys. Res.*, 92:5,249-5,286.

Gregg, M.C. and Kunze, E. (1991). Shear and strain in Santa Monica Basin, *J. Geophys. Res.*, 96:16,709-16,719.

Halpern, D. (1980). A Pacific equatorial temperature section from 172°E to 110°W during winter-spring 1979, *Deep-Sea Res.*, 27: 931-940.

Halpern, D., R.A. Knox, D.S. Luthier, and S.G.H. Philander (1989). Estimates of equatorial upwelling between 140° and 110° W during 1984, *J. Geophys. Res.*, 94:8,018-8,020.

Halpern, D., and Feldman, G.C. (1994). Annual and interannual variations of phytoplankton pigment concentration and upwelling along the Pacific equator, *J. Geophys. Res.*, 99:7,347-7,365.

Halpern, D., Y. Chao, C. Ma, and C.R. Mechoso (1995). Comparison of tropical Pacific temperature and current simulations with two vertical mixing schemes embedded in an ocean general circulation model and reference to observations, *J. Geophys. Res.*, 100:2,515-1,522.

Hamilton, J.M., M.R. Lewis, and B.R. Ruddick (1989). Vertical fluxes of nitrate associated with salt fingers in the world's oceans, *J. Geophys. Res.*, 94:2,137-2,145.

Harrison D.E., and Giese, B.S. (1991). Episodes of surface westerly winds as observed from islands in the western tropical Pacific, *J. Geophys. Res.*, 96:3,221-3,237.

Harrison, W.G. (1983). Nitrogen in the marine environment, IV.2 Use of isotopes. In: E.J. Carpenter and D.G. Capone (eds), *Nitrogen in the marine environment*, Academic Press. pp. 763-807.

Harrison, W.G., T. Platt, and M.R. Lewis (1987). f-ratio and its relationship to ambient nitrate concentration in coastal waters, *J. Plankton Res.*, 9:235-248.

Harrison, W.G., L.R. Harris, D.M. Karl, G.A. Knauer, and D.G. Redalje (1992). Nitrogen dynamics at the VERTEX time-series site, *Deep-Sea Res.*, 39:1535-1552.

Harrison, W.G., L.R. Harris, and B.D. Irwin (1997). The kinetics of nitrogen utilization in the oceanic mixed layer: Nitrate and ammonium interactions at nanomolar concentrations, *Limnol. Oceanogr.*, 41(1):16-32.

Harrison, W.G. and Harris, L.R. (1997). Nitrate utilization in the open ocean: To what extent are uptake rates overestimated as a result of ^{15}N tracer additions, Submitted to *Limnol. and Oceanogr.*.

Hayes, S.P., L.J. Mangum, J. Picaut, A. Sumi, and K. Takeuchi (1991). TOGA/TAO: A moored array for real-time measurements in the tropical Pacific Ocean, *Bulletin of the American Meteorological Society*, 72: 339-347.

Hemantha, W.W., and M.C. Gregg (1996). Surface layer response to weak winds, westerly bursts, and rain squalls in the western Pacific Warm Pool, *J. Geophys. Res.*, 10:977-997.

Henin, C., Y. du Penhoat, and M. Ioulalen (1997). Observations of sea surface salinity in the western Pacific fresh pool: Large scale changes during 1992-1995, *J. Geophys. Res.*, in press.

Herbland, A., and Voituriez, B. (1979). Hydrological structure analysis for estimating the primary production in the tropical Atlantic ocean, *Journal Marine Research*, 37:87-101.

Hsiung, J. (1986). Mean surface energy fluxes over the global ocean, *J. Geophys. Res.*, 91:10,585-10,606.

Inoue., H.Y., M. Ishii, H. Matsueda, and M. Aoyama (1996). Changes in longitudional distribution of the partial pressure of CO_2 (pCO_2) in the central and western equatorial Pacific, west of 160°W, *Geophys. Res. Lett.*, 23:1,781-1,784.

Inoue, H.Y. and Sugimura, Y. (1992). Variations and distributions of CO_2 in and over the equatorial Pacific during the period from the 1986/88 El Niño event to 1988/89 La Niña event, *Tellus*, 44B:1-12.

Ishii, M. and Inoue, H.Y. (1995). Air-sea exchange of CO_2 in the central and western equatorial Pacific in 1990, *Tellus*, 47B:447-640.

Jourdan, D. and Gautier, C. (1995). Comparison between global latent heat flux computed from multi-sensor (SSM/I and AVHRR) and from in-situ data, *J. Atmos. and Oceanic Tech.*, 12:46-72.

Kamykowski, D. and Zentara, S.J. (1986). Predicting plant nutrient concentrations from temperature and sigma-t in the upper kilometer of the world ocean, *Deep-Sea Res.*, 33:89-105.

Karl, D. and Knauer, G.A. (1984). Vertical distribution, transport, and exchange of carbon in the northeast Pacific Ocean: evidence for multiple zones of biological activity, *Deep-Sea Res.*, 31:221-243.

Karl, D., Knauer, G.A., and Martin, J.H. (1988). Downward flux of particulate matter in the ocean, *Nature*, 332:438-440.

Karl, D., R. Letelier, J. Tupas, J. Dore, J. Christian, and D. Hebel (1997). The role of nitrogen fixation in biogeochemical cycling in the subtropical North Pacific Ocean, *Nature*, 388:533-538.

Kawano, T., I. Asanuma, K. Matsumoto, H. Okano, D. Turk, and M.R. Lewis (1998). Primary production in the western equatorial Pacific, *Ocean Optics*, XIII, Proc. SPIE Int. Soc. Opt. Eng.

Keeling, C.D. and Revelle, R. (1995). Effect of El Niño/Southern Oscillation on the atmospheric content of carbon dioxide, *Meteoritics*, 20:437-450.

Kessler, W.S., M.J. McPhaden, and K.W. Wieckmann (1995). Forcing of the Intraseasonal Kelvin waves in the equatorial Pacific, *J. Geophys. Res.*, 100:10,613-10,631.

Knap, A., T. Jickells, A. Pszenny, and J. Galloway (1986). Significance of atmospheric-derived fixed nitrogen on productivity of the Sargasso Sea, *Nature*, 320(13):158-160.

Kristiansen, S., T. Farbrot, and P.A. Wheeler (1994). Nitrogen cycling in the Barents Sea - Seasonal dynamics of new and regenerated production in the marginal ice zone, *Limnol. Oceanogr.*, 39:1,630-1,642.

Landry, M.R., R.T. Barber, R.R. Bidigare, F. Chai, K.H. Coale, H.G. Dam, M.R. Lewis, S.T. Lindey, J.J. McCarthy, M.R. Roman, D.K. Stoecker, P.G. Verity, and J.R. White (1997). Iron and grazing constrains on primary production in the central equatorial Pacific: An EqPac Synthesis, *Limnol. Oceanogr.*, 42(3):405-418.

Laws, E.A. (1991). Photosynthetic quotients, new production and net community production in the open ocean, *Deep-Sea Res.*, 38:143-176.

Ledwell, J.R., A.J. Watson, and C.S. Law (1993). Evidence for slow mixing across the pycnocline from an open-ocean tracer-release experiment, *Nature*, 364:701-703.

Lee, H.K. (1997). Latent heat flux over the tropical Pacific ocean estimated from TOGA-TAO data. *MSc. Thesis*, University of Hawaii.

Legendre, L. and Le Fevre, J. (1989). Hydrodynamical singularities as controls of recycled versus export production in oceans, In: W.H. Berger, V.S. Smetancek, and G. Wefer (Eds), *Productivity of the Ocean: Present and Past*, John Wiley and Sons Limited, 49-63 pp.

Lehninger, A.L. (1982). *Principles of Biochemistry*, Worth Publishers, Inc., New York.

Lehodey P., M. Bertignac, A. Lewis, and J. Picaut (1997). El Niño Southern Oscillation and tuna in the western Pacific, *Nature*, 389:715-718.

Levitus, S. (1994). NOAA Atlas NESDIS 2, *World Ocean Atlas 1994*, U.S. Government Printing Office, Washington D.C.

Lewis, M.R., W.G. Harrison, N.S. Oakey, D. Hebert, and T. Platt (1986). Vertical nitrate fluxes in the oligotrophic ocean, *Science*, 234:870-873.

Lewis, M.R., M.E. Carr, G.C. Feldman, W. Esaias, and C. McClain (1990). Influence of penetrating solar radiation on the heat budget of the equatorial Pacific Ocean. *Nature*, 346:543-545.

Lewis, M.R. (1992). Satellite ocean color observations of global biogeochemical cycles, In: P.G. Falkowski and A.D. Woodhead (Eds.), *Primary productivity and biogeochemical cycles in the sea*, New York: Plenum, 139-156 pp.

Liss, P. and Merlivat, L. (1986). In: P. Buat-Menard (ed), Air-sea gas exchange rates: Introduction and synthesis, *The role of air-sea exchange in geochemical cycling*, Dordrecht/Holland: D. Riedel Publ. Comp., 113-127 pp.

Liu, W. T. and Gauthier, C. (1990). Thermal Forcing on the Tropical Pacific From Satellite Data, *J. Geophys. Res.*, 95:13,209-13,217.

Longhurst, A.R. and Harrison, W.G. (1989). The biological pump: Profiles of plankton production and consumption in the upper ocean, *Prog. Oceanog.*, 22:47-123.

Lukas, R. and Lindstrom, E. (1991). The mixed layer of the western equatorial Pacific ocean, *J. Geophys. Res.*, 96:3,343-3,357.

Mackey, D.J., J. Parslow, H.W. Higgis, F.B Griffiths and J.E O'Sullivan (1995). Plankton productivity and biomass in the western equatorial Pacific: Biological and physical controls, *Deep-Sea Res.*, 42:499-533.

Mackey, D.J., J. Parslow, F.B Griffiths, H.W. Higgis, and B. Tilbrook (1997). phytoplankton productivity and the carbon cycle in the western equatorial Pacific under El Niño and non- El Niño conditions, *Deep-Sea Res.*, 44:1,951-1,978.

Marra, J., R.R. Bidigare, and T.T. Dickey (1990). Nutrient and mixing, chlorophyll and phytoplankton growth, *Deep-Sea Res.*, 37:127-143.

Martin, J.H., R.M. Gordon, and S.E. Fitzwater (1991). The case for iron, *Limnol. Oceanogr.*, 36:1,793-1,802.

McCarthy, J.J, C. Garside, J.L. Nevins, and R. Barber (1996). New production along 140°W in the equatorial Pacific during and following the 1992 El Niño event, *Deep-Sea Res.*, 43:1,065-1,093.

McClain, C. R., R. Murtugudde, and S. Signorini (1999). A simulation of biological processes in the equatorial Pacific Warm pool at 165°E. In press, *J. Geophys. Res.*.

McDougall, T.J. and Ruddick, B.R., (1992). The use of ocean microstructure to quantify both turbulent mixing and salt-fingering, *Deep-Sea Res.*, 39:,1931-1,952.

McPhaden, M.J., S.P. Heyes, L.J. Mangum (1990). Variability in the Western Equatorial Pacific Ocean during the 1986-87 El Niño/Southern Oscillation Event, *J. Phys. Oceanogr.*, 20:190-208.

McPhaden, M.J.and Picaut, J. (1990). El Niño-Southern Oscillation displacement of the western equatorial Pacific Warm Pool,*Science* 250:1385-1388.

McPhaden, M.J., F. Bahr, Y. Du Penhoat, E. Firing, S.P. Hayes, P.P. Niiler, P.L. Richardson, and J.M. Toole (1992), The response of the western equatorial Pacific Ocean to westerly wind bursts during November 1989 to January 1990, *J. Geophys. Res.*, 97:14, 289-14,303.

McPhaden, M.J., A.J. Busalacci, R. Cheney, J.R. Donguy, K.S. Gage, D. Halpern, M. Ji, P. Julian, G. Meyers, G.T. Mitchum, P.P. Niiler, J. Picaut, R.W. Reynolds, N. Smith, K. Takeuchi (1998). The tropical Ocean Global Atmosphere (TOGA) observing system: a decade of progress, *J. Geophys. Res.*, 103:14,169-14,240.

Michaels, A.F. and Silver, M.W. (1988). Primary production, sinking fluxes and the microbial food web, *Deep-Sea Res.*, 35: 473-490.

Michales, A.F., D.A. Siegel, R.J. Johnson, A.H. Knap, and J.N. Galloway (1993). Episodic inputs of atmospheric nitrogen to the Sargasso Sea: contributions to new production and phytoplankton blooms, *Global Biogeochemical Cycles*, 7(2):339-351.

Moran, M. (1981). Formulae for determination of chlorophyllous pigments extracted with N,N-Dimethylformamide, *Plant Physiology Journal*, 69:1,376-1,381.

Morel, F.M.M., J.G. Rueter, and N.M. Price (1991). Iron nutrition of phytoplankton and its possible importance in the ecology of ocean regions with high nutrient and low biomass, *Oceanography*, 4:56-61.

Moum, J.N., D.R. Caldwell, and C.A. Paulson (1989). Mixing in the equatorial surface layer and thermocline, *J. Geophys. Res.*, 94:2,005-2,021.

Murray, J.W., R.T. Barber, M.R. Roman, M.P. Bacon, and R.A. Feely (1994). Physical and biological controls on carbon cycling in the equatorial Pacific, *Science*, 266:58-65.

Murray, J.W., J.N. Downs, S. Strom, C.L. Wei, and H.W Jannasch (1989). Nutrient assimilation, export production and 234 Th scavenging in the eastern equatorial Pacific, *Deep-Sea Res.*, 36:1,471-1,489.

Murphy, J. and Riley, J.P. (1962). A modified single solution method for the determination of phosphate in natural waters. *Anal. Chim. Acta.*, 27:31-36.

Nielsen, T.G. and Kiorboe, T. (1991). Effect of a storm event on the structure of the pelagic food web with special emphasis on planktonic ciliates, *J. Plank. Res.*, 13:35-51.

Niiler, P. and Stevenson, J. (1982). The heat budget of tropical ocean warm-water pools, *J. Marine. Res.*, 36:465-480.

Oakey, N.S. (1985). Statistics of mixing parameters in the upper ocean during JASIN phase 2, *J. Phys. Oceanogr.*, 15:1,662-1,675.

Oakey, N.S. (1982).Determination of the rate of dissipation of turbulent energy from simultaneous temperature and velocity shear microstructure measurements, *J. Phys. Oceanogr.*, 15:1,662-1,675.

Oakey, N.S. (1988). Estimates of mixing inferred from temperature and velocity microstructure, In: J.C.J. Nihoul, and B.M. Jamart (eds), *Small-scale turbulence and mixing in the ocean*, Elsevier, Amsterdam, pp. 239-247.

Oberhuber, J. M. (1988). An atlas based on the 'COADS' data set: the budgets of heat, buoyancy and turbulent kinetic energy at the surface of the global ocean. Max-Planck Institut fr Meteorologie, Rep. 15, Hamburg, 20 pp. plus figures.

Osborn, T.R. and Cox, C.S. (1972). Oceanic finestructure, *Geophysical Fluid Dynamics*, 3:321-345.

Osborn, T.R. (1980). Estimates of the local rate of vertical diffusion from dissipation measurements, *J. Phys. Oceanogr.*, 10:83-89.

Osborn, T.R., and Lueck, R.G. (1985). Turbulence measurements with submarine, *J. Phys. Oceanogr.*, 15:1,502-1,520.

Ozmidov, R.V. (1965). On the turbulent exchange in a stably stratified ocean, *Izv. Acad. Sci. USSR Atmos. Ocean. Phys.*, 1:853-860.

Owens, N.J.P. (1988). Rapid and total automation of shipboard ^{15}N analysis: examples from the North Sea., *J. Exp. Mar. Biol. Ecol.*, 122:163-171.

Pacanowski, R. and Philander, S.G.H. (1981). Parameterization of vertical mixing in numerical models of tropical oceans, *J. Phys. Oceanogr.*, 11:1,443-1,451.

Peltzer, E. and Hayward, N.A. (1996). Spatial and temporal variability of total organic carbon along 140°W in the equatorial Pacific ocean in 1992, *Deep-Sea Res.*, 43:1,155-1,180.

Peña, M.A., M.R. Lewis, and W.G. Harrison (1990). Primary productivity and size structure of phytoplankton biomass on a transect of the equator at 135°W in the Pacific Ocean, *Deep-Sea Res.*, 37:295-315.

Peña, M.A., M.R. Lewis, and W.G. Harrison (1992). New production in the central equatorial Pacific, *Mar. Ecol. Prog. Ser.*, 80:265-274.

Peña, M.A. (1994). New production in the tropical Pacific region, *Ph.D. Thesis*, Dept. of Oceanography, Dalhousie University.

Peña, M.A., M.R. Lewis, and J.J. Cullen (1994). New production in the warm waters of the tropical Pacific Ocean, *J. Geophys. Res.*, 99:14,255-14,268.

Peters H., M.C. Gregg, and J.M. Toole (1988). On the parametrization of equatorial turbulence, *J. Geophys. Res.*, 93:1,199-1,218.

Philander, S.G.H., W.J. Hurlin, and A.D. Siegel (1987). Simulation of the seasonal cycle of the tropical Pacific ocean, J. Phys. Oceanogr., 17:1,986-2,002.

Philander, S.G.H. (1990). *El Niño, La Niña, and the Southern Oscillation*, Academic, San Diego, Calif., 293 pp.

Platt, T., P.Jauhari, S.Sathyendranath (1992). The importance and measurement of new production, In: P.G. Falkowski and A.D. Woodhead (eds), *Primary productivity and biological cycles in the sea*, Plenum Press, New York, pp. 273-284.

Price, N.M., P.J. Harrison, M.R. Landry, F. Azam, and K.J.F. Hall, (1986). Toxic effects of latex and Tygon tubing on marine phytoplankton, zooplankton and bacteria, *Mar. Ecol. Prog. Ser.*, 34:41-49.

Quay, P. (1997). Was carbon balance measured in the equatorial Pacific during JGOFS?, *Deep-Sea Res.*, 44:1,765-1,800.

Radenac, M.H and Rodier, M. (1996). Nitrate and chlorophyll distributions in relation to thermohaline and current structures in the western tropical Pacific during 1985-1989, *Deep-Sea Res.*, 43:725-752.

Raimbault, P., G. Slawyk, B. Boudjellal, C. Coatanoan, P. Conan, B. Coste, N. Garcia, T. Moutin, and M. Pujo-Pay (1999). Carbon and nitrogen uptake and export in the equatorial Pacific at 150° W: Evidence of an efficient regenerated production cycle, *J. Geophys. Res.*, 104:3,341-3,356.

Rasmusson, E.M. and Carpenter, T.H. (1982). Variations in tropical sea surface temperature and surface wind fields associated with the Southern Oscillation El Niño, *Mon. Weather Rev.*, 110:354-384.

Reed, R.K. (1985). An estimate of the climatological heat fluxes over the tropical Pacific ocean. *J. Climate and Appl. Meteor.*, 24:833-840.

Redfield, A.C. (1994). On the proportions of organic derivatives in sea water and their relation to the composition of phytoplankton. In: *James Johnston memorial volume*, Liverpool University Press, 177-192 pp.

Rodier M. and Le Borgne, R. (1997). Export flux of particles at the equator in the western and central Pacific ocean, *Deep-Sea Res.*, 44: No. 9-10, 2,085-2,113.

Sambrotto, R.N., G. Savidge, C. Robinson, P. Boyd, T. Takahashi, D.M. Karl, C. Langdon. D. Chipman, J. Marra, L. Codispoti (1993). Elevated consumption of carbon relative to nitrogen in the surface ocean, *Nature*, 363:248-250.

Sarmiento, J.L. and Siegenthaler, U. (1992). New production and the global carbon cycle, In: P.G. Falkowski and A.D. Woodhead (eds), *Primary productivity and biological cycles in the sea*, Plenum Press, New York, 317-332 pp.

Sarmiento, J.L. and Bender, M. (1994). Carbon biogeochemistry and climate change, *Photosynthesis Research*, 39:209-234.

Sathyendranath, S., T. Platt, E.P.W. Horne, W.G. Harrison, O. Ulloa, R. Outerbridge, and N. Hoepffner (1991). Estimation of new production in the ocean by compound remote sensing, *Nature*, 353:129-133.

Shinoda, T., and Lukas, R. (1995). Lagrangian mixed layer modeling of the western equatorial Pacific, *J. Geophys. Res.*, 100:2,523-2,541.

Siegel, D.A., J.C. Ohlman, L. Walshburn, R.R. Bidigare, C.T. Nosse, E. Fields, and Y. Zhou (1995). Solar radiation, phytoplankton pigments and the radiant heating of the equatorial Pacific warm pool, *J. Geophys. Res.*, 100:4,885-4,891.

Siegel, D.A, D.J. McGillicuddy Jr., and E.A. Fields (1998). Mesoscale eddies, satellite altimetry and new production in the Sargasso sea, *J. Geophys. Res.*, submitted.

Smith, S.D. (1980). Wind stress and heat flux over the ocean in gale force winds, *J. Phys. Oceanogr.*, 10:709-726.

Smith, G.D. (1985). *Numerical solution of partial differential equations: Finite difference methods*, Oxford: Clarendon Press.

Sokal, R.R. and Rohlf, F.J. (1995). *Biometry: The principles and practice of statistics in biological research*, W.H. Freeman and Company, New York.

Song, X. and Friehe, C.A. (1997). Surface air-sea fluxes and the upper ocean heat budget at 156°E, 4°S during the Tropical Ocean-Global Atmosphere Coupled Ocean Atmosphere Response Experiment, *J. Geophys. Res.*, 102:23,109-23,129.

Strickland, J.D.H. and Parsons, T.R. (1972). In: *A practical handbook of sea water analysis*, Bull. Fish. Res. brd. Can., 167: 311 pp.

Sprintal, J. and McPhaden, M.J. (1994). Surface layer variations observed in multiyear time series measurements from the western equatorial Pacific, *J. Geophys. Res.*, 99:963-979.

Stephens, M.S., G. Samuels, D.B. Olson, and R.A. Fine (1995). Sea-air flux of CO_2 in the North Pacific using shipboard and satellite data, *J. Geophys. Res.*, 100:13,571-13,583.

Sundermeyer, M.A. and Price, J.F. (1996). Lateral mixing in the North Atlantic Tracer Release Experiment: Observations and numerical simulations of Lagrangian particles and passive tracer, (submitted).

Tans, P.P., I.Y. Fung, and T. Takahashi (1990). Observational constrains on the global atmospheric CO_2 budget, *Science*, 247:1,431-1,438.

Thorpe, S.A. (1977). Turbulence and mixing in a Scottish loch, *Phil. Trans. Roy. Soc. London*, A, 286:125-181.

Toggweiler, J.R. (1989). In: W.H. Berger, V.S. Smetacek, G. Wefer, (eds), *Productivity in the ocean: Past and present*, Willey, New York, 65-83 pp.

Toole, J.M., H. Peters, and M.C. Gregg (1987). Upper ocean shear and density variability at the equator during Tropic Heat., *J. Physic. Oceanogr.*, 17:1,397-1,406.

Tsuchiya, M. (1968). In: *Upper Waters of the Intertropical Pacific Ocean*, Johns Hopkins Oceanographic Studies, 4, 50 pp.

Wacongne, S. (1989). Dynamical regimes of a fully nonlinear stratified model of the Atlantic Equatorial Undercurrent, *J. Geophys. Res.*, 94:4,801-4,815.

Walsh, J.J. (1996). Nitrogen fixation within a tropical upwelling ecosystem: Evidence for a Redfield budget of carbon/nitrogen cycling by the total phytoplankton community, *J. Geophys. Res.*, 101:20,607-20,616.

Wanninkhof, R. (1992). Relationship between wind speed and gas exchange over the ocean, *J. Geophys. Res.*, 97:7,373-7,382.

Wanninkhof, R., R.A. Feely, D.K. Atwood, G. Beberian, D. Wilson, P.P. Murphy, and M.F. Lamb (1995). Seasonal and lateral variations in carbon chemistry of surface waters in the eastern equatorial Pacific during 1992, *Deep-Sea Res.*, 42:387-409.

Wang, W. and McPhaden, M.J. (1997). The surface layer heat balance in the equatorial Pacific ocean, Part 1: Mean seasonal cycle, *J. Phys. Oceanogr.*, submitted.

Weare, B.C., T. Strub, and M. D. Samuel (1981). Annual mean surface heat fluxes in the tropical Pacific Ocean, *J. Phys. Oceanogr.*, 11:705–717.

Webster, P.J. and Lukas, R. (1992). The Tropical Ocean/Global Atmosphere Coupled Ocean-Atmosphere Response Experiment (COARE), *Bull. Am. Meteorol. Soc.*, 73:1,377-1,416.

Wells, M.L., G.K. Vallis, and E.A. Silver (1999). Tectonic processes in Papua New Guinea and past productivity in the eastern equatorial Pacific Ocean, *Nature*, 398:601-604.

Wijesekera, H.W. and Gregg, M.C. (1996). Surface layer response to weak winds, westerly bursts, and rain squalls in the western Pacific Warm Pool, *J. Geophys. Res.*, 101:977-997.

Wilkerson, F.P. and Dugdale, R.C. (1992). Measurements of nitrogen productivity in the equatorial Pacific, *J. Geophys. Res.*, 97: 669-679.

Wilks, D.S. (1995). In: *Statistical methods in the atmospheric science: An introduction*, Academic Press, San Diego, 325-341 pp.

Wyrtki, K. (1981). An estimate of equatorial upwelling in the Pacific, *J. Phys. Oceanogr.*, 11:1,205-1,214.

Zentara, S.J. and Kamykowski, D. (1977). Latitudinal relationship among temperature and selected plant nutrients along the west coast of North and South America, *J. Mar. Res.*, 35:321-337.

Zhang, G.J. and McPhaden, M.J. (1995). The relationship between sea surface temperature and latent heat flux in the equatorial Pacific, *J. Clim.*, 8:589-605.